Forschungszentrum Jülich
in der Helmholtz-Gemeinschaft

Institut für Kernphysik
COSY

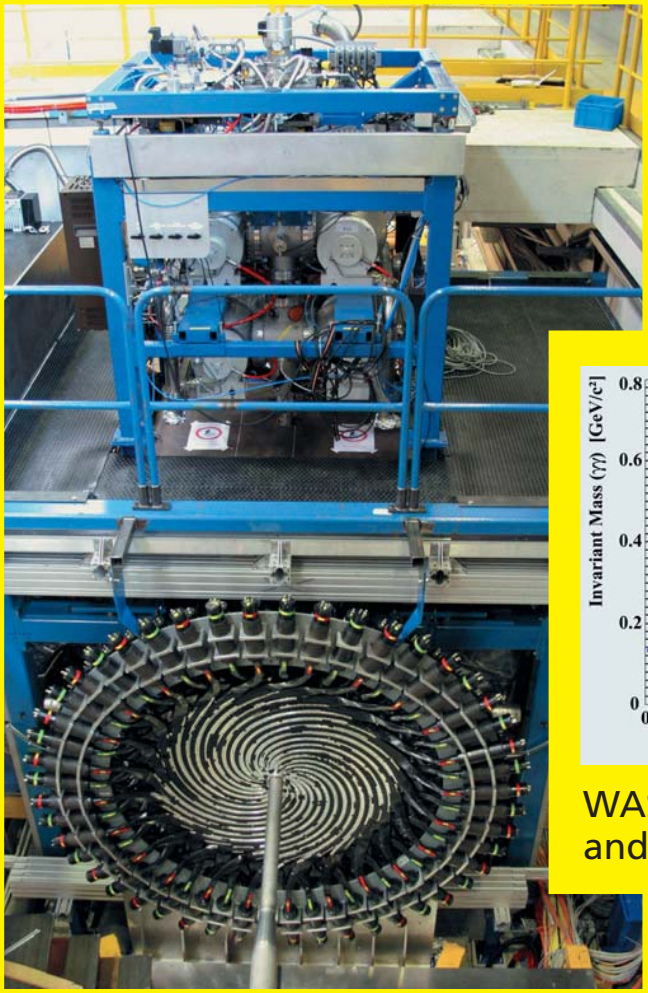

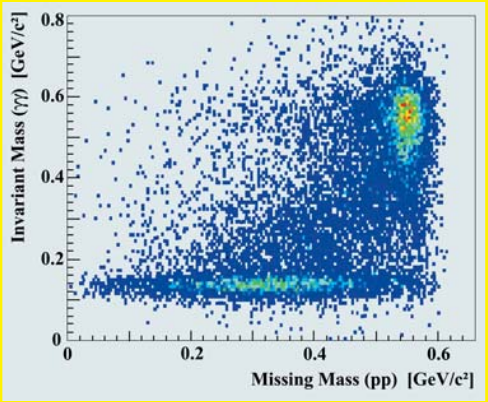

WASA at COSY: Installation and First Measurements

ANNUAL REPORT 2006

JÜl-4234

Annual Report 2006

Institut für Kernphysik / COSY

Cover picture:

One and a half years after starting the dismount at CELSIUS, the WASA detector has been installed and successfully commissioned at COSY. The photograph shows the spiral elements of the Jülich quirl, encircling the COSY beam line (bottom), and the pellet generator above the interaction point in the course of the installation phase. First data on the reaction $p\,p \to p\,p\,\eta$ ($\to \gamma\gamma$) have been reconstructed during commissioning from the WASA forward- and central-detector information (abscissa and ordinate of the experimental spectrum, respectively).

Preface

The past year 2006 has been a very successful one for the institute: first off, a major milestone has been achieved with the in-time installation of the WASA detector at an internal target station of COSY and its subsequent commissioning. WASA-at-COSY is ready to take data and the collaboration is looking forward to its first data production run, approved by the COSY-PAC and scheduled for spring 2007. Furthermore, after very productive scientific programs, the internal experiment COSY-11 and the external beam experiments at BIG KARL have finished their data taking phases, and are now completing the analysis of the existing data.

The following highlights top the list of the important scientific results:

- Pentaquark studies: the TOF-collaboration has very carefully analysed their dedicated high-statistics data sample, and did not find a signal for the $\Theta^+(1540)$. This finding has been supported by the ANKE-collaboration in a different final state.
- Bound η-nucleus states: data with unprecedented precision for the $^3\mathrm{He}\eta$ system have been obtained both at ANKE and at COSY-11 in the dp-reaction, exploiting the unique possibilities at the internal COSY beam during the ramp-up of the energy. The very rapid rise of the total cross section close to threshold implies a very large $^3\mathrm{He}\eta$ scattering length and hence the presence of a quasi-bound state extremely close to threshold.
- Hyperon-nucleon interactions: chiral effective field theory has successfully been applied to the interactions between nucleons and hyperons. This paves the way to a model-independent approach of strange quark effects in nuclei.
- Accelerator studies: the COSY accelerator has been used for spin manipulations of a polarized deuteron beam, and clear indications for a deuteron spin resonance have been obtained.

All results mentioned have recently been submitted for publication. More details and further results can be found in the main text.

In addition to WASA, the two other major installations continue to be developed further:

- ANKE has taken an important step towards double polarization experiments with the first installation and commissioning of the polarized internal target.
- TOF is preparing for an upgrade with straw-detectors to further improve the tracking resolution. In view of the non-confirmation of the pentaquark at COSY and elsewhere, the earlier plans to implement a polarized target have been dropped.

As the FAIR project at GSI Darmstadt is taking shape, the IKP continues to become more and more involved in the preparations for the hadron physics program with antiproton beams:

- The accelerator group plays the dominant role in the international consortium of FZJ, TSL Uppsala and GSI Darmstadt to design the High Energy Storage Ring at FAIR. The ion optical design of the HESR, the RF systems, beam diagnostics, magnet and cryo-design and the stochastic cooling system are in the responsibility of the Jülich accelerator group.
- Beam-dynamics investigations in the equilibrium of internal targets and beam cooling have been carried out at COSY.
- The experimental groups are widely engaged in the design of the PANDA detector at HESR, with projects and commitments ranging from inner tracking to the pellet target. In particular, a cleanroom has been installed to develop the silicon pixel microvertex detector, and the IKP straw concept has been adapted by PANDA as the basis for the proposed Straw Tube Tracker. Furthermore, the IKP-Moscow group has taken a leading role in the pellet-target development.
- The possibilities to effectively produce polarized antiprotons for a later upgrade are being pursued by the PAX collaboration with essential test measurements at COSY (and possibly elsewhere).

We are looking forward to the constitution of the FAIR GmbH and the formal start of the project, and we hope for the timely flow of investment money in order to prepare and build the accelerator and detector components as planned.

Within the new funding opportunities by the Helmholtz association, IKP has succeeded in:

- A virtual institute "Spin and strong QCD", headed by Prof. U.-G. Meißner , has been installed.
- A HGF-University junior-researcher position on "Few-Nucleon Systems in Chiral Effective Field Theory" has been raised in collaboration with Bonn University by Prof. E. Epelbaum.

More than 20 teaching positions at 11 Universities demonstrate the strong dedication of the institute for the education of students and young researchers. In this respect I want to emphasize that in 2006 the 3rd COSY Summer School took place which was attended by more than 30 Diploma and Ph.D. students from 9 countries.

Finally I would like to express my sincere gratitude to all our colleagues and co-workers, since without their help and support, we would not have been able to achieve our milestones. For WASA-at-COSY, our special thanks go to the former WASA-collaboration and to ZAT and ZEL. We also acknowledge the continuous support by the board of management of the Research Center and HGF.

Jülich, January 2007 Rudolf Maier

Contents

1 Physics at COSY

1.1 Overview

During the year 2006, the WASA detector has been installed at an internal target position of COSY and commissioning has started. **WASA** can detect both neutral and charged particles with a large angular and momentum acceptance and, thus, complements the two other large COSY experiments, **ANKE** and **TOF**, which are "photon blind".
From 2007 on **WASA**, **ANKE** and **TOF** will be the only running experiments at COSY since the remaining other installations — **COSY-11**, **PISA BIG KARL** (with ENSTAR, GEM and HIRES) — are decommissioned after successfully completing their scientific programs.
At **ANKE** the polarized internal target (PIT) has been installed in 2006, first double polarization experiments are carried out early in 2007. The non-magnetic spectrometer **COSY-TOF** will be upgraded with straw trackers in summer 2007, which will significantly increase the mass resolution for *e.g.* hyperon studies.

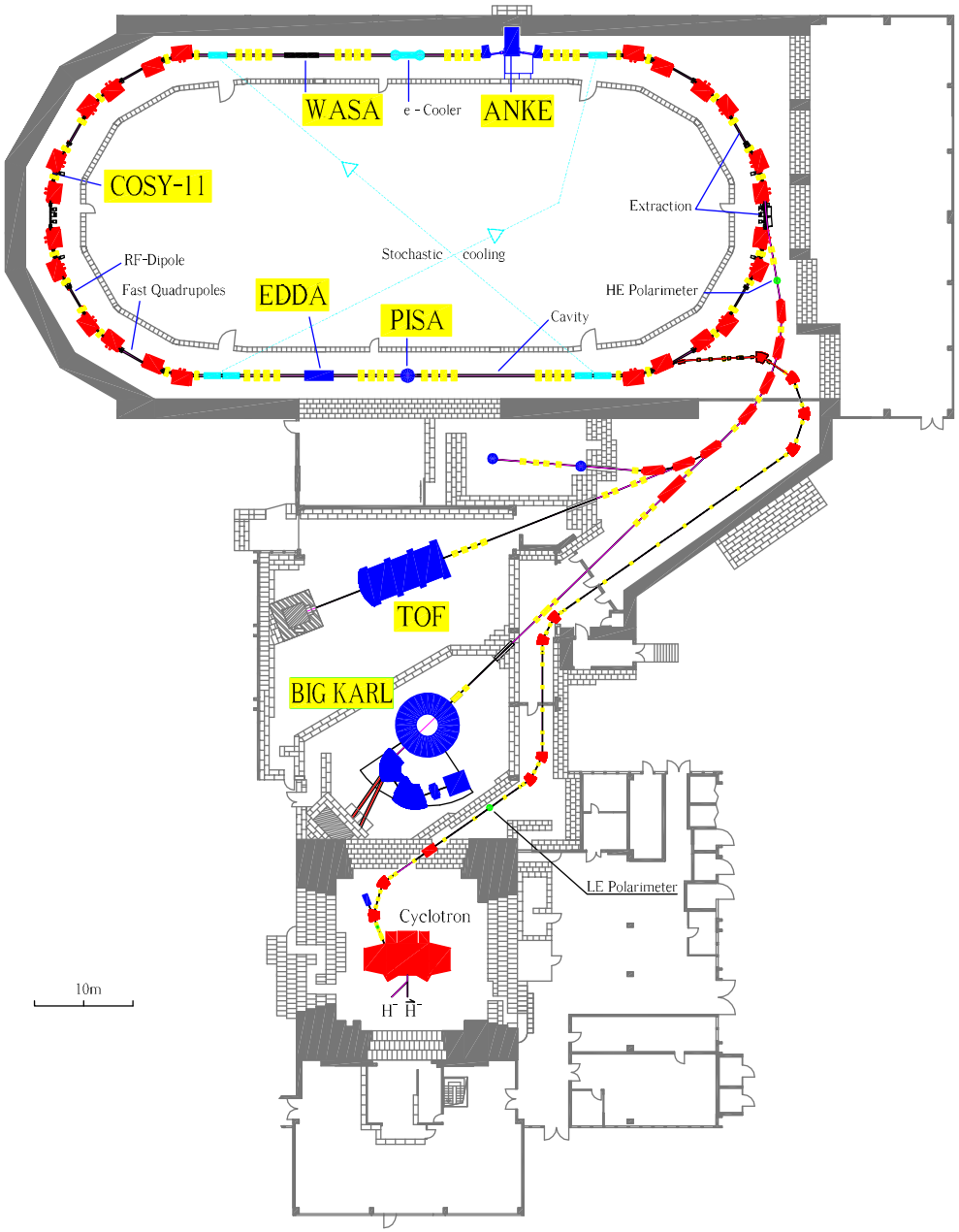

1.2 Major Physics Results at COSY

1.2.1 Pentaquark Searches

End of 2004 the reaction $pp \to pK^0\Sigma^+$ was investigated with the **COSY-TOF** spectrometer at 3.059 GeV/c incident beam momentum to obtain decisive information on the exotic Θ^+ state where the situation is still confusing. The main objective was to clarify whether or not the Θ^+ pentaquark is populated at 1.53 GeV/c^2 in the pK^0 subsystem with a data sample of much higher statistical significance compared to the data previously published by the COSY-TOF collaboration for the same channel.
The analysis was carried out with three independent analysis programs, which differ in the algorithms and event selection methods, but are based on a common calibration of all detector components. The invariant mass spectra of the pK^0 subsystem as extracted from the three analyses are shown in Fig. 1 after background subtraction and acceptance correction together with a 3rd order polynomial parameterization.

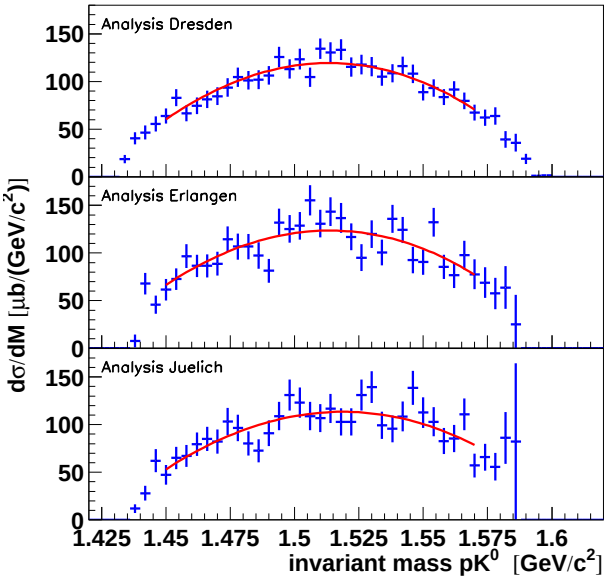

Fig. 1: Invariant masses of the pK^0 system for the three analyses together with a 3rd order polynomial parameterization.

To determine the statistical significance with which a narrow structure might be present, a Gaussian corresponding to the experimental resolution of about $5-6$ MeV (σ) was added where the mass was varied from 1.50 GeV/c^2 to 1.55 GeV/c^2. The analysis of these spectra does not confirm the existence of the Θ^+ pentaquark. This is expressed as an upper limit for the cross section

$$\sigma_{pp\to\Theta^+\Sigma^+} < 0.3\,\mu\text{b}$$

at a 95% confidence level.
The reaction $pp \to pK^0\pi^+\Lambda$, measured at **ANKE** at a beam momentum of $p_p = 3.65$ GeV/c, allows one to investigate the Kp system, and to search for signatures from the pentaquark baryon $\Theta^+(1540)$. The reaction has been identified by detecting four particles simultaneously, the π^+ coming from the reaction vertex, the proton from vertex/Θ^+ decay, and the products of the Λ decay: proton and π^-. Besides individual particle identification, the final state is fixed by the missing mass technique. A sizable background remains after cuts on masses are made, and this background is removed by the side band subtraction method.

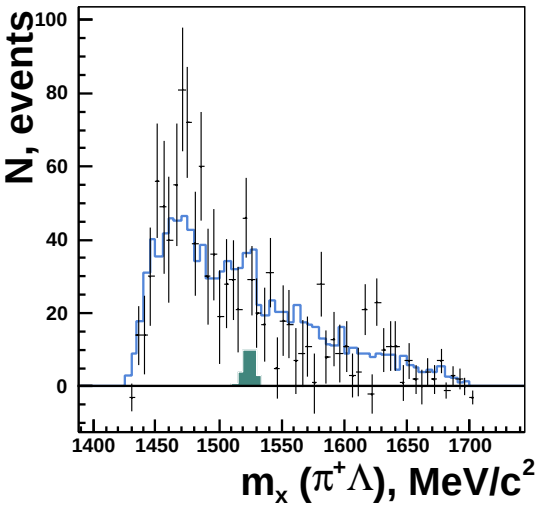

Fig. 2: Missing mass spectrum of $\pi^+\Lambda$ system. The solid line denotes the sum of all contributions. The gray region corresponds to the maximum permissible $\Theta^+(1540)$ signal.

The missing mass distribution $m(\pi^+\Lambda)$, presented in Fig. 2, is the one where the signal from the pentaquark is expected to appear. The solid line includes contributions from non-resonant production as well as from the formation of an intermediate $\Delta^{++}(1232)$, inclusion of which is required by other differential distributions. The grey area in Fig. 2 corresponds to the maximum possible signal from Θ^+ production. The fit results in a Θ^+ peak area, comparable with the statistical fluctuation of the background. Therefore, only an upper limit for the possible Θ^+ production can be deduced:

$$\sigma_{pp\to\Theta^+\pi^+\Lambda} < 0.058\,\mu\text{b}\,.$$

Since the acceptances of both four-body phase-space production and production with an intermediate $\Delta^{++}(1232)$ are very similar, a total cross section for the $pK^0\pi^+\Lambda$ final state can be calculated independent of the decomposition into separate channels. After the normalisation and efficiency corrections, the following total cross section for the $pK^0\pi^+\Lambda$ final state has been deduced:

$$\sigma_{\text{tot}} = (1.41 \pm 0.05 \pm 0.33)\,\mu\text{b}\,,$$

where the first error is statistical, while the second is systematic.

1.2.2 $\Lambda(1405)$ Production in pp Collisions

The $\Lambda(1405)$ is a particularly interesting state because its structure is not yet understood and is difficult to be obtained from quark models. The $\Lambda(1405)$ can be the spin-multiplet partner of $J^P = 3/2^-$ $\Lambda(1520)$, a meson-baryon resonance, or a $\bar{K}N$ quasibound state. Recent theoretical investigations based on chiral dynamics predict two poles for the $\Lambda(1405)$, one coupling strongly to $\pi\Sigma$ states and the other one mostly to $\bar{K}N$ states.

The reaction $pp \to pK^+Y^{0*}$ has been studied with **ANKE** at a beam momentum of 3.65 GeV/c to investigate the production of excited hyperon resonances Y^{0*} decaying via $\Sigma^0\pi^0$. In case of $\Lambda(1405)$ production there are two protons, one positively charged kaon and a negatively charged pion in the final state: $pp \to pK^+\Lambda(1405) \to pK^+\Sigma^0\pi^0 \to pK^+\Lambda\gamma\pi^0 \to pK^+p\pi^-\pi^0\gamma$. At ANKE those particles are measured with *different* parts of the detection system.

Missing- and invariant-mass techniques are used to identify the $\Lambda(1405)$ resonance. Cutting on the invariant mass of $p\pi^-$ one can detect protons and negative pions from Λ decay. Furthermore the missing mass $MM(pK^+p\pi^-)$ is requested to be larger than the π^0 mass to separate the $\Lambda(1405)$ hyperon, in particular from the $\Sigma(1385)$. In Fig. 3 the missing mass $MM(p_{FD}K^+)$ spectrum obtained under these conditions is shown. The position of the most prominent peak is at the mass of the $\Lambda(1405)$.

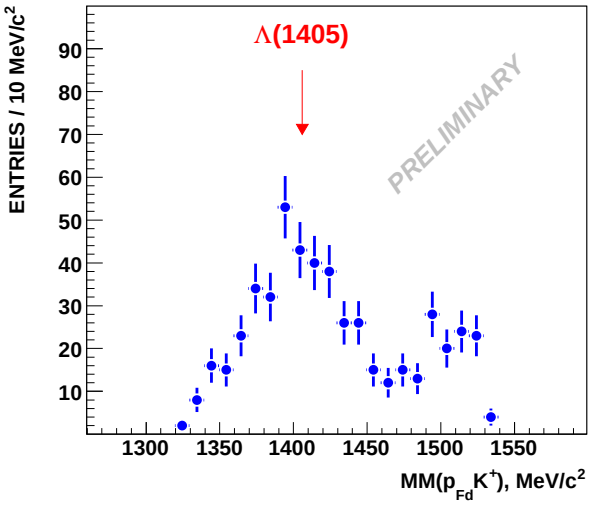

Fig. 3: Missing mass $MM(p_{FD}K^+)$ measured in pp collisions at a beam momentum of 3.65 GeV/c.

This is the first observation of direct production of the $\Lambda(1405)$ in pp collisions decaying via $\Sigma^0\pi^0$. The preliminary number of events in the $\Lambda(1405)$ peak is 250 ± 50.

1.2.3 $K\bar{K}$ Production in pd interactions

The study of meson production in proton-nucleus collisions near threshold is of interest because of the intricate reaction mechanism that allows the momentum transfer to be shared among several nucleons and this feature becomes yet more critical as the mass of the meson is increased. Clean spectra can be obtained by exclusive measurements. Therefore, for the study of $K\bar{K}$ production in pd collisions the ^{3}He has been measured with the magnetic spectrograph **BIG KARL** and the two kaons with the **MOMO** wall in coincidence. The measurements were performed at overall excess energies of $\varepsilon_{KK} = 35.1$ MeV, 40.6 MeV, and 55.2 MeV. There is evidence for the production of the ϕ meson at all three energies but the physics background arising from a prompt K^+K^- production looking like phase space is very large. Fits to the excitation energy spectra have been undertaken in terms of phase space and phase space modulated by a ϕ peak.

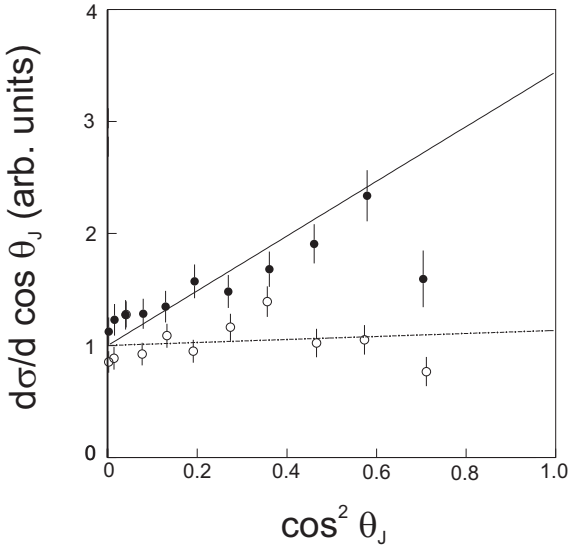

Fig. 4: Angular distributions of the kaons as a function of the Jackson angle for the lowest beam energy. The data are divided into those with $Q_{KK} < 28$ MeV (no ϕ's, closed circles) and $Q_{KK} > 28$ MeV (open circles). For the lines see text.

In the Gottfried-Jackson frame, the total momentum of the K^+K^- system is zero, which means that it is the ϕ rest frame. Since the ϕ is a vector meson, the distribution in the relative momentum of the kaons from its decay is sensitive to its polarization with respect to some quantization axis:

$$\frac{\mathrm{d}\sigma(\phi \to 2K)}{\cos(\theta_{\mathrm{GJ}})} \propto \rho_{11}\sin^2\theta_{\mathrm{GJ}} + \rho_{00}\cos^2\theta_{\mathrm{GJ}}. \qquad (1)$$

Here the spin-density matrix elements ρ_{00} and ρ_{11} correspond to the populations with magnetic sub-state $m = 0$ and the average of $m = \pm 1$ respectively. On the other hand, the production of an S-wave K^+K^- pair would lead to a flat distribution in the decay angle θ_{GJ}. Figure 4 shows the distribution in this angle separately for the ϕ-rich region and the remainder. In order to demonstrate the very different slopes in the two regions, the data have been arbitrarily scaled such that the cross sections have

similar values when $\cos\theta_{GJ} = 0$. These slopes are determined by the fraction of the cross section associated with ϕ production and the ϕ polarization. The straight lines in the figure are obtained by using the ϕ contribution determined from the fits to the Q_{KK} distribution, assuming that the meson is produced purely with $m = 0$. This *ansatz* describes the main features of the data in both energy regions. Alternatively, fitting Eq. (1) to the ϕ-rich data gives $\rho_{00} = 0.82 \pm 0.05$, where the error bar is statistical.

The MOMO data on the $pd \to {}^3\mathrm{He}\,K^+K^-$ reaction can also be investigated in terms of the $K^-{}^3$He interaction. Such few-body nuclear systems involving the $\bar{K}$-meson as a constituent have found considerable interest after the prediction of extremely dense and deeply bound states by Akaishi and Yamazaki. They argued that the $\bar{K}N$ interaction is characterized by a strong I=0 attraction, which allows the few-body systems to form narrow $\bar{K}$-nuclear states with a binding energy of more than 100 MeV. Evidence for such bound states produced in K^- absorption at rest on different nuclear targets has been claimed by the at KEK and by the FINUDA collaborations. However, the interpretation of these data in terms of deeply bound states still is heavily debated.

A strongly modified $\bar{K}N$-effective scattering length extracted from the proposed very attractive K^-A potential would also lead to a pronounced deformation of the $K^-{}^3$He relative-energy spectra, see dash-dotted line in Fig. 5. However, the measured $K{}^3$He relative energy distribution rather shows a phase-space like shape, pointing at a weak $K^-{}^3$He interaction. An exotic deeply bound state is thus strongly disfavored by the data.

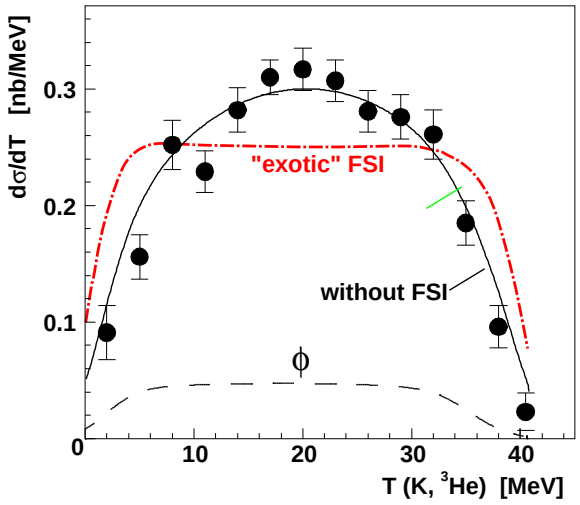

Fig. 5: Distribution of the $K{}^3$He relative energy for the $pd \to {}^3\mathrm{He}\,K^+K^-$ reaction at an excess energy of 40.6 MeV. The solid line describes the incoherent sum of a pure phase-space distribution and the $\phi(1020)$ contribution (dashed line). The dash-dotted line shows the effect for a strongly modified $\bar{K}N$ scattering length in nuclear medium leading to the deeply bound states.

1.2.4 η-Nucleus Interaction Studies

The low energy $\eta\,{}^3$He system has been investigated in the $dp \to {}^3\mathrm{He}\,\eta$ reaction in high statistics experiments using the **ANKE** and **COSY-11** facilities. The anomalous energy dependence found in earlier measurements at SATURNE as well in photoproduction measurements at MAMI suggests that the strong $\eta\,{}^3$He final state interaction (*fsi*) might lead to the formation of a new state of matter in the form of an $\eta\,{}^3$He quasi-bound state for nuclei much lighter than originally postulated. This question is far from being settled and further high quality data are required.

At ANKE and COSY-11 differential and total cross sections have been measured near threshold using a continuous ramp of the beam energy from sub-threshold energies up to excess energies Q of 11.3 MeV and 8.3 MeV, respectively. The differential cross sections extracted both at ANKE and COSY-11 expose contributions from higher partial waves already at low excess energies. As can be seen by the angular asymmetry parameter α (Fig. 6), defined by

$$\left(\frac{\mathrm{d}\sigma}{\mathrm{d}\Omega}\right)_{\mathrm{c.m.}} = \frac{\sigma_{\mathrm{tot}}}{4\pi}\left[1 + \alpha\cos\theta_{\mathrm{c.m.}}\right], \qquad (2)$$

above an η c.m. momentum p_η of 40 MeV/c ($Q \sim 2$ MeV) α is positive and increases monotonically with p_η but with a magnitude much larger than that found at SPES-II.

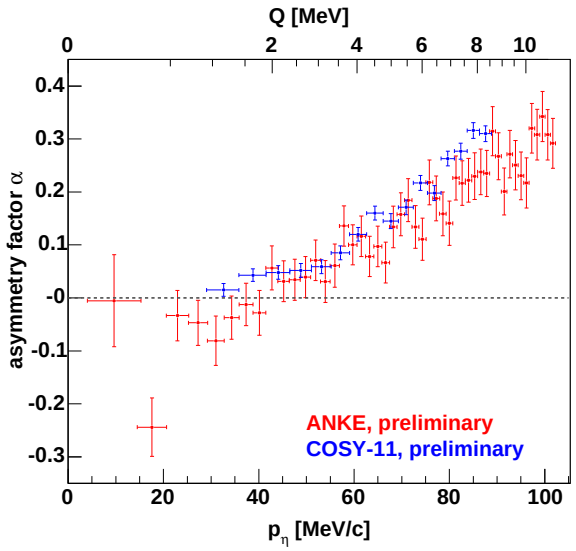

Fig. 6: Asymmetry parameter α for different values of the η c.m. momentum p_η. The shown error bars correspond to the statistical uncertainties.

The $dp \to {}^3\mathrm{He}\,\eta$ total cross sections obtained at 195 bins (ANKE) and 20 bins (COSY-11) in excess energy Q are displayed in Fig. 7. While the SPESII results do not define firmly the energy dependence close to threshold, the high-resolution ANKE data displayed in Fig. 7b) show that the total cross section reaches its maximum value

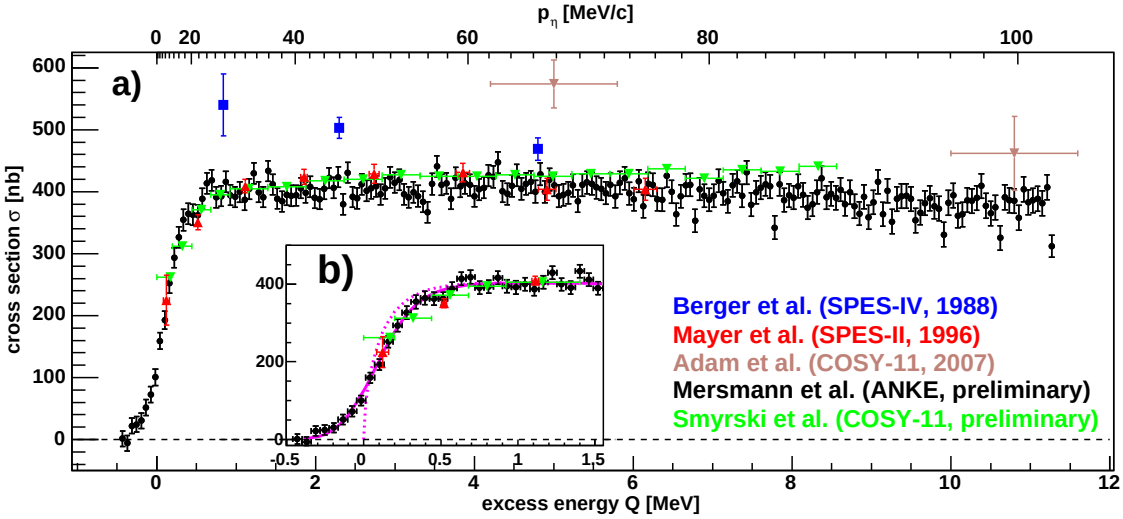

Fig. 7: Comparison of the extracted total cross section data for the reaction $dp(pd) \to {}^3\mathrm{He}\,\eta$. The error bars represent the statistical uncertainties.

within $\Delta Q = 0.5\,\mathrm{MeV}$ of threshold and remains nearly constant after that. This behavior is in complete contrast to phase-space expectations and indicates a very strong final state interaction. In the presence of such a strong final state interaction, the s-wave amplitude f_s can be approximated in terms of the complex $\eta\,{}^3\mathrm{He}$ scattering length (a) and effective range (r_0)

$$f_s = f_B \big/ \left(1 - iap_\eta + \tfrac{1}{2}ar_0p_\eta^2\right) , \qquad (3)$$

where f_B is assumed to be slowly varying. The shape of the η production below the nominal threshold shown in Fig. 7 is a very sensitive measure of the momentum width of the COSY beam, and this resolution has to be taken into account in the analysis. A preliminary evaluation of the ANKE data (solid and dotted lines of Fig. 7b) results in a surprisingly large real part of the meson-nucleus scattering length $a_{He\eta}$ which in turn is a prerequisite for the existence of a quasi-bound $\eta\,{}^3\mathrm{He}$ system. Additionally, for the description of the data very close to threshold the consideration of the effective range was found to be essential. Here the solid line represents a fit to the data including the beam momentum width while the dotted line shows the same fit but corrected for the finite momentum width. The COSY-11 data are expected to allow for a similar analysis in the near future.

1.2.5 Vector Meson Production

Quasi-free ϕ-meson production in pn interactions has been studied at **ANKE** using a deuteron cluster-jet target. The energy dependence of the total pn cross section has been extracted up to 80 MeV by exploiting the intrinsic momentum of the neutron in the deuteron. In order to select the quasi-free $pn \to d\phi$ process from the measured $pd \to d\phi\, p_{\mathrm{sp}}$ events, the K^+K^- decay mode of the ϕ-meson has been detected in coincidence with a fast deuteron. The missing mass of the (K^+, K^-, deuteron) candidates has been calculated and a gate put around the proton mass. The momentum distribution of the unobserved proton for the events in the ϕ mass region shows the expected distribution for a spectator.

Figure 8 shows the energy dependence of the quasi-free $pn \to d\phi$ production together with the total cross sections $pp \to pp\phi$ also obtained at ANKE. Though the $pn \to d\phi$ cross sections are consistent with a phase-space behavior, the kaon angular distributions show the presence of higher partial waves at rather low energy.

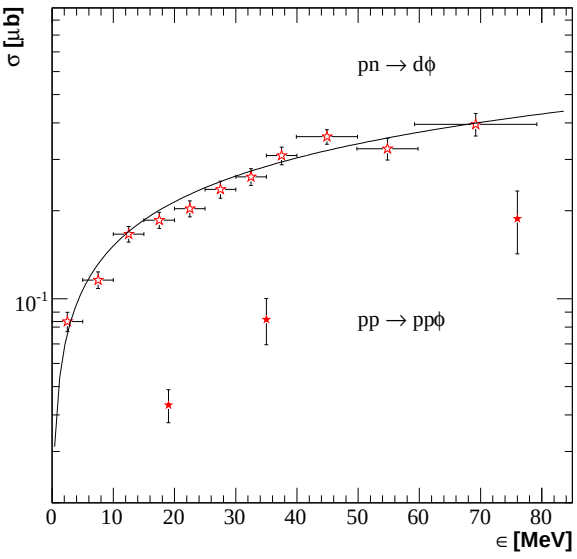

Fig. 8: Total cross section for the quasi-free $pn \to d\phi$ reaction as a function of the excess energy (error bars indicate the statistical uncertainties). The curve represents a phase-space $\sqrt{\varepsilon}$ behavior. For comparison, the values obtained for $pp \to pp\phi$ with total error bars are also included.

The Okubo-Zweig-Iizuka (OZI) rule states that processes with disconnected quark lines in the initial or final state are suppressed. Accordingly, the production of ϕ-mesons from initial non-strange states is expected to be substantially suppressed relative to ω-meson production. The cross-section ratio for ϕ- and ω-production under similar kinematical conditions should then be in the order of $R_{\rm OZI}=\sigma_\phi/\sigma_\omega=\tan^2\alpha_{\rm V}=4.2\times10^{-3}$, where $\alpha_{\rm V}=3.7^\circ$ is the deviation from the ideal ϕ-ω mixing angle. Data from πN interactions as well as from mesonic and radiative decays indicate a ϕ-to-ω ratio of $3\times R_{\rm OZI}$.
Data for the $pp\phi$ production from ANKE in an excess energy range from 18.5 to 75.9 MeV (see Fig. 8), together with SPESIII and COSY-TOF $pp\omega$ results, show similar enhanced ϕ-to-ω ratios in this close to threshold region. The weighted mean value for the ratio from 18.5 to 75.9 MeV is

$$R\left(\frac{\sigma(pp\to pp\phi)}{\sigma(pp\to pp\omega)}\right) = (3.3\pm0.6)\cdot10^{-2} = (7.9\pm1.4)\times R_{\rm OZI}\ .$$

With the existing ANKE $pn\to d\omega$ data measured at 57^{+21}_{-15} MeV and the new results on $pn\to d\phi$ presented here, the production ratio at this single energy is found to be

$$R\left(\frac{\sigma(pn\to d\phi)}{\sigma(pn\to d\omega)}\right) = (4.0\pm1.9)\cdot10^{-2} \approx 9\times R_{\rm OZI}\ .$$

This value is similar to that found in the pp case, though the error bar — dominated by the ω measurement — is much larger.
The combined results of ϕ-meson production in pp and pn collisions at ANKE allow one to resume theoretical works on the understanding of strangeness production. The enhanced ϕ-to-ω production ratio in the near-threshold region may be a signal for additional dynamic effects related to the role of strangeness in few nucleon systems.

1.2.6 Surprises in pn Final State Interactions

The pn interaction at small relative momenta has been studied in the final state interaction of the $pp\to\pi^+pn$ reaction, where the pion was measured under zero degree with the magnetic spectrometer **BIG KARL**. The proton beam was electron cooled at injection energy, then accelerated and finally stochastically extracted. The result of this procedure was an almost background free beam with very small divergence and beam spot of 0.5 mm radius. While the cooling has only a small effect on the horizontal beam divergence it substantially improves the vertical one. Also the beam momentum spread profits from cooling as shown in Fig. 9. The unique combination of a high resolution spectrometer and cooled beam yields a missing-mass resolution of 5×10^{-5}.
In previous experiments the deuteron strength was always leaking into the continuum. Thus a theorem had to be

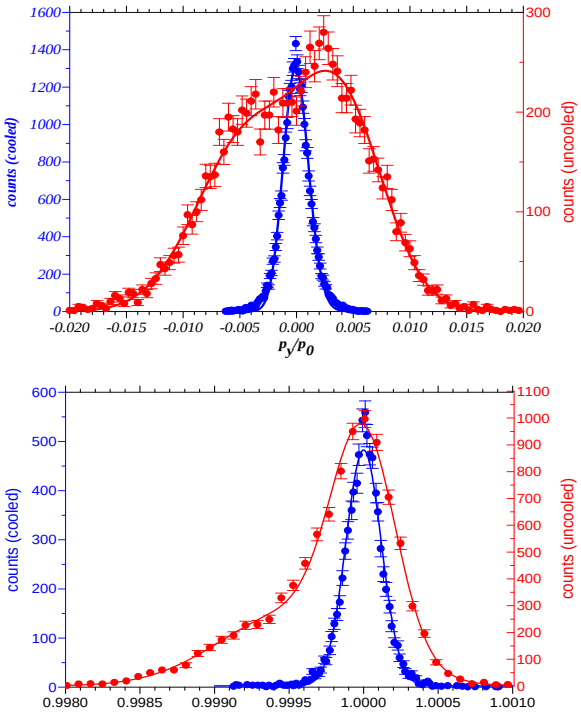

Fig. 9: Top: Vertical divergence of the uncooled beam (red dots) and the cooled beam (blue). The solid curves are Gaussian fits; the uncooled beam is fitted by two Gaussians. Bottom: Momentum spread of the uncooled and cooled beam.

applied which connects the bound-state wave function to that of the continuum. Then the continuum cross section is given by the deuteron cross section in the same state, which is the isospin-triplet state:

$$\frac{d^2\sigma}{d\Omega\,dx}(pp\to\pi^+\{pn\}_t) = R\frac{p(x)}{p(-1)}\frac{\sqrt{x}}{2\pi(x+1)}\frac{d\sigma}{d\Omega}(pp\to\pi^+d) \qquad (4)$$

Here x denotes the excitation energy ε in the np system in units of B_t, $x=\varepsilon/B_t$, and $p(x)$ and $p(-1)$ are the pion c.m. momenta for the pn continuum or deuteron, respectively. We have used an additional factor R, which in the original approach is $R=1$. In the experiments performed so far only approximately one half of the continuum cross section was accounted for by this method. The other half was then attributed to the isospin singlet state. This has a narrow resonance at 48 keV excitation energy. When folding with the experimental resolution the resonance is no more visible.
The high resolution data from BIG KARL, where in addition to the unbound pn-system also the bound deuteron was identified, show that, surprisingly, the singlet-state strength is $<10^{-6}$ as compared to the triplet state. This raises the question about the nature of the experimentally observed strength. One speculation is that there might be an interference with the spin $l=2$ state, which is known to exist in the deuteron on a 4% level. If so, the sign of the interference is still unknown. In order to answer this

question additional data were taken close to and below the maximum of the Δ-resonance. In Fig. 10 a spectrum showing the deuteron as well as the continuum is shown as an example.

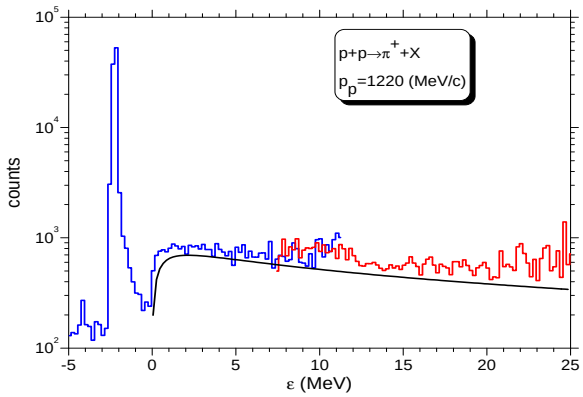

Fig. 10: Comparison of the data with the fsi theorem. The different colors indicate runs with different magnetic spectrometer settings.

It is well known that the phase of an amplitude changes its sign at the pole of a resonance. And indeed: if one applies the above mentioned theorem, one can adjust the factor R in Eq. 4 to fit the data. These factors are compiled in Fig. 11. Presently further model calculations are performed in order to prove whether the effect is in the order of magnitude which one can expect from the d-state strength in the deuteron. But then still the question remains where the isospin singlet strength is gone. Also the influence of higher order correction to the theorem Eq. 4 has to be studied.

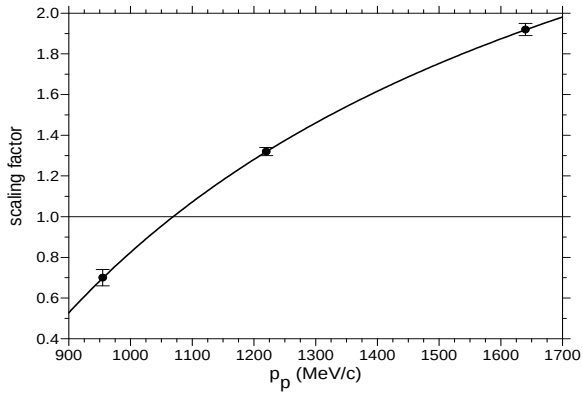

Fig. 11: Dependence of the factor R on the beam momentum. The curve is shown to guide the eyes.

1.2.7 Pion Production

Single pion production in nucleon-nucleon collisions, $NN \to NN\pi$, is the first inelastic process that can be used to test our understanding of the underlying meson-baryon dynamics of the NN interaction. By far the cleanest reaction to study is $pp \to d\pi^+$, where the differential cross section and multitude of spin observables that have been measured over the years can confront the different theoretical models. In contrast, very little was known about the $pp \to pp\pi^0$ reaction, though the unexpectedly large π^0 production rate observed at IUCF near threshold led to a flurry of theoretical and experimental activity. Now in cases where the excitation energy E_{pp} of the final protons is very small, due to the Pauli principle, this reaction will excite only the $J^p = 0^+$ ($^1S_0$) diproton state. Despite having kinematics very similar to those of $pp \to d\pi^+$, this reaction involves different transitions in the NN system and, in particular, the role of the Δ isobar is expected to be much suppressed because the S-wave ΔN intermediate state is forbidden.

The $pp \to pp\pi^0$ differential cross section has been measured with the **ANKE** spectrometer for pion c.m.s. angles between 0° and 15.4° at a proton beam energy of 0.8 GeV. The spectra in the diproton excitation energy E_{pp} showed the expected pp final state enhancement in the $^1S_0$ state and a cut of $E_{pp} < 3$ MeV was applied to the data. The resulting differential cross section exhibits a very strong angular dependence with the value dropping by 30% in the interval $\cos\theta_\pi = 0.97 - 1$. This steep fall is rather unexpected even in the light of the previous CELSIUS results showing a minimum in the forward direction. As seen in Fig. 12, such a steep variation is also obtained in a recent phenomenological calculation, although the absolute scale is too low. There must be an extremely strong cancelation in the forward direction between different partial wave amplitudes and so a relatively minor change in a single partial wave may cause a large change in the cross section.

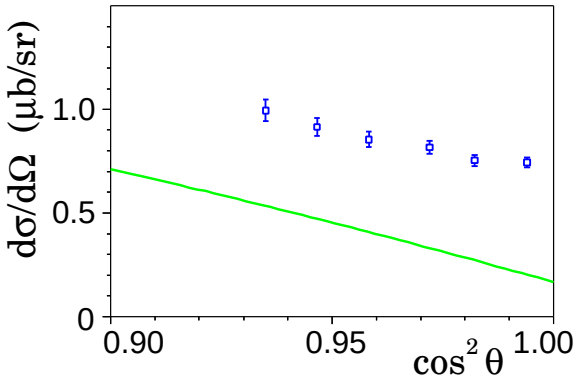

Fig. 12: The $pp \to \{pp\}_s\pi^0$ differential cross section for $E_{pp} < 3$ MeV as a function of $\cos^2\theta$. The curve is a model result by J. Niskanen.

It should be noted that, unlike the complicated spin structure connected with the $pp \to d\pi^+$ reaction, only two spin amplitudes which are functions of $\cos^2\theta_\pi$ are required to describe the $pp \to \{pp\}_s\pi^0$ reaction. These can be isolated, up to an unmeasurable overall phase, by determining the proton analysing power and the initial pp spin correlation C_{xx}. Both of these experiments can be carried out at small angles using ANKE and the resulting amplitude analysis will tie down even further πNN dynamics at intermediate energies.

1.2.8 η Production in $\vec{p}p$ Interactions

The **COSY-11** collaboration has determined the analysing power for the $\vec{p}p \rightarrow pp\eta$ reaction since its theoretical value is sensitive to the assumption on the type of the exchange meson that excites one of the colliding nucleons to the $S_{11}(1535)$ state. The measurements have been performed in the close-to-threshold region at beam momenta of $p_{\mathrm{beam}} = 2.010$ and 2.085 GeV/c, corresponding to the excess energies of $Q = 10$ and 36 MeV, respectively. The measured amplitudes of the analysing power A_y^{max} for both excess energies are presented in Fig. 13.

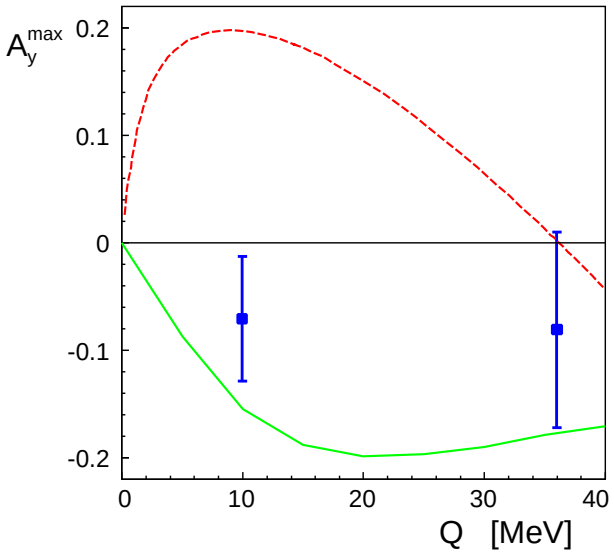

Fig. 13: Theoretical predictions for the amplitudes of the analyzing power's energy dependence confronted with the amplitudes determined by the COSY-11 group at $Q = 10$ and 36 MeV for the vector (red dashed line, model calculations by G. Fäldt and C. Wilkin) and pseudoscalar (solid green, Nakayama *et al.*) meson-exchange dominance model. The experimental values of the amplitude (A_y^{max}) of the analysing power were derived under the assumption that the shape of A_y as a function of $cos(\theta)$ does not depend on the excess energy.

The Figure shows that the predictions of the model based on π-meson dominance are fairly consistent with the data, whereas the calculations based on the dominance of the ρ exchange differ from the data by more than four standard deviations.
The χ^2 analysis applied to the tested production models excludes the correctness of the assumption of a pure vector-meson dominance (ρ exchange) with a significance level of 0.006 corresponding to a discrepancy between the model and the data larger than four standard deviations, and provides strong evidence for the supposition that the production of η mesons in nucleon-nucleon collision is dominated by the pion exchange.
One should, however, keep in mind that the interpretation of the data is at present model dependent and that the interference in the exchange of both types of mesons is not excluded and should be studied theoretically and experimentally by the measurement of further spin observables. It is also worth to mention that the analysing powers of the $\vec{p}p \rightarrow pp\eta$ reaction for both excess energies studied are consistent with zero within one standard deviation. This may suggest that the η meson is predominantly produced in the s-wave, an observation which is in agreement with the results of the analysing power measurements performed by the DISTO collaboration where, interestingly, in the far-from-threshold energy region the A_y were found to be also consistent with zero within one standard deviation.

1.3 Status of Experimental Facilities

1.3.1 Installation and Commissioning of the WASA Detector

After installation at COSY during summer, the WASA detector has been successfully commissioned in the second half of 2006. Thus the physics program (for details we refer to the "WASA-at-COSY" proposal nucl-ex/0411038) will start in the beginning of 2007 as orignially scheduled.

Installation

Mechanical preparations included an adjustment of the original detector main frame by 285 mm to adapt for the difference in height of the beamline of COSY compared to CELSIUS. The alignment procedure for main frame, forward cone and solenoid was extensively tested prior to installation. The fixation of the forward cone with the central drift chamber (MDC) to the main frame was changed to allow for an easier precise alignment. The carriages of the calorimeter have been modified for use with the rail system for the central detector installed in 2005.
After the setup of the cryogenic plant the first current in the superconducting solenoid was produced already in June. The vacuum system has been finished middle of July, followed by completion of detector installation and cabling and first pellets being produced middle of August, just ahead of the first commissioning run.

Pellet Target

After installation, during both commissioning phases in August and November 2006, a continuously stable pellet-target operation has been achieved: Hydrogen pellets have been produced for more than a week at rates up to 4 kHz at the interaction point (Fig. 14). During the December shutdown, first deuterium pellets have been produced after the transfer to COSY.
The manufacturing of glass nozzles and vacuum-injection capillaries has been started at the Central Department of Technology (ZAT) of the FZJ. One future focus will be to further improve the target performance with hydrogen, *i.e.* both to increase the average rate of pellets in COSY beam, and to minimize variations in the time structure of the pellet beam.

Beam Development

A major part of the COSY machine development weeks in the second half of 2006 was dedicated to the commissioning with the WASA solenoid and the pellet target. The electron cooler solenoid was used for partial compensation of the phase-space coupling by the WASA solenoidal field. Due to the residual phase-space coupling and the asymmetric acceptances in COSY ($\sim 50\,\pi$ mm mrad horizontally, $\sim 15\,\pi$ mm mrad vertically) the beam intensity in COSY was reduced by a factor of three to $2.4 \cdot 10^{10}$ with the WASA solenoid on.

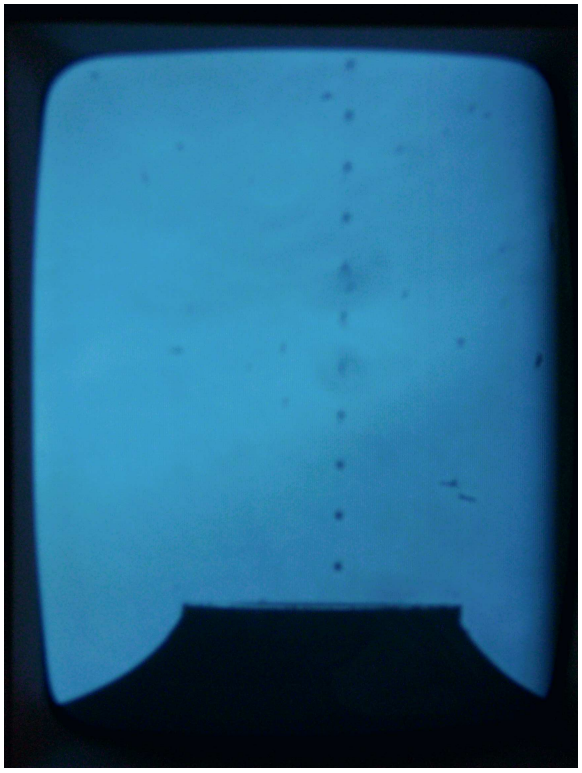

Fig. 14: Stream of droplets from the nozzle of the pellet generator (top, not seen) to the vacuum injection (bottom).

Figure 15 shows a comparison of beam lifetimes with the pellet target switched off and on. The fitted beam lifetimes result in 859 minutes without target and 2.4 minutes with target on. Assuming an integrated target thickness of the residual gas in the COSY ring of $2.5 \cdot 10^{12}\,\mathrm{cm}^{-2}$ hydrogen atoms a target thickness of $8.8 \cdot 10^{14}\,\mathrm{cm}^{-2}$ can be deduced. A later improvement of the COSY tune in flat top increased the beam lifetime without target to 57 hours. An improvement of the target lead to an estimated target thickness of $1.7 \cdot 10^{15}\,\mathrm{cm}^{-2}$.

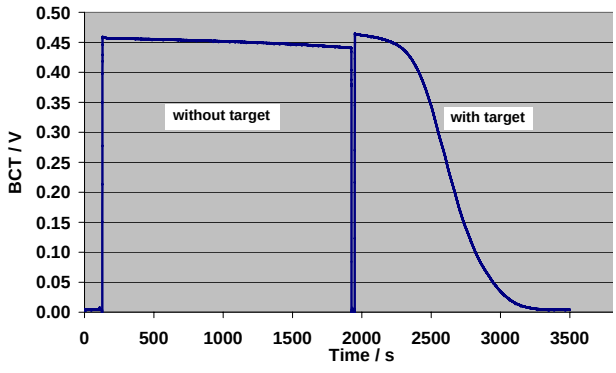

Fig. 15: Beam intensity as function of time without and with pellet target.

An alternative estimate of the target thickness comes from the measurement of the decreasing revolution frequency with the ring RF switched off which is a measure for the energy loss of the beam in the target. This leads to a target thickness of $2.5 \cdot 10^{15}\,\mathrm{cm}^{-2}$, which is in good agreement with the beam-lifetime measurement.

Detector Components

In the central detector setup (Fig. 16) the Hamamatsu 1924 phototubes used in the forward part of the scintillating electromagnetic calorimeter (SEC) have been replaced by an upgraded version 1924A with a significantly improved linearity. During commissioning, all detector channels of both calorimeter and plastic-scintillator barrel were working, and the superconducting solenoid was operated at a magnetic field of 1 Tesla. The magnetic field was shut down twice by the quench detector without any damage and with a fast restart within a few hours. The shutdowns were caused by two general external power failure and voltage peak events. That demonstrates both safety and reliability of the solenoid control system.

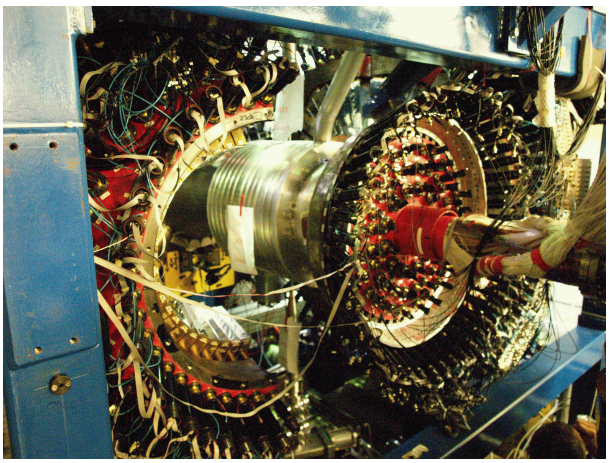

Fig. 16: The WASA central detector during installation before closing the calorimeter half spheres: Outer half sphere (left) and (in beam direction) COSY beam pipe wrapped with MDC cabling, calorimeter end cap with circular arrangement of plastic barrel photomultipliers, and superconducting solenoid (center).

The front-end electronics for the MDC have been completely exchanged by a solution based on the CMP16 amplifier-discriminator chip originally developed for the CERN CMS experiment. Except for few per cent of individual non-working straws, that were not repaired before installation to avoid the risk of collateral damage, the entire MDC was equipped with electronics and read out during commissioning.

To improve the tagging efficiency in the WASA forward detector at high energies, an additional layer of scintillator material has been added to the Forward Range Hodoscope (FRH). For protons with kinetic energies close to 1 GeV the precision of the energy determination based on the d*E*-*E* technique is expected to improve by 25 % as compared to the original setup.

Data Acquisition

A DAQ system compatible with existing systems at other COSY experiments has been designed for WASA at COSY by the FZJ Central Institute for Electronics (ZEL), including the development of new digitization modules: Slow and fast TDCs for straw and scintillation detectors, and — in cooperation with Uppsala University — slow and fast QDCs (Flash ADCs with FPGA integration logic) for the SEC and the plastic scintillators, respectively. After prototyping and mass production, the complete front end electronics were available in time to read out the full detector information.

The readout time of $\approx 80\,\mu$s measured during commissioning happens to correspond to the time needed for one pellet to pass the COSY beam ($80-100\,\mu$s), thus limiting the number of events measured per pellet to one. With the final implementation of the synchronization system scheduled for beginning of 2007, this number is expected to increase to $2-4$ events per pellet.

Commissioning

The first commissioning phase was used to integrate both pellet target and superconducting solenoid into COSY operation, and to debug both front-end electronics and the trigger system. Data were taken during the second phase at kinetic energies of 1.22 GeV/c for calibration, 2.2 GeV/c for η production, and 3.35 GeV/c for η' production. The data taking was also used to study and improve different trigger conditions and diagnostics.

After a rough calibration, the information only from the scintillators in the forward detector, *i.e.* the missing mass with respect to two protons, and the invariant mass of two photons in the SEC were combined. A clear enhancement at the η mass is visible (see spectrum on the cover page of this Annual Report), demonstrating that after dismount at CELSIUS, transfer, and installation at COSY, the WASA facility is operational and ready to start its physics program.

Outlook

During the first half of 2007, a first η production run is scheduled, aiming to collect a data sample of 10^8 η decays, to allow both a high statistics Dalitz-plot analysis of the $\eta \to 3\pi^0$ decay, and a background investigation for the very rare decay $\eta \to e^+e^-$.

1.3.2 Towards Double-Polarization Measurements at ANKE

A key feature of the experiments planned at ANKE is the use of polarised beams and targets which allow one to perform double-polarisation measurements. The focus is on the study of three-body final states with the aim of extracting basic spin-dependent two-body scattering information close to threshold. Since the necessary equipment has been installed, it is time to advance experiments using a polarised target cell in conjuction with a polarised beam.

As an example, it is important to measure the charge-exchange (CE) break-up of polarised deuterons on a polarised hydrogen target. At low excitation energies E_{pp} of the final pp system, the observables in $\vec{d}\,\vec{p} \to (pp)n$ can be directly related to the np spin-dependent amplitudes β, γ, δ and ε. Impulse approximation applied to $dp \to (pp)_{^1S_0}n$ leads to the following predictions for the differential cross section, deuteron analysing powers, and spin-spin correlation parameters:

$$\begin{aligned}
\frac{d^4\sigma}{dtd^3k} &= \tfrac{1}{3} I \left\{ S^-(k, \tfrac{1}{2}q) \right\}^2 , \\
IA_y^d &= 0 \,, \; IA_y^p = -2\Im(\beta^*\gamma) \,, \\
IA_{xx} &= |\beta|^2 + |\gamma|^2 + |\varepsilon|^2 - 2|\delta|^2 R^2 \,, \\
IA_{yy} &= |\delta|^2 R^2 + |\varepsilon|^2 - 2|\beta|^2 - 2|\gamma|^2 \,, \\
IC_{y,y} &= -2\Re(\varepsilon^*\delta)R, \; IC_{x,x} = -2\Re(\varepsilon^*\beta).
\end{aligned}$$

Within this approximation, a measurement of the differential cross section, A_{xx}, and A_{yy} allows the extraction of $|\beta|^2 + |\gamma|^2$, $|\delta|^2$, and $|\varepsilon|^2$ over a range of values of q (three-momentum transfer) near the forward direction. As seen from Fig. 17, we have shown that this can be successfully done at 1170 MeV for $q \leq 130$ MeV/c.

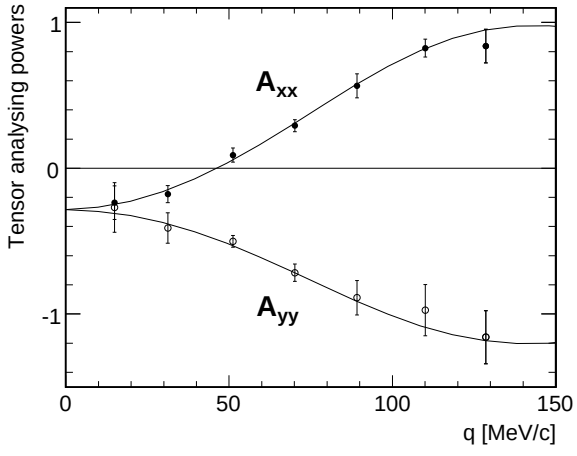

Fig. 17: Cartesian tensor analysing powers A_{yy} (open symbols) and A_{xx} (closed) of the $\vec{d}p \to (pp)n$ reaction for $E_{pp} < 3$ MeV at T_d=1170 MeV compared to the impulse approximation predictions.

The values of A_y^d are consistent with zero for all momentum transfers and this provides further support for the impulse-approximation interpretation. A measurement of the deuteron-proton spin correlation will allow us to determine the relative phases of these amplitudes and not just their overall magnitudes. Numerical predictions have been made for the transverse spin-correlation coefficients and the results are shown in Fig 18.

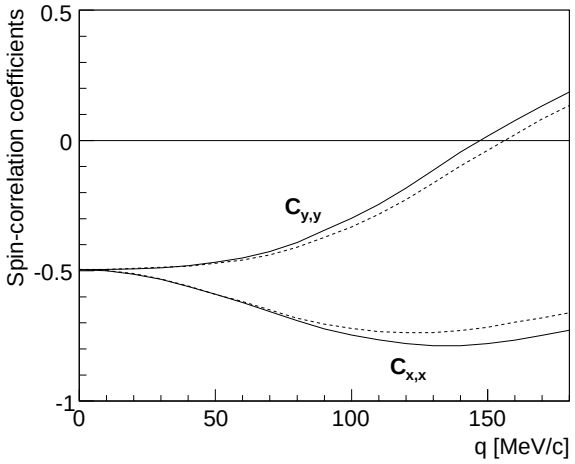

Fig. 18: Predicted values of the spin-correlation coefficients in the CE reaction at 585 MeV/nucleon for cuts in excitation energy of $E_{pp} < 1$ MeV (solid line) and $E_{pp} < 3$ MeV (dashed line).

The predicted $C_{x,x}$ and $C_{y,y}$ are both expected to be very large and show considerable structures over the ANKE measurement range. We are quite fortunate to have found such a large (predicted) signal with such an interesting behaviour. Measurements of this observables are the primary aim of the experiment planned at COSY for the begining of 2007.

In order to calibrate the polarisations of both the beam and target, it is necessary to measure in parallel reactions where the analysing powers are known. The ones chosen for this purpose are elastic dp scattering and quasi-free $np \to d\pi^0$, with a fast spectator proton. These reactions have high counting rates and characteristic kinematics, with two charged particles that can be detected at ANKE. The experiment is crucial in: (i) teaching us how to handle simultaneously the polarised beam and polarised target (cell-type), and (ii) establishing polarisation standards for double-polarised nuclear reactions at COSY energies.

- After its first installation in the summer of 2005, commissioning studies were carried out. These included storage cell tests to determine the dimensions of the COSY beam. The cell, which was made from pure aluminium foil, had a length of 400 mm, and a cross section of $20 \times 20\,\text{mm}^2$.
- In November 2005, tests with such a storage cell were undertaken using polarised hydrogen atoms from the polarised atomic beam source (ABS). The COSY beam consisted of electron-cooled unpolarised protons, stacked at injection, and accel-

erated to $T_p = 600\,\mathrm{MeV}$. It was possible to store 1.5×10^{10} protons in the flat top.

- In March 2006, a first asymmetry measurement was carried out with a COSY beam of unpolarised 831 MeV protons and a polarised hydrogen target. The $p\vec{p} \to d\pi^+$ reaction has been used to measure the polarisation of the $\vec{\mathrm{H}}$ jet. Assuming that both polarisation P_+ and P_- were equal, an average target polarisation of $P = 0.44 \pm 0.03$ was measured. This value has been increased up to $P = 0.75 \pm 0.11$ in a later commissioning beam time.

- The target thickness with a hydrogen beam from the ABS injected into the cell in HF state **1** ($\mathrm{m_I} = \mathrm{m_J} = +\frac{1}{2}$) was estimated to be about 1.2×10^{13} H atoms/cm^2.

- The analysis of the $pp \to pp\pi^\circ$ and $pp \to pn\pi^+$ reactions showed that events from the extended target can be cleanly identified in the ANKE forward detector system when there are two charged particles in the final state. The missing-mass distribution of the $pp \to pp\pi^0$ reactions is shown in Fig. 19. Data with the hydrogen target ($\mathrm{H_2}$) show prominent peaks corresponding to the production of a π^0. The background is very similar to that measured with the nitrogen target ($\mathrm{N_2}$) and the natural assumption is that for hydrogen this comes from the cell walls.

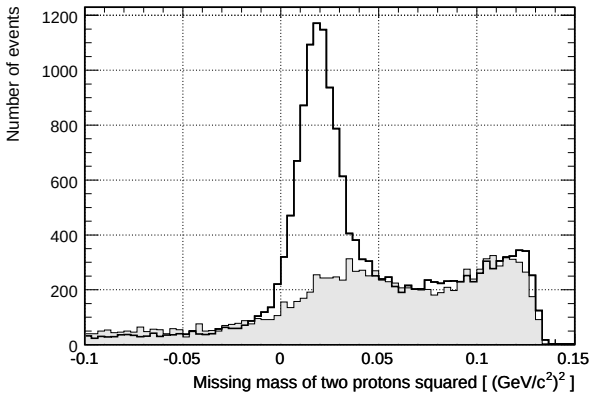

Fig. 19: Missing-mass distribution for the reactions $pp \to ppX$ measured with the storage cell and the 831 MeV proton beam. The open histograms represent the results obtained with the hydrogen gas while the shaded areas show the "background" contributions measured with nitrogen in the cell.

After this first experiment is done, we can embark on other reactions described in ANKE spin programme.

2 External Experiments

2.1 ATRAP Experiment at CERN — Physics with Cold Antihydrogen

The ATRAP experiment at the CERN antiproton decelerator AD aims for a test of the CPT invariance by a comparison of hydrogen (H^0) to antihydrogen ($\bar{H}^0$) atom spectroscopy and a measurement of the gravitational force on antimatter atoms.
The $\bar{H}^0$ production was routinely operated at ATRAP in a nested Penning trap configuration before the planned interruption of antiproton production at AD/CERN from November 2004 up to August 2006. The ATRAP collaboration used this time for preparing the next generation of experiments. Thus ATRAP-II now allows for much larger flexibility, increased performance, higher robustness, and better efficiency. All production stages for the physics with $\bar{H}^0$ were installed during 2006, tested, and optimized resulting in a complete new setup of the ATRAP apparatus and feasibility tests for the production and storage of cold antihydrogen atoms.

Fig. 20: Photograph and model of the inner part of the ATRAP-II experiment, as described in the text.

ATRAP-II uses a new super-conducting magnet with a central bore as large as 0.5 m in diameter giving ample space for installations needed. The insert for this bore is shown in Figure 20 with from top to bottom: The head with all the connectors for the individual parts, the heat shield, the liquid He-dewar, the adjustment table, the Ioffe-trap, and the $\bar{p}$ trapping electrodes which have a factor of three larger diameter as those used before in ATRAP-I.
Another essential part is a new setup for the positron (e^+) loading into the ATRAP-II installation using an external trap which can be continuously filled with clouds of positrons and then transported on request via a long transfer-line. Thus the efficiency of ATRAP-II is increased drastically since the loading of $\bar{p}$'s and e^+'s can be performed in parallel and not consecutively as done so far.
The IKP contributed successfully with the construction of a new ten layer scintillating fiber hodoscope divided into three rings with straight and bended fibers, where one of these units is presented in Figure 21 still at the workshop of the IKP before its installation into the ATRAP-II setup. The performance will be presented in a separate contribution.

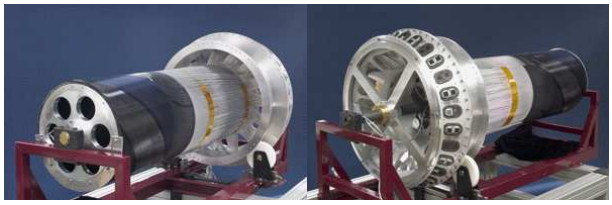

Fig. 21: Both sides of one part of the detection system.

The trapping of neutral $\bar{H}^0$ atoms uses the force on the magnetic moment in a magnetic field gradient. Such a magnetic quadrupole field trap with two pinch coils was built with substantial support from the ZAT of the Research Center Jülich (where parts of the assembly and much help was provided by the company ACCEL) and installed into the experiment. A blow up, its composite, and the encapsulated device is pictured in Figure 22.

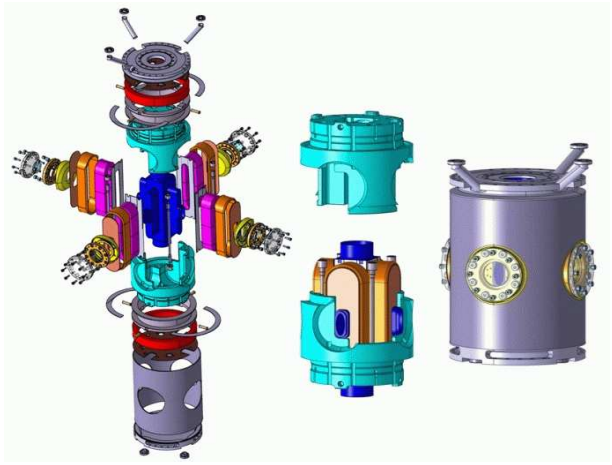

Fig. 22: Ioffe-Trap: a blow up, its composite, and the encapsulated device.

Using this trap it has been demonstrated with clouds of up to about 500000 $\bar{p}$'s that substantial numbers of $\bar{p}$'s sur-

vive the radial magnetic field of a quadrupole magnetic trap — enough to produce $\bar{H}^0$ atoms within this field using the charge-exchange method, developed by ATRAP in 2003. Whether trapping of $\bar{H}^0$ produced in a nested Penning trap works as well during positron cooling of antiprotons remains to be seen in further studies. When moving the $\bar{p}$ cloud adiabatically along the axis for several centimeters some losses are observed but a large fraction remains trapped, a promissing first result.
Also substantial numbers of $\bar{e}^+$ can be stored in the appropriate location within the magnetic gradient field as based upon successful tests with electrons. Thus, ATRAP demonstrated that — in spite of earlier claims to the contrary in the literature — quadrupole magnetic fields seem to have a role to play for $\bar{H}^0$ production experiments.
Summarizing, the ATRAP-II apparatus has successfully been installed at the AD and all single components work as well as specified including the construction of a magnetic quadrupole trap for exciting physics experiments with $\bar{H}^0$ to come during the next years.

2.2 Pionic Atoms at PSI

The pionic hydrogen experiment has been completed by a high statistics study of pionic deuterium (πD). The hadronic shift ε_{1s} of the ground state represents the coherent scattering at threshold of pions at a proton and a neutron given in leading order by the isoscalar scattering length a^+. Significant second order corrections from multiple scattering, structure effects also depend on the isovector scattering length a^-. Consequently, ε_{1s} provides a powerful constraint for a^+ and a^- as determined from pionic hydrogen. The hadronic width in πD is related to s-wave pion production by charge symmetry and detailed balance allowing for an independent precision determination of the threshold parameter of the reaction $pp \to d\pi^+$.
In order to identify or exclude atomic effects on the hadronic parameters, the transition $\pi D(3p-1s)$ was measured at three different densities corresponding to 3.5, 10, and 20 bar D_2 pressure (Fig. 23). The pure hadronic effects are then found by extrapolating to density zero in case. The analysis is in progress.

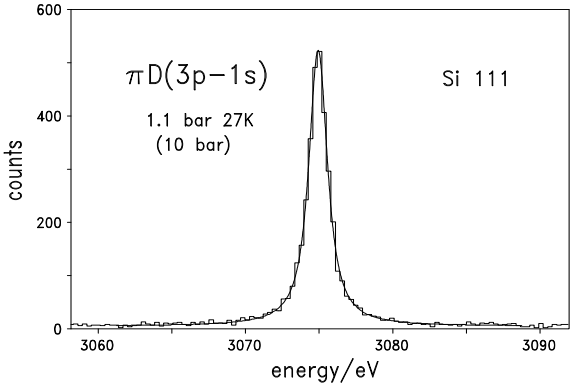

Fig. 23: $\pi D(3p-1s)$ X-ray transition measured with a high resolution Bragg crystal spectrometer using the Si 111 reflection.

2.3 Search for Nuclear Dichroism at the Cologne Tandem

Theoretical work on the coherent process of nuclear dichroism, an effect analogous to optical dichroism, predict longitudinal tensor polarization $p_{z'z'}$ in an initially unpolarized beam of spin-1 particles after passage through targets consisting of unpolarized spin-0 nuclei. To study this prediction, in collaboration with scientists from Minsk, Belarus, an experiment has been performed at the Insitute for Nuclear Physics of the University of Cologne using the HVEC tandem Van-de-Graaff accelerator with unpolarized deuterons of energies up to 20 MeV and amorphous carbon targets of different areal thicknesses. The polarization of the trans-mitted deuterons has been measured with a ^{3}He polarimeter, based on the $d + {}^3\mathrm{He} \to {}^4\mathrm{He} + p$ reaction, by detection of the emitted protons in four detectors positioned at polar angles of 24.5° around the deuteron-beam axis and a forward detector.

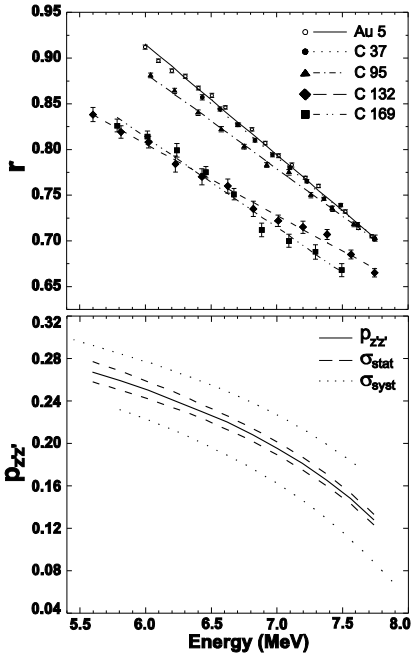

Fig. 24: Ratio of the protons detected in all four side detectors to those in the forward detector for the C targets and a calibration Au target of areal thicknesses given in mg/cm^2 as function of the energy of the transmitted deuterons (upper part). The lower part shows the measured longitudinal tensor polarization for the 169 mg/cm^2 target, where the dotted band gives the error caused by the uncertainty of the target thickness at the beam spot.

The deduced $p_{z'z'}$ exceeds that, predicted for the coherent dichroism mechanism, by about two orders of magnitude, which might be explained by incoherent multiple forward scattering. The final data evaluation and interpretation is in progress.

3 Theoretical Investigations

The IKP theory group studies the strong interactions in their various settings — spanning topics in hadron structure and dynamics, the nuclear many-body problem and high-energy Quantum Chromodynamics (QCD). The main focus is on the formulation and application of effective field theories for precision hadron and nuclear physics based on the symmetries of QCD. Some of the highlights of these activities are discussed below.

3.1 Dispersive Corrections to the Pion-Deuteron Scattering Length

The pion-deuteron scattering length $a_{\pi d}$ is a quantity of high interest, since it appears to be the natural source for the extraction of the isoscalar pion-nucleon scattering length. To make this extraction possible a calculation of the few-body corrections is necessary to very high accuracy. This is possible only within a well defined effective field theory — namely chiral perturbation theory (CHPT).

Recently $a_{\pi d}$ was measured to be $a_{\pi d}^{\rm exp} = (-26.1 \pm 0.5 + i(6.3 \pm 0.7)) \times 10^{-3} \; m_\pi^{-1}$, where m_π denotes the mass of the charged pion. In the near future a new measurement with a projected total uncertainty of 0.5% for the real part and 4% for the imaginary part of the scattering length will be performed at PSI. The imaginary part for the πd scattering length can be expressed by unitarity in terms of the πd total cross section through the optical theorem: $4\pi {\rm Im}(a_{\pi d}) = \lim_{q\to 0} q\,\{\sigma(\pi d \to NN) + \sigma(\pi d \to \gamma NN)\}$, where q denotes the relative momentum of the πd pair. The ratio $R = \lim_{q\to 0}(\sigma(\pi d \to NN)/\sigma(\pi d \to \gamma NN))$ was measured to be 2.83 ± 0.04. At low energies diagrams that lead to a sizable imaginary part of some amplitude are expected to also contribute significantly to its real part. Those contributions are called dispersive corrections. As a first estimate Brückner speculated that the real and imaginary part of these contributions should be of the same order of magnitude. This expectation was confirmed within Faddeev calculations. Given the high accuracy of the measurement and the size of the imaginary part of the scattering length, another critical look at this result is called for. Here we report on the first calculation for these terms within CHPT.

This work became possible by recent progress in our theoretical understanding of the reaction $NN \to NN\pi$. Based on a new power counting that traces explicitly the large initial momentum, it was possible to show that field theoretically consistent amplitudes emerge as the result of various cancellations amongst different loop diagrams. This lead to a new structure for the transition operator and to a good description of the experimental data. The same amplitudes were then used to calculate both the absorptive as well as the dispersive corrections to the πd scattering length. The diagrams included are sketched in Fig. 25. Especially the crossed diagrams (c and d) were not considered consistently before. Many works also did not consider intermediate nucleon-nucleon (NN) interactions. Using the CD-Bonn potential for the NN distortions we found for the dispersive correction from the purely hadronic transition (in units of $10^{-3}\, m_\pi^{-1}$)

$$a_{\pi d}^{\rm disp} = (-6.3 + 2 + 3.1 - 0.4) = -1.6,$$

where the numbers in the first bracket are the individual results for the diagrams shown in Fig. 25, in order. At the same time the corresponding imaginary parts agree well with the empirical values.

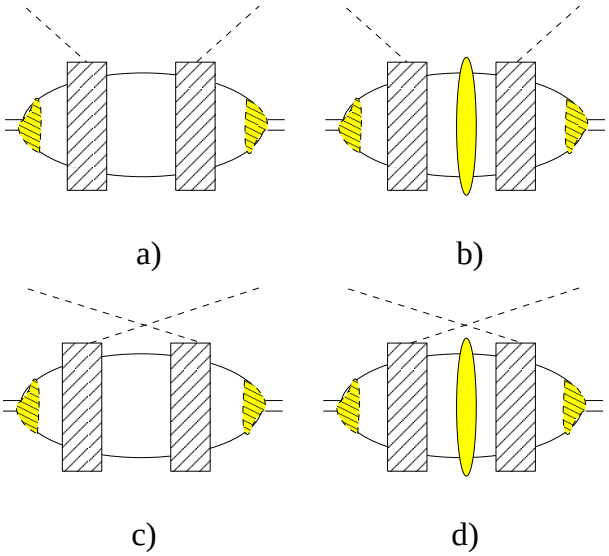

Fig. 25: Dispersive corrections to the πd scattering length. Solid (dashed) lines denote propagating nucleons (pions). The outermost filled hatched areas denote the deuteron wave functions, the hatched squares the $NN \to \pi NN$ transition operators, and the filled ellipses intermediate NN interactions.

We also studied the dispersive corrections that come from the γNN intermediate state. For this contribution the real part was even smaller whereas the imaginary part was sizable and consistent with the data. These novel results are different from what was found before based on less systematic approaches.

3.2 The Four-nucleon Force in Chiral Effective Field Theory

Recent advances in the development of few-body methods coupled with a significant increase in computational resources allow one, nowadays, to perform accurate microscopic calculations of three- and even four-nucleon scattering observables and of the spectra of light nuclei. This opens the door for precise and nontrivial tests of the underlying dynamics. Modern two-nucleon forces were demonstrated to be able to describe the bulk of few-nucleon observables at low and moderate energies. Three-nucleon forces have deserved much attention as

well and were shown to be important *e.g.* for our understanding of the spectra of light nuclei. In contrast, four-nucleon forces (4NFs) have not yet been explored in few-body calculations. Although the 4NFs are expected to be less important than the two- and three-nucleon ones, this needs to be verified via explicit calculations. We made an important step in this direction and derived the leading 4NF in the framework of chiral effective field theory which appears at next-to-next-to-next-to-leading order (N^3LO) in the chiral expansion. It is governed by the exchange of pions and the lowest-order nucleon-nucleon contact interaction and includes effects due to the nonlinear pion-nucleon couplings and the pion self-interactions constrained by the chiral symmetry of QCD. The resulting 4NF is local and does not contain any unknown parameters. Its application in future few-body studies will, therefore, provide a challenging test of our understanding of the nature of the nuclear forces.

We made first estimates of 4NF effects by calculating the expectation values of the 4NF using different ^{4}He wave functions. To simplify the calculations, we assumed that the momentum part of the ^{4}He wave function is totally symmetric with respect to any permutations of the nucleons and can be written as a function of one variable, namely the c.m. kinetic energy of the 4N system. The eighteen fold integrals over the nucleon momenta were carried out using the Monte Carlo method. The 4NF is found to yield an attractive contribution to the ^{4}He binding energy of the order of few hundred keV. This is qualitatively in line with modern predictions for the α-particle which leave little room for the contribution of the possible 4NFs. Clearly, to ultimately clarify the role of the 4NF one needs to perform a complete analysis of few-nucleon systems at N^3LO. This work is in progress.

3.3 Nuclear Lattice Simulations

Lattice QCD is a tool to calculate nuclear properties from first principles. Due to the enormous computational demand, so far only two-nucleon systems have been considered. However, it is possible to explore systematically the influence of the QCD symmetries on the structure of nuclei. To achieve this goal, we have started systematic investigations of nuclei in the framework of nuclear lattice simulations. Here, the fundamental degrees of freedom are nucleons and their interactions are given by chiral effective field theory. The nuclear lattice approach addresses the few- and the many-body problem in nuclear physics by applying non-perturbative lattice methods to low-energy nucleons and pions. The nucleons are located on the lattice sites whereas pions and external fields live on the links. Furthermore, π times the inverse lattice spacing sets the UV cutoff in momentum space. By using hadronic degrees of freedom and concentrating on low-energy physics, it is possible to probe larger volumes, lower temperatures and far larger numbers of nucleons than in lattice QCD. To study light nuclei at leading order, using lattice pions and auxiliary fields, we include the physics of instantaneous one-pion exchange and S-wave contact interactions. To avoid a clustering (zero range) instability, we include higher derivative contact interactions by applying Gaussian smearing to the S-wave contact interactions. This is the minimal modification to overcome the clustering instability — in the future, we will instead include higher-derivative interactions consistent with the power counting of chiral nuclear effective field theory. By construction the lattice path integral is positive in the limit of exact Wigner SU(4) symmetry for any even number of nucleons. This SU(4) positivity and the approximate SU(4) symmetry of the low-energy interactions play an important role in suppressing sign and phase oscillations in the Monte Carlo simulations. At this order, we have three parameters in the effective potential which we fix from the deuteron binding energy, the $^1S_0$ scattering length and the average effective S-wave range. Our lattice results agree within 5% for all deuteron properties with the experimental values. We have also shown that the transfer matrix method employed leads to completely negligible stochastic errors. The triton (or ^{3}He, since we work in the isospin limit) binding energy comes out as 8.9(2) MeV and the triton root-mean-square radius is within 30% of the data. The observed overbinding might be an artefact of the still small lattice volume of $(9.85\ \mathrm{fm})^3$ — we are presently investigating systematically finite volume effects. For ^{4}He, the binding energy is within 25% while the root-mean-square radius is within 10%. We have also investigated nucleon density correlation functions for the deuteron, the triton and ^{4}He, as shown in Fig. 26. The description of these light nuclei will improve when higher derivative operators are treated systematically by matching phase shifts on the lattice at higher momentum. We have also investigated the computational scaling of our lattice method, this shows that simulations for light nuclei with up to eight nucleons can be done without much difficulty.

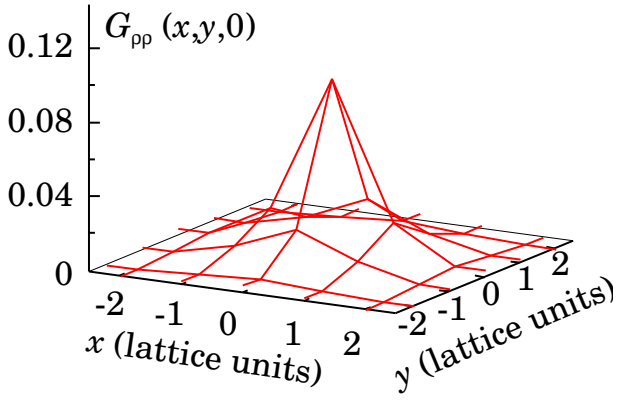

Fig. 26: The nucleon density correlation $G_{\rho\rho}(\vec{n}_s)$ for ^{4}He in the xy-plane.

3.4 Hyperon-nucleon Forces

Hyper-nuclear physics allows one to study the effects of strange quarks within the nucleus. A systematic and controlled analysis of the characteristics of these hypernuclei can be performed in a three-flavor chiral effective field theory based on hadronic degrees of freedom. As a first step in this direction, we have constructed the leading order chiral effective potential in Weinbergs approach to nuclear physics. At this order, the potential consists of pseudoscalar meson (Goldstone boson) exchanges and four-baryon contact interactions. Very different from the two-nucleon interactions, such a leading order calculation is expected to work to some accuracy for three reasons: The hyperon-nucleon (YN) system does not exhibit unnaturally large scattering lengths, the known empirical information is much poorer and also, the extension to SU(3) leads to 5 independent contact S-wave interactions in contrast to two for NN. At this order, the Goldstone boson exchanges are given in terms of two known parameters, the pion-nucleon coupling and the SU(3) ratio $F/(D+F) = 0.4$. We also have included the Coulomb potential utilizing a modified Vincent-Phatak approach consistent with the EFT power counting. The effective potential needs regularization for large momenta. Employing an exponential regulator in the Lippman-Schwinger equation, we can fit the 35 low-energy data (total cross sections and the capture ratio at rest) with a total χ^2 between 28 and 35 when varying the cutoff between 550 and 700 MeV, see the green band in Fig. 27.

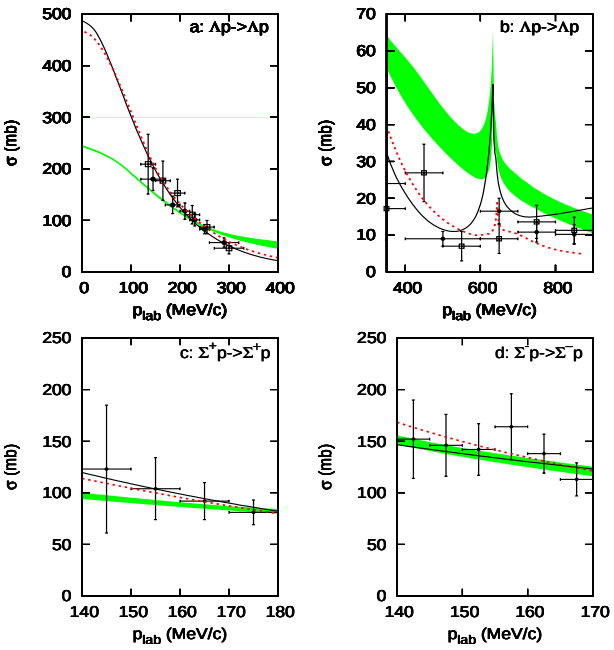

Fig. 27: Total cross sections for $\Lambda p \to \Lambda p$ and $\Sigma^{\pm} p \to \Sigma^{\pm} p$ with proper account of the Coulomb interaction. The shaded band is the chiral EFT result, the dashed (solid) curve represents the Jülich 04 (Nijmegen NSC97f) model.

The description of the data is as good as for the existing meson-exchange models (that have more parameters and are less systematic), see the solid and dashed lines in Fig. 27. With a singlet Λp scattering length of -1.9 fm (as imposed in our fits), the hyper-triton is bound and the binding energy comes out within 0.5% of the empirical value. The corresponding triplet Λp scattering length is -1.23 fm. These scattering lengths are smaller than in standard meson-exchange models. Preliminary results for the four-body hyper-nuclei ${}^{4}_{\Lambda}$H and ${}^{4}_{\Lambda}$He show that the chiral EFT predicts reasonable Λ separation energies. These investigation show that an extension of the successful EFT description of the NN system can be extended to the YN interaction. In the future, we will performed a simultaneous fit to NN and YN data starting at NLO and also investigate the hyperon-hyperon interaction which is of relevance for the nuclear equation of state at large densities.

3.5 Electromagnetic Excitation Spectra of Short-lived Neutron-rich Nuclei

The excitation spectra of neutron-rich isotopes are needed for the astrophysical r-process. Since experimental information about isotopes with a short life time still is missing, theoretical approaches have to rely on extrapolations of information obtained in stable nuclei. The nuclear mean field, for instance, can be derived from phenomenological interactions which reproduce the bulk properties of known nuclei quite well. There are some open problems, however. Relativistic mean field theories systematically overestimate the excitation energies of the energetically low lying electric dipole strength by about 3 MeV, as discussed in a recent review by Ring and coworkers. We show that this shortcoming of mean field theories can be cured, if one incorporates the phonon degree of freedom into the theoretical approach. Phonons define the smallest energy scale available for nuclear excitations and therefore should be treated together with the single particle degrees of freedom. The phonons fragment the mean field single particle spectrum and generate quite naturally non-trivial low lying electric dipole modes. We have generalized the so called extended theory of Finite Fermi Systems to a self-consistent approach and have performed calculations with phenomenological interactions of the Skyrme type. A prediction for the electric dipole strength of the exotic isotope ^{166}Sn (recall that the chain of known even-even Sn isotopes ends with ^{136}Sn which has a life-time of 0.25 s) is shown in Fig. 28. The maximal dipole strength is found close to the energy $E = 80A^{-1/3} = 14.6$ MeV expected from the empirical systematics of the giant dipole resonances in stable nuclei. In comparison with the known isotope ^{132}Sn one observes a stronger fragmentation of the dipole strength, however, and a relatively large concentration of strength near 4 MeV. The predictive power of phenomenological interactions of the Skyrme type or of the relativistic mean field type is limited mainly to excitations of natu-

ral parity. For unnatural parity modes which are relevant for neutrino-induced reactions, one has to incorporate the pion. Therefore the next logical step is to apply the nucleonic interactions derived from effective field theory in the present investigations.

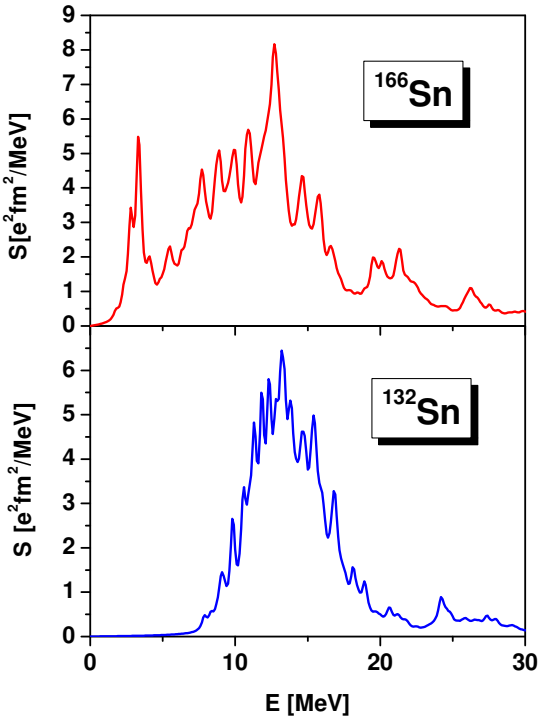

Fig. 28: Predictions for the electromagnetic dipole strength of ^{166}Sn and ^{132}Sn.

3.6 ϕ-meson Production off Nuclei

The renormalization of the meson spectral function in nuclear matter has attracted substantial interest in connection with the measurements of the di-lepton invariant mass spectra from heavy ion collisions. Recently experimental results on ω and ϕ meson modification at normal nuclear densities have been reported in experiments involving photon and proton beams. The most remarkable result obtained in all these experiments is the anomalous A-dependence of the ϕ-meson production from nuclear targets. At the same time the A-dependence of the ω-meson production both in γA and pA interactions is well understood. We have analyzed coherent and incoherent ϕ-meson photoproduction from nuclei by applying a single and coupled channel optical model. The data on coherent ϕ photoproduction collected at Cornell at photon energies of 6.4 and 8.3 GeV can be well reproduced by a single channel calculation taking into account the ϕ-meson distortion compatible with the ϕN total cross section $\sigma_{\phi N} = 10$ mb. This result is in good agreement with the Vector Meson Dominance analysis of the forward $\gamma p \to \phi p$ differential cross section, which indicates that $\sigma_{\phi N} \simeq 11$ mb. Coherent ϕ-meson photoproduction shows litte coupled channel effects due to the contribution from the $\omega \to \phi$ transition. The data on incoherent ϕ-meson photoproduction off various nuclei collected at SPRING-8 at photon energies from 1.5 to 2.4 GeV can be reproduced by the single channel optical model calculations only under the assumption that the ϕ-meson is substantially distorted in nuclei, which corresponds to $23 \leq \sigma_{\phi N} \leq 63$ mb. This result is in agreement with previous incoherent ϕ-meson photoproduction data analyses. Moreover, we found that taking into account the coupled channel effects, *i.e.* assuming direct ω-meson photoproduction followed by the $\omega N \to \phi N$ transition as well as pion photoproduction followed by the $\pi N \to \phi N$ scattering, it is possible to reproduce the A-dependence measured at SPRING-8, see Fig. 29. To draw firmer conclusions, the t-dependence of incoherent photoproduction should be measured for all nuclei under consideration because in the coupled channel analysis, each of the two-step processes leads to a different t-dependence.

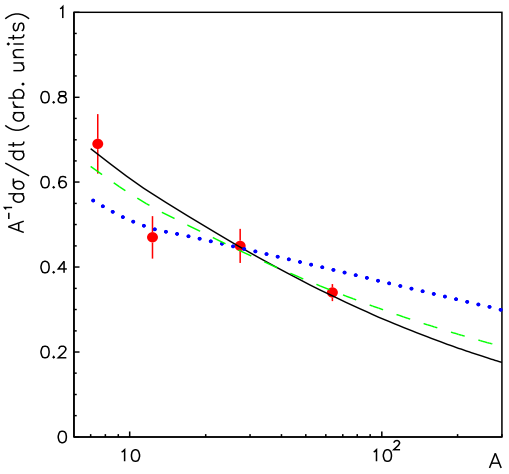

Fig. 29: Incoherent ϕ-meson photoproduction cross section as a function of the mass number. The circles show the data from SPRING-8. The solid line is the coupled channel scattering calculations with a total ϕN cross section of 11 mb and the ωN cross section of 23 mb, while the dashed line is obtained with $\sigma_{\phi N}$=11 mb and $\sigma_{\omega N}$=30 mb. The dotted line is the single channel result for $\sigma_{\phi N}$=11 mb. Both experimental results and calculations are divided by A. The normalization of the calculations is fixed for the Al target.

3.7 Unitarity Cutting Rules in Perturbative QCD

We have formulated the first consistent unitarity cut interpretation of multi-Pomeron exchanges, alias the topological cross sections, in hard perturbative (pQCD) processes off nuclear targets. At the partonic level, a typical final state in small-x deep inelastic scattering (DIS) off nuclei and hard proton-nucleus collisions can be characterized by the multiplicity of color-excited nucleons. Within the

Reggeon field theory (RFT), each color-excited nucleon is associated with the unitarity cut of the Pomeron exchanged between the projectile and the nucleus.

Our solution is based on the separation of color-diagonal and color-excitation transitions in the multiparton S-matrices which describe the non-Abelian intranuclear evolution of color dipoles. The obtained topological cross sections admit an RFT interpretation in terms of the uncut, and two kinds of the unitarity-cut Pomerons, which describe transitions between color dipoles in $SU(N_c)$ representations with dimensions differing by the factor N_c^2 and color-rotations within higher representations, respectively. This distinction between the two kinds of cut Pomerons has been missed in all the earlier discussions of the cutting rules and is the major novelty of this work.

Upon the proper identification of the uncut and cut Pomeron exchanges the topological cross sections for di-jet production follow in a straightforward way from the earlier derived nonlinear $k_\perp$ factorization quadratures for the inclusive di-jet cross sections. The concept of a coherent (collective) nuclear glue proves extremely useful for the formulation of the whole multitude of the RFT vertices of multi-Pomeron — cut and uncut — couplings to particles and between themselves. A departure of our unitarity cutting rules from the ones suggested by the pre-QCD Abramovsky-Kancheli-Gribov (AKG) rules stems from the coupled-channel features of non-Abelian intranuclear pQCD. We demonstrate this breaking of the AGK rules by explicit derivation of the leading unitarity correction to the total, coherent diffractive, single cut Pomeron and two cut Pomeron cross sections.

The second novelty of our pQCD cutting rules is a Cheshire Cat smile — the non-cancellation of spectator parton interactions in the topological single-jet cross sections which must be contrasted to an exact cancellation of spectator effects in the fully inclusive single-jet cross section. We propose a multiplicity re-summation as a tool for the elimination of spectator effects in topological cross sections for single-jet production. Possible applications of our cutting rules to a description of long range correlations in DIS and proton-nucleus collisions at RHIC were outlined.

3.8 Projectile Electron Losses in the Collision with Neutral Targets

At the forthcoming FAIR facility at GSI/Darmstadt one will accelerate U^{28+} ions. An important problem in this connection is the projectile electron loss in the collision of these U^{28+} ions with the rest gas atoms (molecules). This electron loss process can lead to degraded focusing and loss of the beam to the walls. These charge-changed fast ions strike the accelerator container walls and give rise to sputtering and activation of the surface. Evidently, it is important to study the interaction of highly charged heavy ions with neutral (rest gas) targets, for practical as well as theoretical reasons. It is a theoretical challenge to treat the many-electron (relativistic) scattering problem in a realistic nonperturbative way. In the spirit of Glauber theory we present a nonperturbative approach for the treatment of single and multiple electron losses of highly charged ions colliding with neutral atom targets. The key quantity is the impact dependent probability $P(b)$. It is calculated in the eikonal approximation. We can now write the probability W^{N_e} for the loss of $N_e = N_p - N$ electrons, where N_p is the number of electrons of the highly charged ion ($N_p = 64$, in the case of our application to U^{28+}) as $W^{N_e}(b) = (N_p!)/(N!N_e!)P(b)^{N_e}(1-P(b))^N$. The corresponding cross section is obtained by an integration over the impact parameter d^2b. In Fig. 30 we show the dependence of the multiple electron loss cross section on the number $N_e = N_p - N$ of electrons lost. In our approach we use a parametrization for a suitably averaged excitation probability $P(b)$ where two parameters were fixed. This was done by fitting to the experimentally observed cross section for $N_e = 14, 15$. The agreement is quite good, in view of the approximations made.

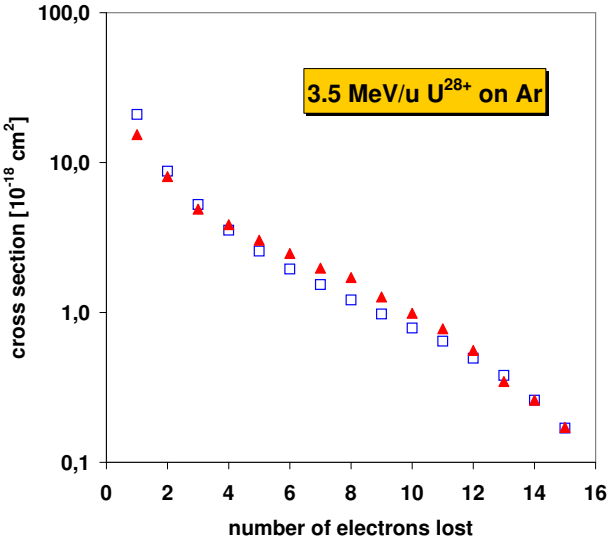

Fig. 30: Dependence of the multiple electron loss cross section on the number of loss electrons. Triangles are the experimental data, squares are the result of our calculation.

We conclude that the main physics is described quite well in our approach. A detailed code, called LOSS, is available which describes ion-atom loss processes using realistic electron wave functions for many-electron ions like U^{28+}. In our future collaboration it is planned to extend the LOSS code so that impact parameter dependent probabilities can be calculated in non-relativistic as well as relativistic collisions. This will provide a solid theoretical basis to assess the questions concerning the acceleration of U^{28+}.

4 COSY: Operation and Developments

4.1 Overview

In the past, nearly uninterrupted operation throughout the year had always been a top priority for COSY. But after a major refocusing two top priorities have emerged for the institute and the accelerator crew. Foremost is the engagement to make FAIR success; second is the integration and commissioning of the WASA-Detector inside the accelerator ring. This new detector opens a new promising window for the future physics program but also requires substantial resources.

In connection with the WASA project there was a limited shutdown of the accelerator for 14 weeks. The increased down-time was needed to install WASA in the COSY ring. After installation a successful commissioning of WASA in the COSY accelerator could be achieved. First experiments with the new detector were carried out.

In the scheduled beam time the accelerator maintained a reliability of over 90% that has been its outstanding hallmark since years. In spite of committing resources to FAIR and WASA the accelerator crew had been successful in reaching new records in polarized and unpolarized proton and deuteron beams. Most notably by advancing the capabilities for spin manipulation inside the ring, performing electron cooling at higher energies, and creating ultra slow energy ramps for threshold experiments. It also contributed its expertise in the context of EU-projects and assisted the research of outside users for instance by performing irradiations at the cyclotron.

Besides the physics program a serious of important beam experiments were carried out. To gain confidence in the results of extensive theoretical investigations for the HESR longitudinal stochastic cooling performance the model was tested with the system parameters at COSY against cooling experiments. A remarkable agreement between model predictions and experiment was achieved. The idea of utilization of an ion beam crystalline state for nuclear physics experiments has a large interest now. The achievement of very low ion temperature in the beam rest frame gives new possibilities in the accelerator physics. Two COSY runs dedicated to electron cooling development were performed at COSY in the year 2006. Experiments on proton beam ordering ("crystallization") that have been started in August 2005 were continued this year.

Further details for the High Energy Storage Ring (HESR) have been worked out. The efforts aimed to advance the design of proposed systems and to increase the knowledge base through beam dynamic simulations and investigations. COSY was used, for instance, as a test bed for the development of a new nondestructive diagnostics that may prove valuable for the FAIR project. The physics of electron cooling has been further explored theoretically as well as through experiments conducted at COSY. The models used to predict cooling times for electron cooling are being perfected to raise their accuracy. Stochastic cooling simulations were continued with new signal paths that provide a reduced undesired mixing between pickup and kicker. The requirements to the stochastic cooling system of the HESR can be met with a bandwidth of 2–4 GHz. For that system two different coupler designs are being evaluated together with appropriate combiner boards. A new ring-slot coupler and a printed loop coupler together with suitable combiner boards are being developed and will be tested at COSY (see contributions on CD-ROM). Competing super conducting magnet designs are still under scrutiny with respect to their technical feasibility and their impact in ring performance. All this is done in close cooperation with the GSI, collaborating partners, and industry to ensure their practical realization.

Extensive studies for a 2 MeV electron cooler at COSY for beam cooling up to the maximum momentum of COSY have been worked out. This challenging task will offer new possibilities to prepare the COSY beam also for the new WASA detector with an internal Pellet target. With respect to the planned cooling systems at the HESR a combination of stochastic cooling and electron cooling can then be studied at COSY for a combined tail and core cooling.

4.2 Operation of COSY

The operation of COSY in 2006 was dominated by a 2-months shutdown in summer for the installation of WASA as internal experiment and the 1-month winter shutdown for further upgrades for WASA, and the installation of four new ring-quadrupole power supplies. Unfortunately, during the summer shutdown a mechanical problem at the cyclotron RF transmitter occurred, whose repair prolonged the summer shutdown by another three weeks. By this and several power supplies faults the overall yearly reliability decreased to 84/Fig. 31). One week of GEM beam time had to be shifted to the beginning of 2007.

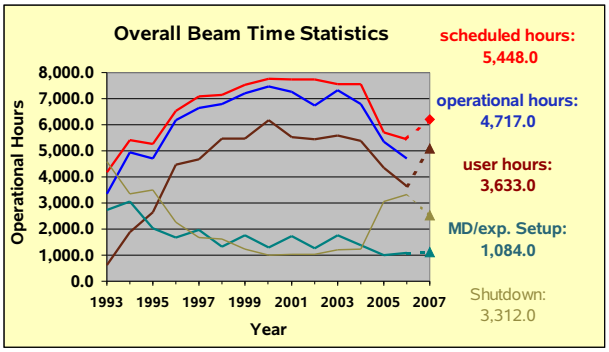

Fig. 31: Beam time statistics over the years since COSY operational start.

The distribution of ion species is shown in Fig.32. More than 60% of the time unpolarized protons were required for the experiments, nearly one quarter of the beam time

were carried out with poalrized deuterons, polarized protons were not requested during 2006.

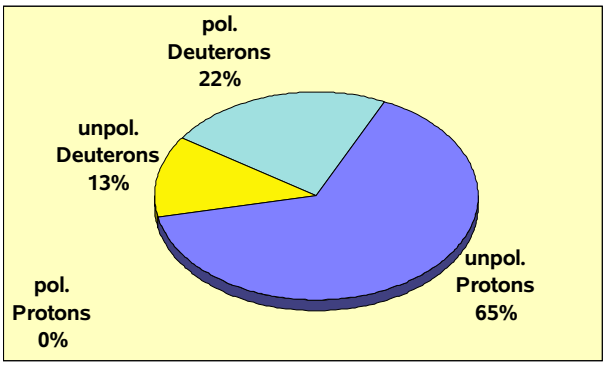

Fig. 32: Ion specific beam-time distribution in 2006.

4.3 Investigation of Spin Manipulation

The ability to manipulate spin with rf fields is important for existing and planned accelerators. Using an rf dipole, beams of spin-1/2 and spin-1 particles were successfully spin-flipped. The second phase of the experiment focused on a general understanding of spin manipulation. The observed but unexpected reduction of the rf spin resonance strength for deuterons was studied. Now Chao's new matrix formalism is investigated, which should allow an analytical description of the polarization's behavior inside a spin resonance. It was earlier found that, for deuterons, the measured rf spin resonance strength was about 7 times less than predicted. This discrepancy was found by studying the ratio $\varepsilon_{\mathrm{FS}}/*\varepsilon_{\mathrm{Bdl}}$ of the deuteron's measured rf spin resonance strength $\varepsilon_{\mathrm{FS}}$ to the $*\varepsilon_{\mathrm{Bdl}}$ calculated from the rf magnet's $\int Bdl$. The $\varepsilon_{\mathrm{FS}}$ was obtained by fitting spin-flipping data to the Froissart-Stora equation. This discrepancy was recently studied using a 1.85 GeV/c vertically polarized deuteron beam stored in COSY by sweeping the rf dipole's frequency through an rf-induced spin resonance. The dependence of $\varepsilon_{\mathrm{FS}}/*\varepsilon_{\mathrm{Bdl}}$ on: the beam size, the momentum spread $\Delta p/p$, the distance $\Delta\nu_y$ from an intrinsic spin resonance, and the rf dipole's sweep range Δf was studied. No dependence on the beam size, $\Delta p/p$, or Δf could be found. However, a sharp hyperbolic dependence of $\varepsilon_{\mathrm{FS}}/*\varepsilon_{\mathrm{Bdl}}$ on the vertical betatron tune distance ($\Delta\nu_y$) from the intrinsic resonance was discovered (Fig. 33). This seems to be the first clear observation of a deuteron spin resonance. But this did not explain the 7-fold reduction of $\varepsilon_{\mathrm{FS}}/*\varepsilon_{\mathrm{Bdl}}$ far from the intrinsic resonance. Thus, this small $\varepsilon_{\mathrm{FS}}/*\varepsilon_{\mathrm{Bdl}}$ ratio may be due to some unexpected behavior of relativistic spin-1 deuterons in an rf dipole. It is next planned to examine whether this discrepancy also occurs with an rf solenoid. It was recently started testing Chao's proposed new matrix formalism for describing the spin dynamics due to a single spin resonance in a stored polarized beam. This formalism seems to be the first generalization of the Froissart-Stora (F-S) equation since it was published in 1960.

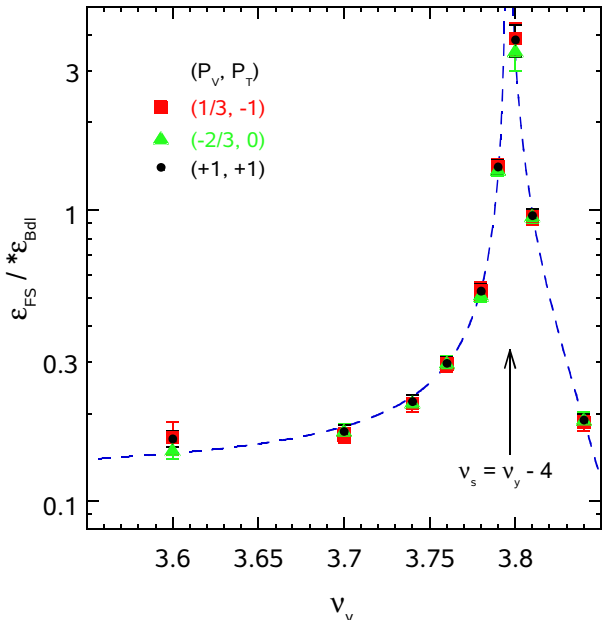

Fig. 33: Resonance strength ratio *vs.* vertical betatron tune. The curve is a fit to an asymmetric hyperbola.

It allows one to calculate analytically the polarization's behavior inside a resonance, which is not possible using the F-S equation. Some Chao formalism predictions using a 1.85 GeV/c polarized deuteron beam stored in COSY were recently tested. This involved sweeping the rf dipole's frequency through a 200 Hz range, at two different sweep rates, while varying the distance from the sweep's end frequency to the rf-induced spin resonance's center. The data were compared with the Chao formalism predictions and those of a phenomenological F-S-based two-fluid model. (The F-S formula itself can make no prediction inside a resonance.) The data seem to strongly favor the validity of the Chao formalism. Tests of this formalism with better precision are planned soon.

4.4 Electron Cooling Experiments

The search of proton ordering in electron cooled beams has been continued this year. Schottky spectra of the proton beam were measured at injection energy (45 MeV) for different electron current values and decreasing proton numbers in the beam. After injection the proton number was reduced by the horizontal scraper leading to a faster beam loss. After reaching a certain proton number that was measured via the Schottky noise power the scraper was taken out and the averaging procedure of the spectrum measurement was started. Instead of a theoretical predicted sudden drop in momentum spread indicating that an ordered state is achieved when the particle number decreases below a critical value the momentum spread decreased and attained a minimum value. As shown in Fig. 34 the momentum spread flattened out and did not decrease below $1.2 \cdot 10^{-6}$ at a proton number be-

low $1 \cdot 10^6$. Additional heating effects such as scattering on residual gas or magnetic field ripples in the COSY bending magnets might be a reason for this outcome. It should be noted that the result was not sensitive on the application of the high voltage power supply feedback. This feedback system is intended to suppress ripples of the 35 kV high voltage power supply. A reduction of the ripples amplitude by a factor of two could be achieved.

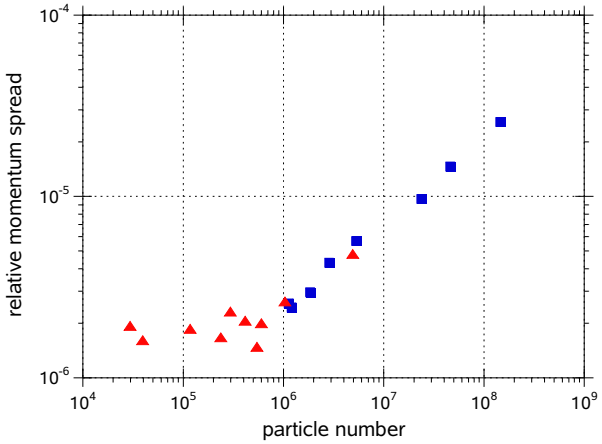

Fig. 34: Proton beam momentum spread *vs.* particle number: squares: feedback OFF, triangles: feedback ON. Electron current 70 mA

4.5 Stochastic Cooling Experiments

Detailed numerical and analytical studies of the Fokker-Planck equation (FPE) for longitudinal filter cooling including the beam-target interaction has been carried out to demonstrate the stochastic cooling capability in the HESR at the FAIR facility. To gain confidence in the model predictions a series of stochastic filter cooling experiments at COSY with the internal ANKE target has been carried out to compare model predictions with the experimental cooling performance. The experiments were carried out at a beam momentum 3.2 GeV/c with about 10^{10} stored protons in the machine that was operated above transition resulting in a negative frequency slip factor. Longitudinal cooling was carried out with band I ranging from 1 to 1.8 GHz. In order to compare momentum distributions predicted by the FPE solutions with those in the experiment beam frequency distributions were measured in the frequency range of the harmonic number 1500 with the band II system. Using the known relation ship between momentum and frequency they were then simply converted to momentum distributions. The frequency distributions were measured every 2.5 min or 5 min in flat top with a duration of about 30 min. First the target beam interaction was investigated in order to determine the mean energy loss per turn ε and the mean square relative momentum deviation per turn δ^2_{loss}. Both quantities enter the FPE to predict the beam-target interaction as well as the cooling properties. In Fig. 35 the measured center of the frequency distributions are shown for cooling off and on. The revolution frequency of the protons can derived by dividing the values by the harmonic number 1500. The time development of the relative momentum spread is shown in Fig. 36 for both cases, cooling off and on. Due to the energy loss in the target the beam centre frequency (black data points in Fig. 35) is shifted linearly towards higher frequencies when cooling is off as expected when the frequency slip factor is negative. The slope of the measured data determines the mean energy loss and resulted in $\varepsilon = -1.8 \cdot 10^{-3}$ eV/turn. From this value the ANKE target thickness of about $N_{\mathrm{t}} \sim 3 \cdot 10^{14}$ atoms/cm^2 was deduced. The red curves represent the model prediction and reflect the linear behavior in good agreement with the data when cooling is off. At larger times the model prediction deviates from the linear development due to particles losses that start when the beam reaches the acceptance limit. A similar good agreement between model prediction and data was obtained for the time development of the relative momentum spread of the beam as shown in Fig. 36.

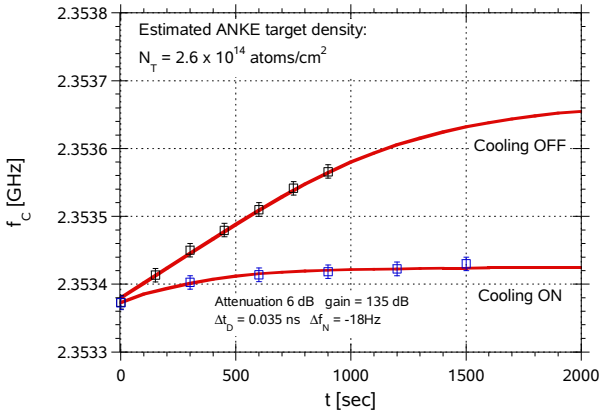

Fig. 35: Measured center frequency at harmonic 1500 (blue symbols: cooling ON, black symbols: cooling OFF) in comparison with the model predictions (red curves).

After determining the parameters of the beam target interaction stochastic cooling was switched on. The system delay was adjusted for cooling by means of BTF measurements and the notch filter was set 18 Hz below the center frequency of the distribution at harmonic one. In momentum space this means that the filter was set above the mean momentum of the protons. Measurements for different attenuations of the electronic gain of the cooling system were then carried out. As an example the Figs. 35 and 36 show the results for the amplifier gain set to 135 dB. The effect of cooling is clearly visible in a reduction of the relative momentum spread which attains an equilibrium value after about 1000 s. The mean energy loss is partly compensated. Also here a remarkable well agreement between measurement and model predictions is found. When cooling was on no particles losses occurred. A detailed representation can be found in a sep-

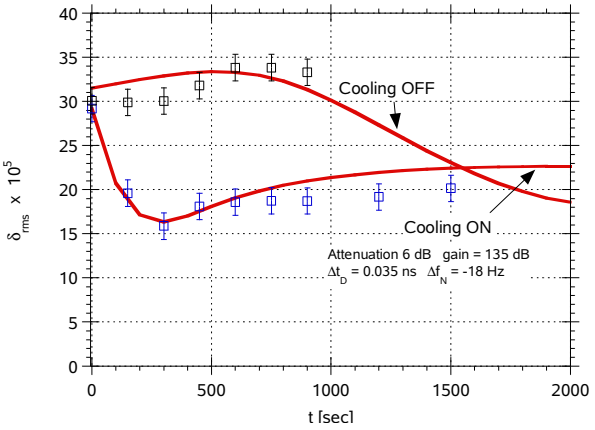

Fig. 36: Measured relative momentum spread at harmonic 1500 (blue symbols: cooling ON, black symbols: cooling OFF) in comparison with the model predictions (red curves). The linear increase of the squared momentum spread determines the mean square relative momentum deviation per turn when cooling is switched off.

arate contribution in the accompanying CD-ROM of this report.

4.6 Studies for the 2 MV Electron Cooler

At COSY electron cooling is applied at low energies, presently at injection energy, to prepare low-emittance beams after acceleration and extraction for internal and external experiments. Stochastic cooling covering the momentum range from 1.5 GeV/c up to the maximum momentum is routinely applied to compensate the mean energy loss and the increasing beam momentum spread as well as a transverse emittance growth in internal experiments. Future experiments with WASA however request higher luminosities ($> 10^{32}\,\mathrm{cm}^{-2}\mathrm{s}^{-1}$) as compared to the currently utilized targets and thus a more powerful cooling is needed to counteract the stronger target-beam interaction. Two possible options could provide a solution. Firstly the bandwidth of the stochastic cooling system is increased and secondly electron cooling up to maximum momentum is applied. Then, for experiments with thick internal targets the combination of stochastic and fast magnetized electron cooling would be the preferred challenging solution. At COSY the combination of the two cooling techniques could not only be studied but also, experiments could significantly benefit from the advantages of both cooling methods. Electron cooling of the beam core and stochastic cooling of the beam tails would be an interesting and novel cooling application. Furthermore, the realization of such an electron cooling system will be an important step to launch an experimental technique that reduces in an important manner parasitic effects in the beam-target interaction emerging from beam halo particles — a step towards a "background less" detection system.

Table 1: Basic Parameters and Requirements.

COSY 2 MeV Electron Cooler	Parameter
Energy Range	0.025–2 MeV
High Voltage Stability	$< 10^{-4}$
Electron Current	0.1–3 A
Electron Beam Diameter	10–30 mm
Cooling Length	3 m
Toroid Radius	1.5 m
Variable Magnetic Field	0.5–2 kG
(cooling section solenoid)	
Vacuum at Cooler	10^{-8}–10^{-9} mbar
Available Overall Length	7 m
Maximum Height	7 m
COSY Beam Axis above Ground	1.8 m

For electron cooling up to the maximum momentum of COSY an electron cooler up to 2 MeV electron energy has to be developed. The basic parameters and requirements are listed in Table 1. The most important restrictions are given by the available space at the COSY ring itself. The height is limited by the building up to 7 m, the length of the cooler in beam direction by the existing electron cooler and the ring itself to 3 m. The acceleration of polarized beams at COSY must to be taken into account. Space for compensating magnets must be foreseen to achieve the conservation of polarization. Model calculations have been performed in which the cooling force is approximated by the well known Parkhomchuk formula.

The effect of intra beam scattering is included by the simple model of relaxation distribution velocity. The increase of the angle spread due to scattering of an internal target is also taken into account. The simulation was made with the following parameters: cooler length 3 m, beta function in the cooling section 13 m, electron beam radius 0.5 cm, electron beam current 2 A, magnetic field 2 kG, initial normalized emittance $10^{-6}\,\pi\,\mathrm{m\,rad}$, 2 GeV proton beam energy and the number of protons $2 \cdot 10^{10}$ (5 mA).

As it is seen in Fig. 37 the ion beam emittance is effectively decreased during 10 s. The acievable equilibrium emittance is a result of a balance between intra-beam scattering and electron cooling.

The proposed electron cooler consists of a high voltage vessel with electrostatic acceleration and deceleration columns, two bending toroids and a cooling drift section. The preliminary scheme of the cooler is depicted in Fig. 38 . The basic features of the design consist in the longitudinal magnet field from the electron gun to the collector in which the electron beam is embedded, the collector and electron gun placed at the common high voltage terminal. The power for the magnet field coils at the accelerating and decelerating columns is generated by turbines operated on SF6 gas under pressure. The gas flux which drives the turbines is also used to cool the magnetic coils and to keep constant the temperature

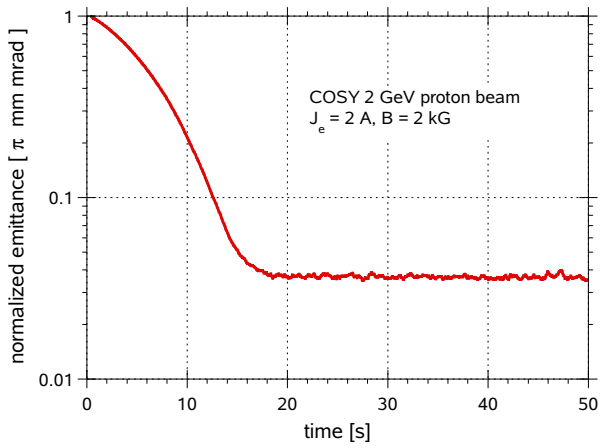

Fig. 37: Normalized beam emittance versus time with electron cooling of a 2 GeV proton beam (without target and parameters as listed in the text).

inside the vessel. The vessel withstands pressures up to 10 bar. The diameter of the high voltage sections amounts to 80 cm. The electron current is equal to 0.05 A. The beam power is 100 kW. The high voltage sections for the 2 MeV electron cooler contains the following parts, high voltage power supply, coils for the magnet field along acceleration and deceleration columns, power source and control units for measurement and control of parameters for each section.

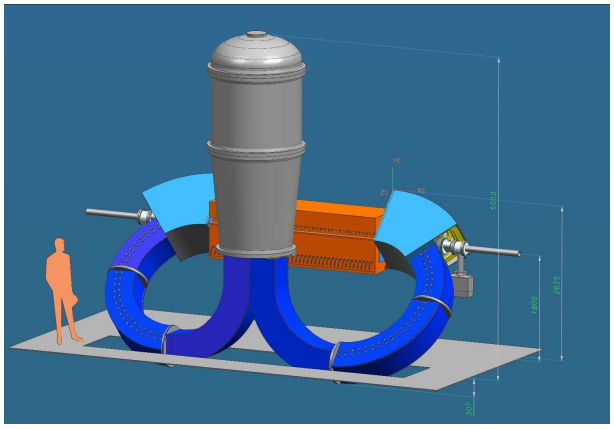

Fig. 38: Layout of the proposed 2 MeV electron cooler for COSY.

Each section has two high voltage power units of 30 kV. The utilization of two power units allow to decrease the voltage for insulation from 60 kV to 30 kV. The whole 2 MV column consists of 34 sections. The electric field between the sections will be 30 kV/cm. The pressured SF_6 gas can be used to prevent sparking. A SF_6 gas pressure of about two bars will be sufficient. Further details and a full description of the high voltage generation system can be found in a separate contribution in the accompanying CD-ROM of this report.

5 Preparations for FAIR

5.1 HESR Technical Progress Summary

The High Energy Storage Ring, HESR, of FAIR is being planned by a consortium formed by GSI, Uppsala University, and the IKP, which is the leading laboratory of this project. Financial support by the European Union via FP6 grants facilitated progress in the technical work for HESR in the fields of RF equipment, electron cooling system, stochastic cooling system, and beam dynamics. Many common meetings of IKP- and GSI-staff members ensure precise exchange of all relevant data and technical efforts. For instance, as a result of this exchange, a dedicated vacuum tank has been designed, built and installed at COSY to test diagnostic devices, which have been developed by the diagnostics group at GSI. The tank can later be used at FAIR.

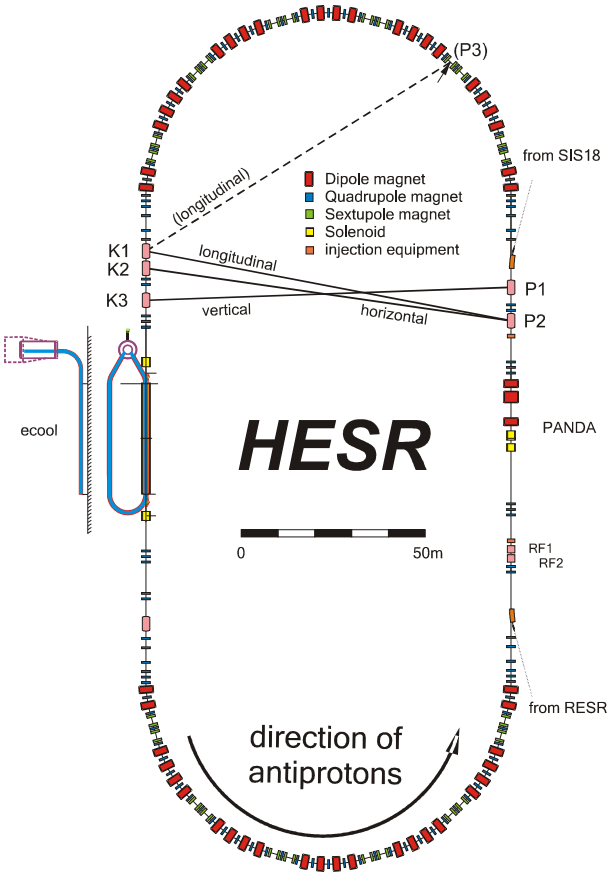

Fig. 39: Schematic layout of the HESR lattice. Equipment for experiment, acceleration and electron cooling, compensation solenoids, and injection is included. The positions of stochastic cooling devices are indicated.

5.1.1 Building Issues

The size of all buildings has been fixed within ±5 m to provide a basis for the planning of civil construction. According to the guideline to plan the HESR such that future developments for antiproton spin physics are not excluded as long as no cost increase is implied, and triggered by recent discussions that this kind of physics might need a symmetric collider option, the HESR buildings have been shifted southwards by 30 m. Transfer beamlines could be redesigned accordingly.

The main systems of the HESR are shown in Fig. 39. Transverse dimensions are not to scale. Position and dimension of all devices is collected in a data base to allow easy generation of floor plans. The coordinates of the injection points have been fixed as well as the coordinates of the end points of the straight sections. Currently two alternatives for the arc are considered: (i) lattice with 6fold symmetry and 1.8 m long straight dipole magnets, and (ii) lattice with 4fold symmetry and 3.3 m long bent dipole magnets. Within the presently required tolerance (±5 m) both alternatives will fit into the same tunnel. The decision which lattice to prefer will be based on beam dynamics, dipole magnet fabrication issues, and economic evaluations which are in progress.

5.1.2 Magnets

For the straight magnets a shortened version of the RHIC D0 magnets can be used. Sagitta arguments restrict the magnetic length to 1.8 m. Even then it is difficult to guide 99% of the beam particles through the good field region of the magnet. However, the use of bent dipole magnets will ensure that the beam always travels in a good field region. Moreover, the number of dipole magnets can be reduced from 48 to 32 if bent dipoles are used. The number of fringe fields and interconnect regions will be reduced accordingly. For bent dipoles two different designs have been studied: (i) cos-theta design and (ii) double helix design. The cos-theta design is well proven (for straight magnets), and "just" modifications for bending have to be applied. These modifications of the production process have been analyzed in a dedicated design study. A list of mock-up studies has been identified, and possible production difficulties can be expected to be managable. A drawback is the rather long time to produce and qualify the first magnet which is in the order of 1.5 years. For the innovative double helix design extremely low contributions to multipole errors can be expected avoiding tedious design and manufacturing of spacers and collars. The quadrupole component induced by the bending can be compensated completely by modulating the wire path of the double helix dipole magnet. A first cold mass can be produced in less than 6 months. Prototype work for the dipole magnets will start soon to allow a serious decision on the magnet type.

For quadrupole magnets a design study has been launched *(i)* to determine a realistic assembly of dipole and quadrupole magnets and *(ii)* to decide whether a hybrid magnet with a sextupole coil on top of the quadrupole coil could be advantageous for the HESR.

Design of sextupole magnets has started on the basis of beam dynamics results. Further work on this magnet type

will make use of the results of the quadrupole magnet developments.
The orbit will be corrected in HESR using an orbit response matrix. Investigations show that in the straights orbit kicks of 2 mrad and in the arcs kicks of 1 mrad will be sufficient to guarantee an orbit with amplitudes smaller than 5 mm.
For injection into the HESR the incoming beam at the end of the transfer line will be guided through a 5° (permanent) dipole magnet followed by a magnetic septum for 10° bending angle which is installed in the HESR. At a suitable position downstream a magnetic kicker element (2 modules of 3.2° kick angle each) will align the incoming beam with the trajectory of the circulating beam. The basic design with the most important parameters of 5°-dipole magnet, magnetic septum, and kicker magnet could be fixed.

5.1.3 Stochastic Cooling

The results of extensive theoretical investigations were compared to measurements using the stochastic cooling system of the COSY accelerator giving confidence in the underlying theoretical model. The requirements for the stochastic cooling system of the HESR can be met with a bandwidth of 2–4 GHz. For that system two different coupler designs are being evaluated together with appropriate combiner boards: (Fig. 40) new ring-slot couplers and (Fig. 41) printed loop couplers in an octagonal arrangement.

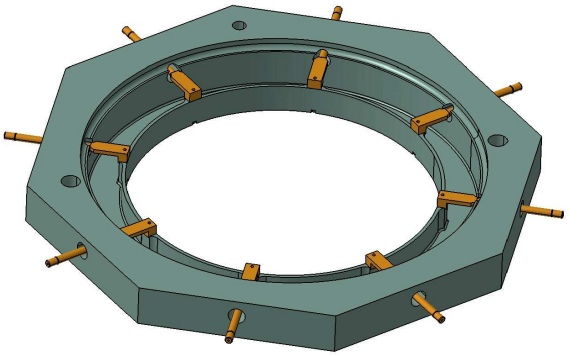

Fig. 40: Ring-slot coupler for possible use in the stochastic cooling system of HESR.

5.1.4 Electron Cooler Progress at Uppsala University

The design work and work on prototyping of subsystems for the HESR high-energy electron cooling system continues at The Svedberg Laboratory, Uppsala University, Sweden (TSL). It was mentioned already in last year's Annual Report that the high-energy electron cooling system is likely to be based on a Pelletron from National Electrostatics Corporation (NEC) in the U.S.A.. The layout of equipment inside the high-voltage tank has been made by TSL in collaboration with NEC and Fermilab.

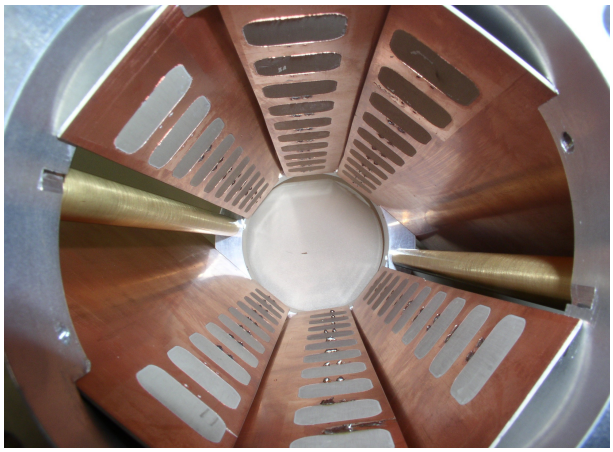

Fig. 41: Octagonal structure consisting of printed loop couplers for possible use in the stochastic cooling system of HESR.

The design of the magnet system is nearing completion. It produces a longitudinal magnetic field, which extends from the electron gun to the collector. The magnetic field is 0.2 T over the interaction section and 0.07 T in the accelerating and decelerating sections. The magnet system includes two 24 m long straight sections, a total of 420° of bends with 4 m bending radius, about 12 m of magnet system inside and below the high-voltage tank, and two 2 m long adiabatic transition sections, where the magnetic field is gradually changing between 0.07 T and 0.2 T. Prototypes of several solenoids are under manufacture. One of these will be a prototype of a solenoid which will be placed in the high-voltage tank, and which will be cooled with the surrounding sulphur hexafluoride gas. The magnet system also includes correctors for fine adjustments of the electron beam position and for compensation for misalignments of sections.
The magnetic field lines in the interaction region need to be very straight. The allowed non-straightness is only 10 μrad r.m.s.. Therefore, a precise magnetic field measuring system needs to be built. This work is performed in collaboration with the BINP in Novosibirsk, Russia, and is based on their experience with such measurements using a magnetic compass needle with a mirror and a laser beam. The sensor head will travel through the solenoid in a carriage, which makes use of rails. These rails are incorporated in the aluminium vacuum chamber. A prototype of the vacuum chamber has been made and a prototype magnetic-field measuring system is under construction, see Fig. 42.
Successful operation of the electron-cooling system requires advanced electron beam diagnostics. The most important components of this electron-beam diagnostics system are pick-up electrodes and electron beam scrapers. The pick-up electrodes have to measure the positions of the electron and antiproton beams with a resolution of 10 μm. The purpose of the electron beam scrapers is to measure the diameter of the electron beam with a resolu-

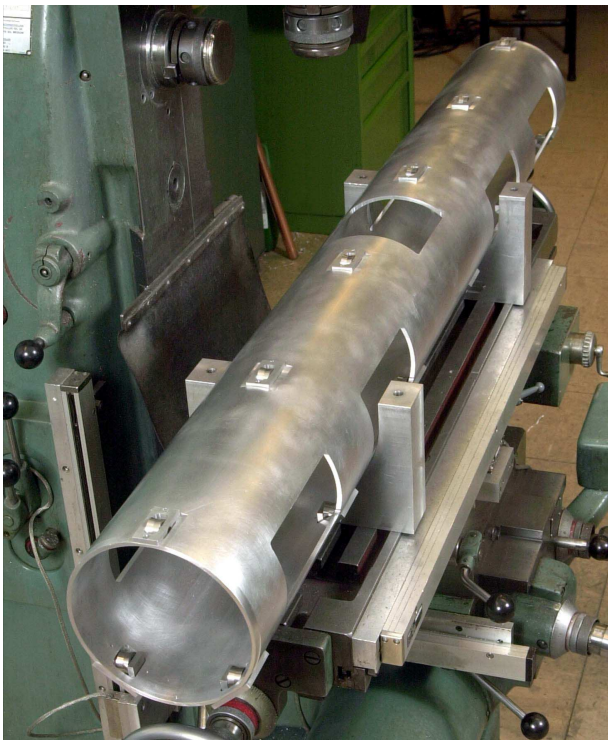

Fig. 42: Cart for magnetic field measuring system.

tion of about 0.2 mm, in order to make sure that electron-beam envelope oscillations are minimized. The pick-up electrodes and electron-beam scrapers on the interaction straight section will be combined into a single unit which is currently being designed.
Experience of measuring the diameter of the electron beam with such scrapers will be acquired by doing experiments using the CELSIUS electron-cooler which is being modified for this purpose at the present time.
The electron gun has been designed and preparations for designing the collector are taking place. This work is performed in collaboration between TSL and the Fermilab.
Tests relating to the precise regulation of the high voltage have been carried out with the Pelletron at Uppsala. These tests indicate that mechanical vibrations of the Pelletron can play an important role. Work to evaluate the tests continues.

5.1.5 RF Cavities

Beam dynamics requirements for RF result in two different cavities: one for bunch manipulation and acceleration/deceleration, and one for storing the particles in a barrier bucket. The first task is accomplished with a symmetric, magnetic alloy loaded cavity, combined with a push-pull tube-amplifier for multi-harmonic signals in the order of 10–3000 V. This cavity with a length of 80 cm and an outer diameter of slightly less than 50 cm has been designed and is being manufactured. The necessary magnetic alloy cores (FineMet®) have been delivered (Fig. 43, right side) and will be installed as soon as the construction work is completed. The barrier bucket cavity has been designed and built as a single tank cavity (Fig. 43, left side). The magnetic alloy cores (VitroPerm®) are also on site and currently are being installed. The barrier bucket cavity will be driven by a 1 kW transistor amplifier which will allow to reliably apply voltages between 1 and 100 Volts.

Fig. 43: Barrier Bucket cavity (left), magnetic alloy core for acceleration cavity (VitroPerm®, right)

5.1.6 Cryogenic Issues

To minimize static losses of the cryogenic system the number of cold/warm junctions will be minimized. The HESR components which have to be operated at room temperature are the injection septa and the injection kickers, the dipole magnets for the PANDA orbit chicane, the RF cavities, the stochastic kicker tanks, and the electron cooler. All other devices can be operated at liquid Helium temperature.Thus, HESR will have a minimum of 9 warm sections. Each arc will be one cold section. The initial pump down time for one arc has been estimated to be in the order of one day using one pumping unit at one end of an arc and with a vacuum gauge at the other end of the arc.

5.2 The PANDA Experiment

One major component of the approved **F**acility for **A**ntiproton and **I**on **R**esearch (FAIR) at the GSI in Darmstadt is the **H**igh **E**nergy **S**torage **R**ing (HESR) with the PANDA (**P**roton **AN**tiproton **D**etector **A**rray) experiment. HESR will provide a phase space cooled antiproton beam of unsurpassed quality, precision and intensity. A momenta range up to 15 GeV/c will be covered allowing the detailed study both of the structure of hadrons in the charmonium mass range and the spectroscopy of double hyper nuclei. To serve this wide physics program the general purpose experiment PANDA is currently planned.
Basic concept of the detector is given by its division into two main parts, the central or target spectrometer and the forward spectrometer. This combines a nearly 4π coverage in the target region together with high acceptance of particles emitted at small polar angles in this fixed target kinematics.
The heart of the central spectrometer is a micro vertex detector located direct around the target for extreme precise tracking information. It is surrounded by the central tracker built either of straw tubes (STT) or a time projection chamber (TPC) in the barrel part, and a set of mini drift chambers (MDC) in the forward direction. Particle identification is done by two ring imaging Cherenkov counters surrounded by a compact electromagnetic calorimeter made out of $PbWO_4$ crystals. The entire system is situated in a 2 T solenoidal magnet which is covered outside with detectors for muon identification and tracking.
The forward spectrometer consists of a 2 T·m dipole magnet with a set of multiwire drift chambers (MuDC) for tracking, a RICH detector for particle identification, calorimeters for charged and neutral particles and a layer of muon counters.
The ongoing activities of the IKP for the PANDA detector are focused in three parts: the micro vertex detector, the straw tube tracker and the simulation of the tracking detectors.

5.2.1 Micro Vertex Detector

The Micro Vertex Detector (MVD) plays a key role in the PANDA experiment to identify open charm and strangeness by detecting secondary decays of particles displaced from the primary interaction point. These decay lengths range from a few 100 μm for charmed mesons and baryons up to several cm for strange hadrons. One of the most important issues for the design of the pixel part of the MVD is the data handling and transfer. In order to allow an open charm trigger based on secondary vertex tagging a quasi online data processing in the DAQ chain is envisaged. This requires a complete data transfer from the MVD to a certain DAQ stage and therefore the MVD itself must be readout without any trigger. All major LHC experiment have developed a hybrid pixel detector and therefore it is natural to evaluate them as possible candidates for the PANDA MVD. Finally the ATLAS pixel chip was chosen as most promising candidate because it combines an easy self trigger mechanism together with relative low power consumption. Consequently the basis of the design is the ATLAS pixel module, a $2 \cdot 6$ cm^2 module with 16 FE chips of 2880 pixel each and a pixel size of $50 \cdot 400$ μm.
To evaluate the data rate requirements detailed Monte Carlo simulations of the MVD layout have been performed. Special focus was given to the maximum track rates per module, FE chip and pixel. Due to the high granulation of the pixel detector the highest single pixel rate of 16 kHz is relatively low and therefore manageable for state-of-the-art pixel FE chips. Also the module rates are acceptable since the rate distribution is very inhomogeneous and therefore the peak rates are averaged over the entire module area. The real bottleneck is the chip data rate with roughly 1 MHz for the $\bar{p}p$ case and about 1.4 MHz for the $\bar{p}A$ case. This has to be compared with the maximum level 1 trigger rate in ATLAS of about 100–125 kHz. If the ATLAS pixel FE will be used in PANDA it has to handle a maximum data output rate 10 times higher than its design requirement.

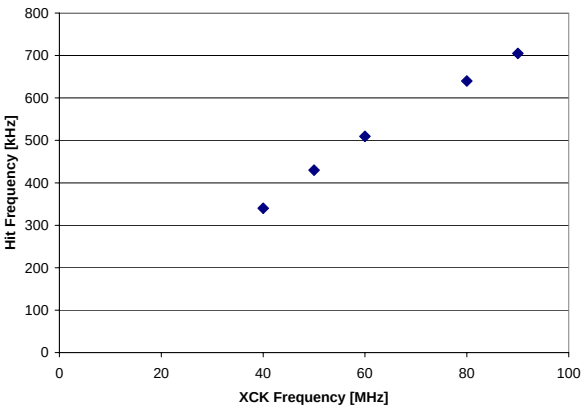

Fig. 44: Measured maximum output hit rate versus clock frequency for an ATLAS FE-I3 single chip, for each event two pixel are hit simultaneously.

For testing the data rate capability of the ATLAS pixel electronics a standard single chip device was used; it consists of one full size FE chip with 2880 pixel cells bump bonded to a small n-in-n pixel sensor. All tests were done with a ATLAS pixel test system allowing a full characterization of all properties of the device under test. Because the ATLAS pixel FE is designed for a triggered readout a special self-trigger circuit implemented for test and source calibration purposes was used. This circuit generates the necessary trigger signal for each hit via a fast 'or' over all single pixel discriminators. An asynchronous hit injection into two pixel simultaneously was used to mimic realistically the application inside PANDA.
Figure 44 shows the achieved data rate for two hits per particle track as function of the chip's master clock frequency which defines the speed of the data transfer. The theoretical expected double hit data rate at 40 MHz was achieved and could be increased linearly until 90 MHz

or 700 kHz track rate. A further increase of the clock frequency was not possible but this was mainly due to limitation of the clock generation and distribution of the test system. The chip itself has shown to be operable until 100 MHz. However, the achieved data rate at 90 MHz nearly matches the required maximum track rate of 720 kHz assuming double hits. A further increase of the data rate seems difficult because this would require either a decrease of trigger signals per event with the risk of loosing small signals or a further clock frequency increase up to regions with possible chip failures.

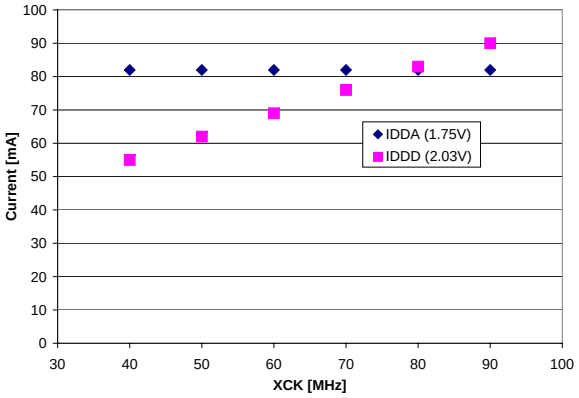

Fig. 45: Current consumption of the ATLAS FE-I3 chip versus clock frequency at standard voltages for the supplies, *i.e.* 1.75 V for the analog supply and 2.03 V for the digital part.

The drawback of the improved data rate capability is the drastic increase in power consumption as illustrated in Fig. 45. Whereas the analog supply current remains constant over the tested frequency range the digital supply increases from 55 mA to about 90 mA. This total 30% increase in power consumption contradicts the strict material budget of the MVD because it requires more cooling capacity. Noise and threshold performance of the chip are nearly independent from the clock frequency, only a slight noise increase of 5% could be observed.
To cope with the expected tremendous amount of tests of different pixel and strip detector prototypes IKP in cooperation with ZEL have developed a powerful, flexible and high speed test system. Main requirement is the easy implementation of new readout chips either for pixel detectors or strip detectors. Hence, we decided for digital board hosting a modern, free programmable FPGA, in our case a Virtex XC4VLX60 with 60,000 logic cell, 2.8 MByte Ram and up to 500 MHz system clocking. The interface to a PC is done with a common PCI interface card which transmits the data optically. The SiS1000 1 Gbit optical link is used for this purpose.
The interface to the readout chips is then done individually. The system provides up to 32 LVDS input and output lines to accommodate any possible readout protocol. If other I/O standards are needed they can easily implemented via an interface card connected between the digital board and the detector. Furthermore two high precision RoboClock chips are available with a range from 24 to 200 MHz, 4 output banks and a phase adjustment accuracy of smaller than 200 ps. Four low output voltages up to 5 V can be generated on board and three differential clock lines are available.

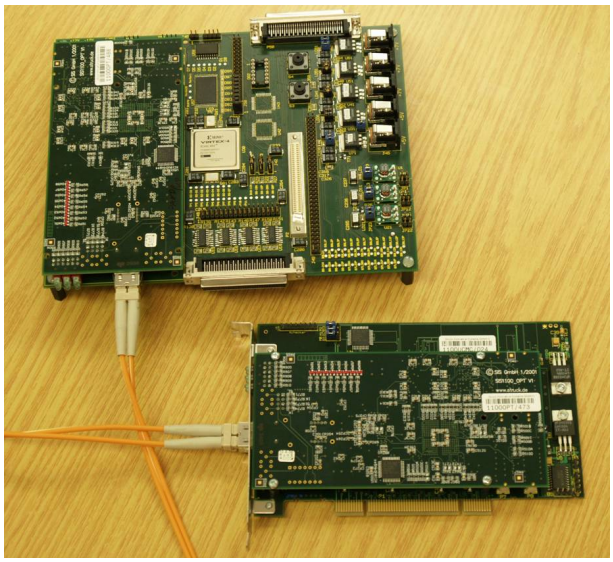

Fig. 46: Picture of the prototype test system, the main board hosting central FPGA is visible in the upper part whereas the lower board shows the PCI card to be installed in the PC.

A picture of the system can be seen in Fig. 46, in the upper part one can see the digital board hosting the FPGA. The PCI card together with optical data link and the optical fibre can be seen in the lower part. Design, layout and production of the first system is finished. Currently the system will be commissioned by implementing the support for the ATLAS pixel FE.

5.2.2 Straw Tube Tracker

The main tracking element of the target spectrometer is the Central Tracker (CT) which occupies a region inside the superconducting solenoid starting at a radial distance of 16 cm from the beam line, up to 42 cm. Along the beam (z) this region extends from 40 cm upstream to 110 cm downstream of the target. The baseline detector technology currently under investigation for the CT is a straw tube tracker (STT). Main focus of the work in 2006 was the development of an realistic layout combining high tracking performance with low material budget. The proposed layout can be divided into three zones and incorporates altogether 21–27 layers of straws grouped into 6 sectors which are arranged in a hexagonal structure, see Fig. 47 (a). At small radii 7 axial layers of 150 cm long straws are located, followed by 10 layers of skewed straws with a skew angle of 3° for optimized z-resolution. At larger radii up to 42 cm again axial straws are located, *i.e.* 4 to 10 layers depending on the φ-position because the outer shape of the STT is circular whereas the inner shape in hexagonal.

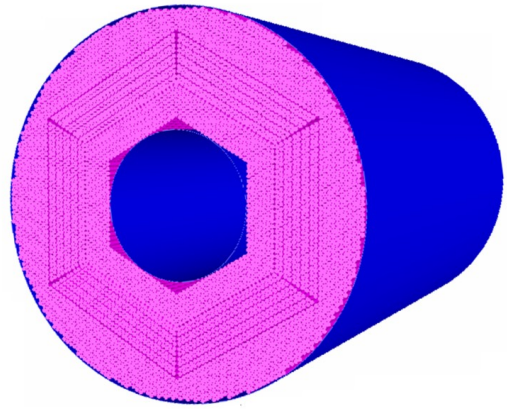

(a) Layout of the STT based on a hexagonal structure.

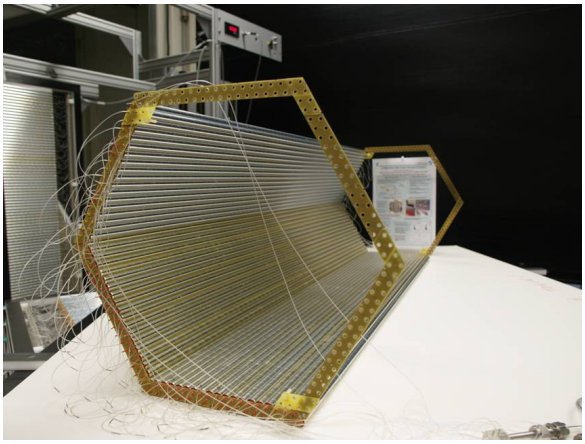

(b) Photo of a mechanical prototype of the hexagonal STT structure.

Fig. 47: Proposed layout for the STT of PANDA; basis of the this layout study are the thin, self supporting Al-mylar film tubes.

The straws are 10 mm diameter Al-mylar film tubes operated with Ar/CO_2 at 1 bar overpressure for self supporting. This type of straws has been developed in IKP for COSY-TOF and showed excellent performance at high rates and radiation doses as well as concerning the used amount of material. In total the 5340 straws for the envisaged PANDA STT will have a mass of about 15 kg without the support structure.

This layout combines the highest layer number which is important for the efficiency and therefore also for the tolerance against straw ageing together with best mechanical stability and precision. It allows a continuous tracking in $r\varphi$ which is necessary for track finding. Having only one zone of skewed straws reduces the lever arm of the z-measurement but this is somehow compensated by the increased number of z-hits. First rough simulations showed that a position resolution in $r\varphi$ of about 150 μm at 98% efficiency for the axial layers can be achieved. The skewed layers give a z-resolution of about 2.9 mm at 90–95% efficiency sufficient for the PANDA needs. This increased numbers of straw layers extends also the low momentum acceptance threshold for slow particle tracks; the achieved relative resolution for transversal momenta σ_{p_t}/p_t is in the order of 1.2% only slightly failing the PANDA requirement of about 1%.

First mechanical tests of the feasibility of such a concept have been done as well. In Fig. 47 (b) one can see a part of a hexagonal support structure equipped with 120 straws to illustrate the realization of this detector. More sophisticated prototypes will be built and tested in the next two years before a decision of the PANDA central tracking device will be taken.

5.2.3 Simulations

Focus of the simulation work done at IKP in the last year was the implementation of a full reconstruction of the STT into the overall PANDA simulation framework. This includes the digitization of the straws, a track finding algorithm and track fitting. Due to the fact that the PANDA collaboration decided during the last to switch the simulation framework to a Root based approach this work has been significantly slowed down. However, a first version of the STT implementation has been successfully developed and tested.

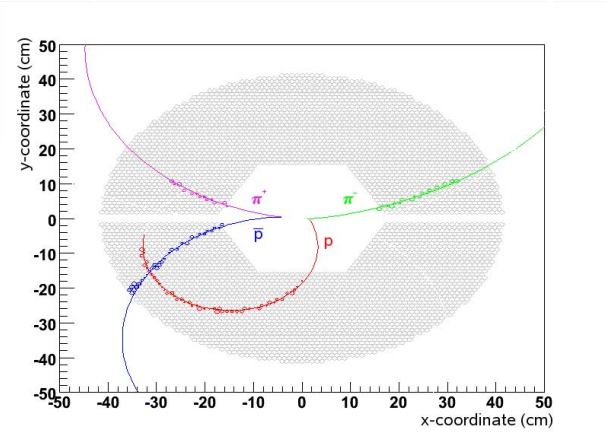

Fig. 48: Event display of $\bar{p}p \to \overline{\Lambda}\Lambda \to \bar{p}\pi^- p\pi^+$ inside the STT; only hits of the STT are considered for reconstructions of the track.

This implementation uses an algorithm depending on the Hough transformation for track finding and a simple helix fitting routine for the track fitting. This leads to an acceptable performance and has been used for testing layout options for the STT as it was mentioned in section 5.2.2. For example in Fig. 48 an event display after reconstruction of the STT can be seen, in this case it is a x-y projection of a $\bar{p}p \to \overline{\Lambda}\Lambda \to \bar{p}\pi^- p\pi^+$ event. The small circles denote the measured hits of the straws and the lines are the fitted tracks. All tracks of the Λ decay prod-

ucts are identified and fitted well. The extrapolation of the tracks leads to clearly visible secondary vertices of the Λ and $\overline{\Lambda}$, respectively, both lying inside the MVD volume. Because no tracking of the MVD was considered for this simulation the transversal vertex resolution is only roughly 4 mm. With only the STT used for tracking the Λ-mass could be reconstructed with a resolution of about 10 MeV/c^2.

Nevertheless, this implementation is only the first step and will be improved in the near future. For instance Kalman filter techniques will be used for improving the fitting of the helices, additional vertex fitting routines will lead to better vertex resolution and incorporating MVD track data will enhance the accuracy of the momentum and hence of the mass reconstruction.

The track finding algorithm shows some weak points, in particular low momentum particles which curls inside the STT are not identified as tracks. Here more sophisticated algorithms or other approaches are needed. However, since track finding is a global tracking task, a high efficiency for the STT-only track finding is less important. Rather, the effort will be directed to common PANDA track finding routines to which this method will contribute.

5.2.4 Pellet Target

The PANDA experiment will require the use of high-density internal targets. Pellet targets seem suitable to meet the various boundary conditions of the experiment. A prototype of the pellet generator for PANDA has been set up in the COSY hall; it has been used to systematically study the breakup of cryogenic jets into droplets. These processes cruically influence the quality of the pellet beam. In particular, vibrations from surrounding equipment may lead to longitudinal and transversal instabilities of the pellet flow. Thus for the PANDA pellet generator it is foreseen to use a vibration-less cooling method (using liquefied Nitrogen and Helium), see Fig. 49.
During several test-runs stable production of H_2 and N_2 pellets with diameters $18-60\,\mu$m has been achieved. Spatial, angular and velocity distributions of the pellets have been measured with CCD cameras at the outlet of the sluice from the TPC. The average velocity of the $30\,\mu$m pellets at the first sluice outlet is ~ 70 m/s. A radial displacement of pellets in the scattering chamber ~ 1.2 m downstream the triple-point chamber of not worse than $\pm 200\,\mu$m has been extrapolated.
From 2007 on, the preparation of the PANDA pellet target (including the Moscow-Jülich pellet generator and an on-line pellet tracking system from Uppsala University) is organized within and supported by INTAS-GSI project 06-1000012-8787.

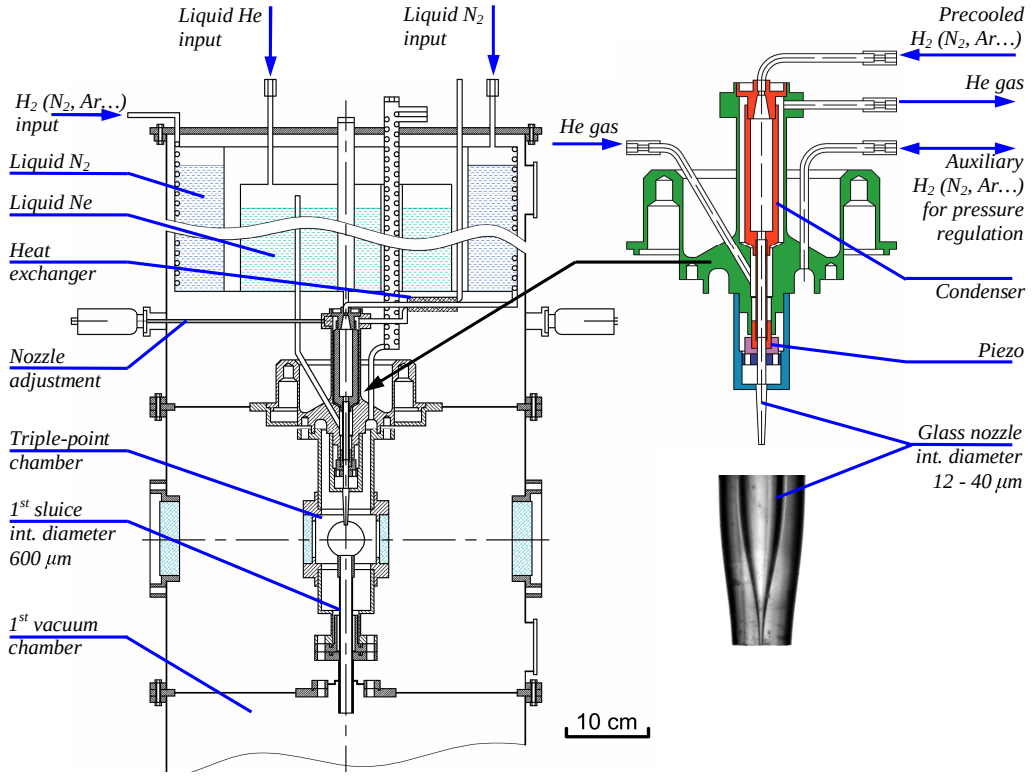

Fig. 49: Main components of the drop generator: the cryostat (total height ~ 0.8 m) with liquid N_2 and He comprises the condenser (upper right) cooled by a stream of evaporated He gas. The condenser houses a few cm^3 of the cryogenic liquid which is driven through a nozzle into the TPC by overpressure. Constant pressure in the TPC is maintained by an auxiliary gas flow. A photo of a glass nozzle with an inner diameter of $12\,\mu$m is shown in the lower right part.

5.3 Polarized Antiprotons at FAIR

As early as 1966, J.D. Bjorken realized the potential of polarized Deep Inelastic Scattering (DIS) to unravel the helicity structure of the proton. Since then, triggered by the EMC spin puzzle an impressive progress in the subject was achieved. High-precision experiments at CERN (SMC), SLAC (143...) and HERA (HERMES) mapped the helicity distributions of charged partons in the proton, the helicity distribution of gluons is presently being pinned down by COMPASS at CERN and polarization experiments at RHIC. However, the spin tomography of the proton would be ever incomplete without the determination of transversity — the quark transverse polarization inside a transversely polarized proton, the last missing leading-twist missing piece of the QCD description of the partonic structure of the nucleon. Unlike the unpolarized quark distribution $q(x, Q^2)$ and the helicity distribution $\Delta q(x, Q^2)$, the transversity $\delta q(x, Q^2)$ can neither by accessed in inclusive DIS nor can it be reconstructed from the knowledge of $q(x, Q^2)$ and $\delta q(x, Q^2)$. The transversity may contribute to some single-spin observables, but is always coupled to other unknown functions because of its chiral properties. The glorious chapter of DIS spin physics from SLAC to CERN to HERA to RHIC must not be closed without having explored the transversity properties of the proton.

An entirely new chapter in studies of the spin structure of the proton will unfold with the advent of the polarized antiproton capability of the Facility for Antiproton and Ion Research (FAIR) at GSI-Darmstadt. A cornerstone of the hadronic physics program at FAIR is the collection, cooling, storing and acceleration of antiprotons in the 15 GeV High Energy Storage Ring (HESR). The PAX Collaboration has suggested to upgrade HESR in the future into an asymmetric polarized proton-polarized antiproton collider and study double polarized antiproton-proton Drell-Yan reactions which will be entirely dominated by the annihilation of valence quarks in the proton with the valence antiquarks in the antiproton. The measured double spin-asymmetry A_{TT} will simply be given by $\left[\delta u(x, Q^2)/u(x, Q^2)\right]^2$. It will probe the large transverse polarization of valence quarks: the theoretical expectations for A_{TT} at FAIR are in the range 0.3–0.4. No other existing or planned future facility will be able to directly measure the transversity in a competitive way.

While polarized protons are readily available, the principal issue of the PAX collaboration is how to polarize antiprotons. The early attempts at LEAR to polarize antiprotons by hadronic scattering did not work, while the production of polarized antiprotons by weak decay of anti-lambda hyperons, as it was done in E704 experiment at FNAL, give impractically low beam intensities. Up to now, the only viable method to produce polarized beams of antiprotons is by "spin filtering", *i.e.* through repeated passage of an antiproton beam through a polarized hydrogen target inside a storage ring. The proof-of-principle experiment has been carried out with protons at TSR, Heidelberg (FILTEX) in 1992. Although the experiment clearly demonstrated that the spin-filtering technique works, the interpretation of the result is not undisputed. Under discussion is in particular the contribution of the atomic electrons in the polarized target to the polarization build-up. In order to make spin filtering a practicable method for polarizing antiprotons, preparatory tests with protons and antiprotons are required. The PAX collaboration has initiated a staged program, which comprises the following steps:

- Depolarization of a polarized proton beam stored in COSY passing through an unpolarized storage cell gas target (accepted proposal for COSY),
- Spin-filtering tests with the proton beam of COSY (see Fig. 50), and
- Spin-filtering tests with antiprotons at AD/CERN.

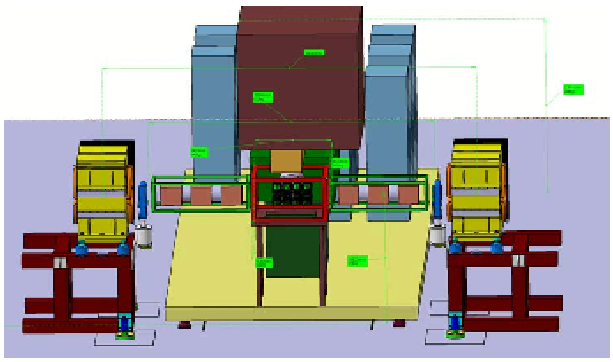

Fig. 50: Experimental setup for the spin filtering studies at COSY and at the AD of CERN. The polarized storage cell target, surrounded by a set of Silicon Microstrip Detectors, is located in a low-beta section, composed of three superconducting quadrupole magnets up- and downstream of the target.

The depolarization and spin-filtering experiments with protons at COSY will help to disentangle the hadronic and the electromagnetic contributions to the polarization build-up. In proton-proton scattering, many double-spin experiments have been carried out with polarized proton beams and targets. Polarized antiproton beams have never been available, thus our present knowledge about the spin dependence of the antiproton-proton interaction does not allow a robust estimation of the polarization build-up of a stored antiproton beam. It is therefore necessary to carry out spin-filtering experiments using stored antiprotons impinging on an internal polarized Hydrogen target. The Antiproton-Decelerator (AD) of CERN is currently the only machine worldwide which provides the required experimental conditions to perform these spin-filtering tests with antiprotons.

If it can be shown *experimentally* that a beam of highly polarized antiprotons can be produced, a new era in the investigation of the nucleon structure would be opened in very much the same way as through the introduction of polarization in the DIS studies.

A Councils

A.1 Hadron Physics Program Advisory Council

Prof. R. Beck	Universität Bonn	
Prof. J.-P. Blaizot	CEA Saclay, FR	
Prof. D.F. Geesaman	Argonne National Laboratory, U.S.A.	
Dr. P. Gianotti	Laboratori Nazionali di Frascati, I	
Prof. M. Harakeh	KVI Groningen, NL	
Prof. E. Jaeschke	Humboldt Universität Berlin	
Prof. K. Königsmann	Albert-Ludwigs-Universität Freiburg	
Prof. R. Kulessa	Uniwersytet Jagiellonski Cracow, PL	
Prof. St. Paul	TU München	Chairperson
Prof. K. Peters	GSI Darmstadt	
Prof. U. Wiedner	Universität Bochum	
Prof. U.-J. Wiese	Universität Bern	

A.2 COSY Program Advisory Committee

Prof. D. Barber	DESY, DE	
Prof. J. Bijnens	Lund University, SE	
Prof. H. Freiesleben	TU Dresden, DE	
Prof. B. Friman	GSI Darmstadt, DE	
Prof. N. Herrmann	Universität Heidelberg, DE	
Prof. T. Johansson	Uppsala Universitet, SE	
Prof. H. Löhner	KVI Groningen, NL	
Prof. A. Magiera	Jagellonian University Cracow, PL	
Prof. W. Meyer	Universität Bochum, DE	
Prof. W.T.H. van Oers	University of Manitoba, CA	Chairperson
Prof. E. Oset	Universitat de Valencia, ES	
Prof. C. Schaerf	INFN Roma II, IT	

B Publications 2006

1. Experiment

1. M. Abd El-Samad, R. Bilger, K.-Th. Brinkmann, H. Clement, M. Dietrich, E. Doroshkevich, S. Dshemuchadse, A.Erhardt, W. Eyrich, A.Filippi, H. Freiesleben, M. Fritsch, R. Geyer, A. Gillitzer, J. Hauffe, D. Hesselbarth, R. Jaekel, B. Jakob, L. Karsch, K. Kilian, H. Koch, J. Kress, E. Kuhlmann, S. Marcello, S. Marwinski, R. Meier, K. Möller, H.P. Morsch, L. Naumann, E. Roderburg, P. Schönmeier, M. Schulte-Wissermann, W. Schröder, M. Steinke, F. Stinzing, G.Y. Sun, J. Waechter, G.J. Wagner, M. Wagner, U. Weidlich, A. Wilms, S. Wirth, G. Zhang, P. Zupranski (COSY-TOF collaboration)
Single-pion production in *pp* collisions at 0.95 GeV/c (I)
European Physical Journal A **30** (2006) 443.

2. M. Abd El-Samad, R. Bilger, A. Böhm, K.-Th. Brinkmann, H. Clement, S. Dshemuchadse, b, W. Eyrich, A. Erhardt, C. Fanara, A. Filippi, H. Freiesleben, M. Fritsch, R. Geyer, J. Hauffe, A. Hassan, P. Herrmann, D. Hesselbarth, B. Jakob, K. Kilian, H. Koch, J. Kress, E. Kuhlmann, S. Marcello, S. Marwinski, A. Metzger, P. Michel, K. Möller, H.P. Morsch, L. Naumann, E. Roderburg, A. Schamlott, P. Schönmeier, M. Schulte-Wissermann, W. Schröder, M. Steinke, F. Stinzing, G.Y. Sun, J. Wächter, G.J. Wagner, M. Wagner, A. Wilms, S. Wirth, U. Zielinski (COSY-TOF collaboration)
Hyperon production in the channel $pp \to K^+\Lambda p$ near the reaction threshold
Physics Letters B **632** (2006) 27.

3. S. Abdel-Samad, K. Kilian, J. Ritman, M. Abdel-Bary
Cryogenic Target With Very Thin 'Gold Finger' Heat Pipe
Nuclear Instruments and Methods A **556** (2006) 20.

4. M. Abdel-Bary, K.-Th. Brinkmann, H. Clement, E. Doroshkevich, S. Dshemuchadse, A. Erhardt, W. Eyrich, H. Freiesleben, A. Gillitzer, R. Jäkel, L. Karsch, K. Kilian, E. Kuhlmann, K. Möller, H.P. Morsch, L. Naumann, N. Paul, C. Pizzolotto, J. Ritman, E. Roderburg, P. Schönmeier, W. Schröder, M. Schulte-Wissermann, G. Y. Sun, A. Teufel, A. Ucar, G.J. Wagner, M. Wagner, P. Wintz, P. Wüstner, P. Zupranski (COSY-TOF collaboration)
Study of spectator tagging in the reaction $np \to pp\pi^-$ with a deuteron beam
European Physical Journal A **29** (2006) 353.

5. M. Bashkanov, D. Bogoslawsky, H. Calen, F. Cappellaro, H. Clement, L. Demiroers, C. Ekström, K. Fransson, J. Greiff, L. Gustafsson, B. Höistad, G. Ivanov, M. Jacewicz, E. Jiganov, T. Johansson, O. Khakimova, M.M. Kaskulov, S. Keleta, I. Koch, F. Kren, S. Kullander, A. Kupsc, A. Kuznetsov, P. Marciniewski, R. Meier, B. Morosov, W. Oelert, C. Pauly, Y. Petukhov, A. Povtorejko, R.J.M.Y. Ruber, W. Scobel, T. Skorodko, B. Shwartz, V. Sopov, J. Stepaniak, V. Tchernyshev, P. Thörngren-Engblom, V. Tikhomirov, A. Turowiecki, G.J. Wagner, M. Wolke, A. Yamamoto, J. Zabierowski, J. Zlomanczuk
Exclusive measurements of $pd \to {}^3\mathrm{He}\,\pi\pi$: The ABC effect revisited
Physics Letters B **637** (2006) 223

6. W. Bertl, R. Engfer, E.A. Hermes, G. Kurz, T. Kozlowski, J. Kuth, G. Otter, F. Rosenbaum, N.M. Ryskulov, A. van der Schaaf, P. Wintz, I. Zychor
A search for μ-*e* conversion in muonic gold
European Physical Journal C **47** (2006) 337.

7. V. Bollini, A. Bubak, A. Budzanowski, J. Cugnon, D. Filges, F. Goldenbaum, A. Heczko, H. Hodde, L. Jarczyk, B. Kamys, M. Kistryn, St. Kistryn, St. Kliczewski, A. Kowalczyk, P. Kulessa, H. Machner, A. Magiera, W. Migdal, K. Nünighoff, N. Paul, B. Piskor-Ignatowicz, K. Pysz, Z. Rudy, R. Siudak, M. Wojciechowski, E. Kozik
Light charged particle and intermediate mass fragment cross sections in GeV proton induced reactions-the PISA experiment
Nuclear Instruments and Methods A **562** (2006) 733.

8. D. Chiladze, A. Kacharava, F. Rathmann, C. Wilkin, S. Barsov, J. Carbonell, S. Dymov, R. Engels, P.D. Eversheim, R. Gebel, V. Glagolev, K. Grigoriev, D. Gusev, M. Hartmann, F. Hinterberger, V. Hejny, A. Khoukaz, I. Keshelashvili, H.R. Koch, V. Komarov, P. Kulessa, A. Kulikov, A. Lehrach, B. Lorentz, G. Macharashvili, R. Maier, Y. Maeda, R. Menke, T. Mersmann, S. Merzliakov, M. Mikirtytchiants, S. Mikirtytchiants, A. Mussgiller, M. Nioradze, H. Ohm, D. Prasuhn, H. Rohdjess, R. Schleichert, H. Seyfarth, E. Steffens, H.J. Stein, H. Ströher, S. Trusov, K. Ulbrich, Yu. Uzikov, A. Wronska, S. Yaschenko
Determination of Deuteron Beam Polarization at COSY
Physics Review ST-AB **9** (2006) 050101.

9. D.Chiladze, J.Carbonell, S. Dymov, V. Glagolev, M. Hartmann, V. Hejny, A. Kacharava, I. Keshelashvili, A. Khoukaz, H.R. Koch, V. Komarov, P. Kulessa, A. Kulikov, G. Macharashvili, Y. Maeda, T. Mersmann, S. Merzliakov, S. Mikirtytchiants, A. Mussgiller, M. Nioradze, H. Ohm, F. Rathmann, R. Schleichert, H.J. Stein, H. Ströher, Yu. Uzikov, S. Yaschenko, C. Wilkin
Vector and tensor analysing powers in deuteron-proton breakup reactions at intermediate energies
Physics Letters B **637** (2006) 170.

10. S.Dymov, M. Büscher, D. Gusev, M. Hartmann, V. Hejny, A. Kacharava, A. Khoukaz, V. Komarov, P. Kulessa, A. Kulikov, V. Kurbatov, N. Lang, G. Macharashvili, T. Mersmann, S. Merzliakov, S. Mikirtytchiants, A. Mussgiller, D. Prasuhn, F. Rathmann, R. Schleichert, H. Ströher, Yu. Uzikov, C. Wilkin, S. Yaschenko
Production of the $^1S_0$ diproton in the $pp \to (pp)\pi^0$ reaction at 0.8 GeV
Physics Letters B **635** (2006) 270.

11. A. Dzyuba, V. Kleber, M. Büscher, V.P. Chernyshev, S. Dymov, P. Fedorets, V. Grishina, C. Hanhart, M. Hartmann, V. Hejny, L. Kondratyuk, V. Koptev, P. Kulessa, Y. Maeda, T. Mersmann, S. Mikirtychyants, M. Nekipelov, D. Prasuhn, R. Schleichert, A. Sibirtsev, H.J. Stein, H. Ströher, I. Zychor
Scalar-isovector $K\bar{K}$ production close to threshold
European Physical Journal A, **29** (2006), 245

12. P. Fedorets, M. Büscher, V.P. Chernyshev, S. Dymov, V.Yu. Grishina, C. Hanhart, M. Hartmann, V. Hejny, V. Kleber, H.R. Koch, L.A. Kondratyuk, V. Koptev, A.E. Kudryavtsev, P. Kulessa, S. Merzliakov, S. Mikirtychiants, M. Nekipelov, H. Ohm, R. Schleichert, H. Ströher, V.E. Tarasov, K.-H. Watzlawik, I. Zychor
Evidence of $a_0^+(980)$-resonance production in the reaction $pp \to d\pi^+\eta$
Physics of Atomic Nuclei **69** (2006) 306.

13. A. Gadea, S.M. Lenzi, S. Lunardi, N. Mrginean, A.P. Zuker, G. de Angelis, M. Axiotis, T. MartÃnez, D.R. Napoli, E. Farnea, R. Menegazzo, P. Pavan, C.A. Ur, D. Bazzacco, R. Venturelli, P. Kleinheinz, P. Bednarczyk, D. Curien, O. Dorvaux, J. Nyberg, H. Grawe, M. Górska, M. Palacz, K. Lagergren, L. Milechina, J. Ekman, D. Rudolph, C. Andreoiu, M.A. Bentley, W. Gelletly, B. Rubio, A. Algora, E. Nacher, L. Caballero, M. Trotta, M. Moszyski
Observation of ^{54}Ni: Cross-Conjugate Symmetry in $f_{7/2}$ Mirror Energy Differences
Physical Review Letters **97** (2006) 152501.

14. M. Hartmann, Y. Maeda, I. Keshelashvilli, H.R. Koch, S. Mikirtytchiants, S. Barsov, W. Borgs, M. Büscher, V.I. Dimitrov, S. Dymov, V. Hejny, V. Kleber, V. Koptev, P. Kulessa, T. Mersmann, S. Merzliakov, A. Mussgiller, M. Nekipelov, M. Nioradze, H. Ohm, K. Pysz, R. Schleichert, H.J. Stein, H. Ströher, K.-H. Watzlawik, P. Wüstner
The Near-threshold production of ϕ mesons in pp collisions
Physical Review Letters **96** (2006) 242301.

15. C.M. Herbach, D. Hilscher, U. Jahnke, V.G. Tishchenko, J. Galin, A. Letourneau, A. PÃ©ghaire, D. Filges, F. Goldenbaum, L. Pienkowski, W.U. Schröder, J. Tõke
Charged Particle Evaporation and pre-Equilibrium Emission in 1.2 GeV Proton-Induced Spallation Reactions
Nuclear Physics A **765** (2006) 426.

16. P. Indelicato, E.-O. Le Bigot, M. Trassinelli, D. Gotta, M. Hennebach, N. Nelms, Chr. David, L.M. Simons
Characterization of a charge-coupled device array for Bragg spectroscopy
Review of Scientific Instruments **77** (2006) 043107.

17. H. Kleines, J. Sarkadi, K. Zwoll, R. Engels, K. Grigoryev, M. Mikirtychyants, M. Nekipelov, F. Rathmann, H. Seyfarth, P. Kravtsov, A. Vasilyev
The control system of the polarized internal target of ANKE at COSY
Nuclear Instruments and Methods A **560** (2006) 503.

18. H. Machner, D.G. Aschman, K. Baruth-Ram, J. Carter, A.A. Cowley, F. Goldenbaum, B.M. Nangu, J.V. Pilcher, E. Sideras-Haddad, J.P.F. Sellschop, F.D. Smit, B. Spoelstra, D. Steyn
Isotopic production cross sections in proton-nucleus collisions at 200 MeV
Physical Review C **73** (2006) 044606.

19. Y. Maeda, M. Hartmann, I. Keshelashvili, S. Barsov, M. Büscher, A. Dzyuba, S. Dymov, V. Hejny, A. Kacharava, V. Kleber, H.R. Koch, V. Koptev, P. Kulessa, T. Mersmann, S. Mikirtytchiants, A. Mussgiller, M. Nekipelov, H. Ohm, R. Schleichert, H.J. Stein, H. Ströher, Yu. Valdau, K.-H. Watzlawik, C. Wilkin, P. Wüustner
Precision measurement of the quasi-free $pn \to d\phi$ reaction close to threshold
Physical Review Letters **97** (2006) 142301.

20. P. Moskal, H.-H. Adam, A. Budzanowski, R. Czyzykiewicz, D. Grzonka, M. Janusz, L. Jarczyk, T. Johansson, B. Kamys, P. Klaja, A. Khoukaz, K. Kilian, J. Majewski, W. Oelert, C. Piskor-Ignatowicz, J. Przerwa, J. Ritman, T. Rozek, T. Sefzick, M. Siemaszko, J. Smyrski, A. Täschner, J. Wessels, P. Winter, M. Wolke, P. Wüstner, Z. Zhang, W. Zipper
A method to disentangle single- and multi-meson production in missing mass spectra from quasi-free $pn \to pn\,X$ reactions
Journal of Physics G **32** (2006) 629.

21. R.Ortega, D. d'Enterria, G. Martinez, D. Baiborodin, H. Delagrange, J. Diaz, F. Fernandez, H. Loehner, T. Matulewicz, R.W. Ostendorf, S. Schadmand, Y. Schutz, P. Tlusty, R. Turrisi, V. Wagner, H.W. Wilschut, N. Yahlali
Constraints on the Time-Scale of Nuclear Breakup from Thermal Hard-Photon Emission
European Physical Journal A **28** (2006) 161.

22. H. Rohdjeß, D. Albers, J. Bisplinghoff, R. Bollmann, K. Büßer, O. Diehl, F. Dohrmann, H.-P. Engelhardt, P. D. Eversheim, J. Greiff, A. Gross, R. Groß-Hardt, F. Hinterberger, M. Igelbrink, R. Langkau, R. Maier, F. Mosel, M. Müller, M. Münstermann, D. Prasuhn, P. von Rossen, H. Scheid, N. Schirm, F. Schwandt, W. Scobel, H.J. Trelle, A. Wellinghausen, W. Wiedmann, K. Woller, R. Ziegler
Radiation damage of polypropylene fiber targets in storage rings
Nuclear Instruments and Methods B **243** (2006) 127.

23. T. Rozek, D. Grzonka, H.-H. Adam, A. Budzanowski, R. Czyzykiewicz, M. Janusz, L. Jarczyk, B. Kamys, A. Khoukaz, K. Kilian, P. Klaja, P. Kowina, P. Moskal, W. Oelert, C. Piskor-Ignatowicz, J. Przerwa, J. Ritman, T. Sefzick, M. Siemaszko, J. Smyrski, A. Taschner, P. Winter, M. Wolke, P. Wustner, Z. Zhang, W. Zipper
Threshold hyperon production in proton-proton collisions at COSY-11
Physics Letters B **643** (2006) 251.

24. S. Tashenov, Th. Stöhlker, D. Banas, K. Beckert, P. Beller, H.F. Beyer, F. Bosch, S. Fritzsche, A. Gumberidze, S. Hagmann, C. Kozhuharov, T. Krings, D. Liesen, F. Nolden, D. Protic, D. Sierpowski, U. Spillmann, U. Steck, A. Surzhykov
First Measurement of the Linear Polarization of Radiative Electron Capture Transitions
Physical Review Letters **97** (2006) 223202.

25. P. Winter, M. Wolke, H.-H. Adam, A. Budzanowski, R. Czyzykiewicz, D. Grzonka, M. Janusz, L. Jarczyk, B. Kamys, A. Khoukaz, K. Kilian, P. Klaja, P. Moskal, W. Oelert, C. Piskor-Ignatowicz, J. Przerwa, J. Ritman, T. Rozek, T. Sefzick, M. Siemaszko, J. Smyrski, A. Täschner, P. Wüstner, Z. Zhang, W. Zipper
Kaon pair production close to threshold
Physics Letters B **635** (2006) 23.

26. I. Zychor, V. Koptev, M. Büscher, A. Dzyuba, I. Keshelashvili, V. Kleber, H.-R. Koch, S. Krewald, Y. Maeda, S. Mikirtichyants, M. Nekipelov, H. Ströher, C. Wilkin
Evidence for an excited hyperon state in $pp \to p\,K^+\,Y^{*0}$
Physical Review Letters **96** (2006) 012002.

2. Theory

27. M.A. Belushkin, H.W. Hammer, U.-G. Meißner
Novel evaluation of the two-pion contribution to the nucleon isovector form factors
Physics Letters B **633** (2006) 507

28. V. Bernard, U.-G. Meißner
The nucleon axial-vector coupling beyond one loop
Physics Letters B **639** (2006) 278.

29. B. Borasoy, P.C. Bruns, U.-G. Meißner, R. Lewis
Chiral corrections to the Roper mass
Physics Letters B **641** (2006) 294.

30. B. Borasoy, H. Krebs, D. Lee, U.-G. Meißner
The triton and three-nucleon force in nuclear lattice simulations
Nuclear Physics A **768** (2006) 179.

31. B. Borasoy, U.-G. Meißner, R. Nissler
K^-p scattering length from scattering experiment
Physical Review C **74** (2006) 055201.

32. B. Borasoy, R. Nissler, U.-G. Meißner
On the extraction of the quark mass ratio $(m_d - m_u)/m_s$ from $\gamma(\eta' \to \pi^0\pi^+\pi^-)/\gamma(\eta' \to \eta\pi^+\pi^-)$
Physics Letters B **643** (2006) 41.

33. A. Bulgac, P. Magierski, A. Wirzba
Scalar Casimir effect between Dirichlet spheres or a plate and a sphere
Physical Review D **73** (2006) 025007.

34. G. Devidze, A. Liparteliani, U.-G. Meißner
$B_{s,d} \to \gamma\gamma$ decay in the model with one universal extra dimension
Physics Letters B **634** (2006) 59.

35. E. Epelbaum, W. Hammer, U.-G. Meißner, A. Nogga
More on the infrared renormalization group limit cycle in QCD
European Physical Journal C **48** (2006) 169.

36. M. Frink, U.-G. Meißner
On the chiral effective meson-baryon Lagrangian at third order
European Physical Journal A **29** (2006) 255.

37. F. Grümmer, J. Speth
Landau-Migdal theory of interacting Fermi systems: A framework for effective theories in nuclear structure physics
Journal of Physics G **32** (2006) R193.

38. H. Haberzettl, K. Nakayama, S. Krewald
Gauge-invariant approach to meson photoproduction including the final-state interaction
Physical Review C **74** (2006) 045202.

39. J. Haidenbauer, H.W. Hammer, A. Sibirtsev, U.-G. Meißner
On the strong energy dependence of the $e^+e^- \leftrightarrow p\bar{p}$ amplitude near threshold
Physics Letters B **643** (2006) 29.

40. J. Haidenbauer, A. Sibirtsev, U.-G. Meißner
Near threshold $p\bar{p}$ enhancement in B and J/Ψ decay
Physical Review D **74** (2006) 017501.

41. K. Hencken, G. Baur, D. Trautmann
Transverse momentum distribution of vector mesons produced in ultraperipheral heavy ion collisions
Physical Review Letters **96** (2006) 012303.

42. Yu.S. Kalashnikova, A.E. Kudryavtsev, A.V. Nefediev, J. Haidenbauer, C. Hanhart
Insights on scalar mesons from their radiative decays
Physical Review C **73** (2006) 045203.

43. H. Krebs, B. Borasoy
Renormalization of two-loop diagrams in scalar lattice field theory
Nuclear Physics B **748** (2006) 1.

44. S. Krewald, V.B. Soubbotin, V.I. Tselyaev, X. Vinas
Density matrix functional theory that includes pairing correlations
Physical Review C **74** (2006) 064310.

45. A. Kucukarslan, U.-G. Meißner
Omega-phi mixing in chiral perturbation theory
Modern Physics Letters A **21** (2006) 1423.

46. V. Lensky, V. Baru, J. Haidenbauer, C. Hanhart, A.E. Kudryavtsev, U.-G. Meißner
Towards a field theoretic understanding of $NN \to NN\pi$
European Physical Journal A **27** (2006) 37.

47. A. Lähde, U.-G. Meißner
Improved Analysis of J/Ψ Decays into a Vector Meson and Two Pseudoscalars
Physical Review D **74** (2006) 034021.

48. J. Ley, C. Düweke, R. Emmerich, A. Imig, H. Paetz gen. Schieck, J. Golak, H. Witala, E. Epelbaum, A. Deltuva, A.C. Fonseca, W. Glöckle, U.-G. Meißner, A. Nogga, P.U. Sauer
Cross sections and tensor analyzing powers A_{yy} of the reaction ^{1}H$(d, \vec{pp})n$ in 'symmetric constant relative energy' geometries at E_d=19 MeV
Physical Review C **73** (2006) 064001.

49. H. Machner, J. Niskanen
Charge independence studied in $NN \to d\pi$ reactions
Nuclear Physics A **776** (2006) 172.

50. U.-G. Meißner, U. Raha, A. Rusetsky
Isospin-breaking corrections in the pion-deuteron scattering length
Physics Letters B **639** (2006) 478.

51. U.-G. Meißner, U. Raha, A. Rusetsky
Kaon-nucleon scattering lengths from kaonic deuterium experiments
European Physical Journal C **47** (2006) 473.

52. E.H. Müller, B. Kubis, U.-G. Meißner
T-odd correlations in radiative K^+_{e3} decays and chiral pertubation theory
European Physical Journal C **48** (2006) 427.

53. Y. Nagai, T. Kobayashi, T. Shima, T. Kikuchi, K. Takaoka, M. Igashira, J. Golak, R. Skibinski, H. Witala, A. Nogga, W. Glöckle, H. Kamada
Measurement of the ^{2}H$(n,\gamma)^3$H reaction cross section between 10 and 550 keV
Physical Review C **74** (2006) 025804.

54. S. Naito, Y. Nagai, T. Shima, H. Makii, K. Mishima, K. Tamura, H. Toyokawa, H. Ohgaki, J. Golak, R. Skibinski, H. Witala, W. Glöckle, A. Nogga, H. Kamada
New data for total ^{3}He$(\gamma,p)D$ and ^{3}He$(\gamma,pp)n$ cross sections compared to current theory
Physical Review C **73** (2006) 034003.

55. N.N. Nikolaev, W. Schäfer
Unitarity cutting rules for the nucleus excitation and topological cross sections in hard production off nuclei from nonlinear $k(T)$-factorization
Physical Review D **74** (2006) 074021.

56. N.N. Nikolaev, W. Schäfer
Quenching of leading jets and particles: The $p(T)$ dependent Landau-Pomeranchuk-Migdal effect from nonlinear $k(T)$ factorization
Physical Review D **74** (2006) 014023.

57. N.N. Nikolaev, W. Schäfer, B.G. Zakharov and V.R. Zoller
Glue in the pomeron from nonlinear $k(T)$-factorization
JETP Letters Â **83** (2006) 192.

58. A. Nogga, C. Fonseca, A. Gardestig, C. Hanhart, C.J. Horowitz, G.A. Miller, J.A. Niskanen, U. van Kolck
Realistic few-body physics in the $dd \to \alpha\pi^0$ reaction
Physics Letters B **639** (2006) 465.

59. A. Nogga, C. Hanhart
Can one extract the π-neutron scattering length from π-deuteron scattering?
Physics Letters B **634** (2006) 210.

60. A. Nogga, P. Navratil, B.R. Barrett, J.P. Vary
Spectra and binding energy predictions of chiral interactions for ^{7}Li
Physical Review C **73** (2006) 064002.

61. H. Polinder, J. Haidenbauer, U.-G. Meißner
Hyperon nucleon interactions: A chiral effective field theory approach
Nuclear Physics A **779** (2006) 244.

62. L. Roca, C. Hanhart, E. Oset, U.-G. Meißner
Testing the nature of the $\Lambda(1520)$ resonance in proton-induced production
European Physical Journal A **27** (2006) 373.

63. D. Rozpedzik, J. Golak, R. Skibinski, H. Witala, W. Glöckle, E. Epelbaum, A. Nogga, H. Kamada
A First estimation of chiral four-nucleon force effects in ^{4}He
Acta Physica Polonica B **37** (2006) 2889.

64. S. Schneider, S. Krewald, U.-G. Meißner
The reaction $\pi N \to \pi\pi N$ in a meson-exchange approach
European Physical Journal A **28** (2006) 107.

65. A. Sibirtsev, J. Haidenbauer, H.W. Hammer, S. Krewald
Resonances and final state interactions in the reaction $pp \to p\,K^+\Lambda$
European Physical Journal A **27** (2006) 269.

66. A. Sibirtsev, J. Haidenbauer, H.W. Hammer, U.-G. Meißner
Phenomenology of the Λ/Σ^0 production ratio in pp collisions
European Physical Journal A **29** (2006) 363.

67. A. Sibirtsev, J. Haidenbauer, S. Krewald, U.-G. Meißner
Kaon-deuteron scattering at low energies
Journal of Physics G **32** (2006) R395.

68. A. Sibirtsev, J. Haidenbauer, U.-G. Meißner
Aspects of ϕ-meson production in proton proton collisions
European Physical Journal A **27** (2006) 263.

69. A. Sibirtsev, H.W. Hammer, U.-G. Meißner, A.W. Thomas
ϕ-Meson Photoproduction from Nuclei
European Physical Journal A **29** (2006) 209.

70. R. Skibinski, J. Golak, H. Witala, W. Glöckle, A. Nogga, E. Epelbaum
Nucleon-deuteron capture with chiral potentials
Acta Physica Polonica B **37** (2006) 2905.

71. A. Wirzba, A. Bulgac, P. Magierski
Casimir interaction between normal or superfluid grains in the Fermi sea
Journal of Physics A **39** (2006) 6815.

72. H. Witala, J. Golak, R. Skibinski, W. Glöckle, a. Nogga, E. Epelbaum, H. Kamada, A. Kievsky, M. Viviani
Testing nuclear forces by polarization transfer coefficients in $d(\vec{p},\vec{p})d$ and $d(\vec{p},\vec{d})p$ reactions E_p^{lab}= 22.7 MeV
Physical Review C **73** (2006) 044004.

3. Accelerator (including conference proceedings)

73. S. Andrianov, A. Chechenin
The normal form for beam physics in matrix representation
Proc. EPAC 2006, Edinburgh, Scotland, ISBN 92-9083-278-9, 978-92-9083-278-2, p. 2122.

74. S. Andrianov, A. Chechenin
The high order aberration correction
Proc. EPAC 2006, Edinburgh, Scotland, ISBN 92-9083-278-9, 978-92-9083-278-2, p. 2125.

75. O. Boine-Frankenheim, R. Hasse, F. Hinterberger, A. Lehrach,A, P. Zenkevich
Cooling equilibrium and beam loss with internal targets in high energy storage rings
Nuclear Instruments and Methods in Physics Research A **560** (2006) 245.

76. A. Chechenin, R. Maier, Yu. Senichev
The Non-linear Space Charge Field Compensation of the Electron Beam in the High Energy Storage Ring of FAIR
Proc. EPAC 2006, Edinburgh, Scotland, ISBN 92-9083-278-9, 978-92-9083-278-2, p. 2802.

77. A. Chechenin, R. Maier, Yu. Senichev, E. Senicheva
The High Order Non-linear Beam Dynamics in High Energy Storage Ring of FAIR
Proc. EPAC 2006, Edinburgh, Scotland, ISBN 92-9083-278-9, 978-92-9083-278-2, p. 2083.

78. J. Conradie, A. Botha, P. Celliers, J. Delsink, D. Theunis Fourie, P. Mansfield, P. Rohwer, J. Van Niekerk, J. Dietrich, I. Mohos
Beam Phase Measurement in a 200 MeV Cyclotron
Proc. EPAC 2006, Edinburgh, Scotland, ISBN 92-9083-278-9, 978-92-9083-278-2.

79. J. Dietrich, V. Parkhomchuk
The Proposed 2 MeV Electron Cooler for COSY-Jülich
Proc. EPAC 2006, Edinburgh, Scotland, ISBN 92-9083-278-9, 978-92-9083-278-2.

80. F. Esser, R. Eichhorn, B. Laatsch, H. Singer, R. Stassen
First cool down of the Jülich accelerator module based on superconducting half-wave resonators
Proc. EPAC 2006, Edinburgh, Scotland, ISBN 92-9083-278-9, 978-92-9083-278-2.

81. A. Garishvili, A. Lehrach, B. Lorentz, S. Martin, F. Rathmann, P. Lenisa, E. Steffens
Design study for an antiproton polarizer ring (APR)
Proc. EPAC 2006, Edinburgh, Scotland, ISBN 92-9083-278-9, 978-92-9083-278-2, p. 223.

82. R. Gebel, O. Felden, R. Maier, P. von Rossen
Recent gain in polarized beam intensities for the cooler synchrotron COSY at Jülich
Proc. EPAC 2006, Edinburgh, Scotland, ISBN 92-9083-278-9, 978-92-9083-278-2, p. 1705.

83. A.D. Krisch, M.A. Leonova, V.S. Morozov, R.S. Raymond, D.W. Sivers, V.K. Wong, R. Gebel, A. Lehrach, B. Lorentz, R. Maier, D. Prasuhn, A. Schnase, H. Stockhorst, F. Hinterberger, K. Ulbrich
Unexpected enhancement and reduction of rf spin resonance strength
Physical Review ST AB **9** (2006) 051001.

84. A. Lehrach, O. Boine-Frankenheim, F. Hinterberger, R. Maier, D. Prasuhn
Beam performance and luminosity limitations in the High-Energy Storage Ring (HESR)
Nuclear Instruments and Methods in Physics Research A **561** (2006) 289.

85. A. Lehrach, R. Maier, D. Prasuhn, O. Boine-Frankenheim, R.W. Hasse, F. Hinterberger
Beam Performance with Internal Targets in the High-Energy Storage Ring (HESR)
Proc. EPAC 2006, Edinburgh, Scotland, ISBN 92-9083-278-9, 978-92-9083-278-2, p. 2197.

86. A. Paal, A. Simonsson, J. Dietrich, I. Mohos
Bunched Beam Current Measurements with 100 pA rms Resolution at CRYRING
Proc. EPAC 2006, Edinburgh, Scotland, ISBN 92-9083-278-9, 978-92-9083-278-2.

87. D. Prasuhn, J. Dietrich, A. Lehrach, B. Lorentz, R. Maier, H. Stockhorst
From COSY to HESR
Proc. EPAC 2006, Edinburgh, Scotland, ISBN 92-9083-278-9, 978-92-9083-278-2, p. 226.

88. H. Rohdjeß, D. Albers, J. Bisplinghoff, R. Bollmann, K. Blüßer, O. Diehl, E. Dohrmann, H.P. Engelhardt, P.D. Eversheim, M. Gasthuber, J. Greiff, A. Groß, R. Groß-Hardt, F. Hinterberger, M. Igelbrink, R. Langkau, R. Maier, F. Mosel, M. Müller, M. Münstermann, D. Prasuhn, P. von Rossen, H. Scheid, N. Schirm, F. Schwandt, W. Scobel, H.J. Trelle, A. Wellinghausen, W. Wiedmann, K. Woller, R. Ziegler
Determining beam parameters in a storage ring with cylindrical hodoscope using elastic proton-proton scattering
Nuclear Instruments and Methods in Physics Research A **556** (2006) 57.

89. H. Rohdjeß, M. Altmeier, F. Bauer, J. Bisplinghoff, R. Bollmann, K. Büßer, M. Busch, O. Diehl, F. Dohrmann, H. P. Engelhardt, J. Ernst, P.D. Eversheim, K.O. Eyser, O. Felden, R. Gebel, A. Groß, R. Groß-Hardt, F. Hinterberger, R. Langkau, J. Lindlein, R. Maier, F. Mosel, D. Prasuhn, P. von Rossen, N. Scheid, M. Schulz-Rojahn, F. Schwandt, V. Schwarz, W. Scobel, H.-J. Trelle, K. Ulbrich, E. Weise, A. Wellinghausen, K. Woller, R. Ziegler

Upper Limits on Resonance Contributions to Proton-Proton Elastic Scattering in the c.m. Mass Range 2.05 – 2.85 GeV/c^2
European Physical Journal A, **28** (2006), 115

90. Yu. Senichev, A. Bogdanov, R. Maier, N. Vasyukhin
Beam dynamics in super-conducting linear accelerator: Problems and solutions
Nuclear Instruments and Methods in Physics Research A **558** (2006) 240.

91. Yu. Senichev, W. Bräutigam, R. Maier, O. Belyaev, Yu. Budanov, V. Stepanov, V. Teplyakov, A. Zherebtsov, I. Zvonarev
Novel H-type rf-deflector
Physical Review ST AB **9** (2006) 012001.

92. Yu. Senichev, N. Vasiukhin
Hamiltonian formalism for halo investigation in high-intensity beams
Nuclear Instruments and Methods in Physics Research A **561** (2006) 166.

93. E. Senicheva, A. Lehrach, D. Prasuhn, D.
The PANDA Insertion Impedance in High Energy Storage Ring of FAIR
Proc. EPAC 2006, Edinburgh, Scotland, ISBN 92-9083-278-9, 978-92-9083-278-2, p. 2865.

94. R. Stassen, R. Eichhorn, F.M. Esser, B. Laatsch, G. Schug, H. Singer
The HW resonators in Jülich
Physica C **441** (2006) 179.

95. H. Stockhorst, B. Lorentz, R. Maier, D. Prasuhn, T. Katayama
Stochastic Cooling for the HESR at the GSI-FAIR Complex
Proc. EPAC 2006, Edinburgh, Scotland, ISBN 92-9083-278-9, 978-92-9083-278-2, p. 231.

96. N. Vasyukhin, R. Maier, Yu. Senichev
The features of high intensity beam dynamics in low energy super-conducting linear accelerator
Nuclear Instruments and Methods in Physics Research A **558** (2006), 333.

C Diploma and Ph.D. Theses 2006

1. Diploma

1. M. Angelstein: *Untersuchungen der Charakteristika eines Szintillatorhodoskopes des Wide Angle Shower Apparatus (WASA) am COoler SYnchrotron" (COSY)*, Fachhochschule Jena

2. M. Evers: *Towards a field theoretically consistent unitatization of quark models*, Universität Bonn

3. B.R. Jany: *Assembly and measurements of the Electromagnetic Calorimeter components for WASA-at-COSY setup*, Jagiellonian University Cracow [arXiv:physics/0606110]

4. E. Matveyev: *Verbesserung der Elektronik einer Emittanzmeßanlage*, Technical University Obninsk

5. M.A. Odoyo: *Development of Software for Slow Control of the High Voltage System of the WASA Central Detector Calorimeter*, Fachhochschule Mannheim.

6. C.F. Redmer: *Groß- und kleinflächige Szintillatorhodoskope in der Teilchen- und Atomphysik*, Ruhr-Universität Bochum

7. D.M. Welsch: *Entwicklung eine Orbitkorrektursystems füqr den Hochenergie Speicherring HESR im Projekt FAIR*, Universität Bonn

8. L. Yurev: *Performance of the Mini Drift Chamber — The central detector of the experiment WASA*, Voronezh State University

2. Ph.D.

9. I. Keshelashvili: *Kaon pair production in pp collisions at the ANKE spectrometer*, Tbilisi University

10. S. Mikirtychiants: *Precision measurement of π^+ and K^+ lifetime*, PNPI Gatchina

11. A. Mussgiller: *Identification and Tracking of Low Energy Spectator Protons*, Universität zu Köln

D Invited Talks and Colloquia

1. Baur, G.
   Reaction theory
   Nustar Annual Meeting
   GSI Darmstadt: 22. – 24.02.2006

2. Baur, G.; Typel, S.
   Investigation of subthreshold resonances with the Trojan horse method
   Fusion06: International Conference on Reaction Mechanisms and Nuclear Structure at the Coulomb Barrier
   S.Servolo Island, Italy: 19. – 23.03.2006

3. Baur, G.
   Direct reactions with exotic nuclei, nuclear structure and astrophysics
   Erice School on Radioactive Beams, Nuclear Dynamics and Astrophysics
   Erice, Italy: 16. – 24.09.2006

4. Büscher, M.
   Experimental Program at COSY
   Joint Sino-German Symposium on Hadron Physics at COSY and CSR (HPC2)
   Lanzhou, China: 13. – 18.01.2006

5. Dietrich, J.
   2 MeV Elektronenkühler für COSY-Jülich
   Leibnitz-Institut für Polymerforschung, seminar talk
   Dresden: 13.10.2006

6. Dietrich, J.
   2 MeV Elektronenkühler für COSY-Jülich
   Universität Erlangen, Institut für Theoretische Physik, seminar talk
   Erlangen: 26.01.2006

7. Dietrich, J.
   Measurements of Beam Profile Based on Light Radiation of Atoms Excited by the Particle Beam
   iThemba Lab, seminar talk
   Faure, South Afrika: 06.12.2006

8. Dietrich, J.
   Muon Cooling
   Goethe-Universität Frankfurt am Main, Winterseminar Beschleunigerphysik, seminar talk
   Riezlern: 05. – 11.03.2006

9. Dietrich, J.
   New Experimental Results on Electron Cooling at COSY-Juelich
   University of Kyoto, Advanced Research Center for Beam Science, seminar talk
   Kyoto, Japan: 07.06.2006

10. Epelbaum, E.
    Three-nucleon forces: new developments
    2006 APS April Meeting
    Dallas, TX: 22. – 26.04.2006

11. Epelbaum, E.
    Chiral Forces and Few-Nucleon Systems
    Workshop on Exotic Hadronic Atoms, Deeply Bound Kaonic Nuclear States and Antihydrogen: Present Results, Future Challenges
    ECT Trento, Italien: 19. – 24.06.2006

12. Epelbaum, E.
    Few-Nucleon Forces and Systems in Chiral Effective Field Theory
    21st Annual Hampton University Graduate School Program
    Jefferson Lab., Newport News: 05. – 23.06.2006

13. Epelbaum, E.
Chiral EFT for Electroinduced Processes in Few-Nucleon Systems Gordon Research Conference on Photonuclear Reactions
Tilton School, Tilton, NH: 30.07. – 04.08.2006

14. Epelbaum, E.
Towards a Systematic Theory on Nuclear Forces and Nuclear Currents
5th International Workshop on Chiral Dynamics: Theory and Experiment
Durham/Chapel Hill, NC: 18. – 22.09.2006

15. Epelbaum, E.
Chiral Extrapoations in Few-Nucleon Systems
Workshop on Lattice QCD, Chiral Perturbation Theory and Hadron Phenomenology
ECT Trento, Italy: 02.10.2006 – 06.10.2006

16. Epelbaum, E.
Isospin Violation in Nuclear Potentials
Carolina Isospin Violation Workshop
Columbia, SC: 01. – 02.12.2006

17. Gillitzer, A.
Experimental access to in-medium properties of η and K mesons
Joint Sino-German Symposium on Hadron Physics at COSY and CSR (HPC2)
Lanzhou, China: 13. – 18.01.2006

18. Gillitzer, A.
Hadrons in the nuclear medium — An experimental review
IVth International Conference on Quarks and Nuclei (QNP06)
Madrid, Spain: 05. – 10.06.2006

19. Gotta, D.
Pionic Hydrogen
The International Workshop Physics with Simple Atomis Systems (PSAS 2006)
Venice, Italy: 13. – 17.06.2006

20. Gotta, D.
Light Antiprotonic Atoms
The International Workshop on Hadronic Exotic Atoms
Trento, Italy: 19. – 23.06.2006

21. Gotta, D.
Pionic Deuterium
The International Workshop on Hadronic Exotic Atoms
Trento, Italy: 19. – 23.06.2006

22. Haidenbauer, J.
Exotica, final-state interactions and the $p\bar{p}$ system
Universität Bonn : Physikalisches Institut; Kolloquium
Bonn: 27.04.2006

23. Haidenbauer, J.
Meson-exchange description of hadronic systems: Recent developments
18th International IUPAP Conference on Few-Body Problems in Physics
Santos, Brasil: 21. – 26.08.2006

24. Haidenbauer, J.
The hyperon-nucleon interaction: conventional versus effective field theory approach
University of Barcelona: Kolloquium
Barcelona, Spain: 31.05.2006

25. Hanhart, C.
CSB pion production, progress in $pn \to d\pi^0$
Carolina Isospin Violation Workshop
Columbia, SC: 01. – 02.12.2006

26. Hanhart, C.
Dispersive Corrections to the Pion Deuteron Scattering Length
QCD and Few-Hadron Systems
Bad Honnef: 16.11.2006

27. Hanhart, C.
Highlights of the ETA06 Workshop on the Eta-Nucleus System
EtaMesonNet Meeting
Mainz: 03.10.2006

28. Hanhart, C.
Pion reactions on two nucleon systems
Physics and Astrophysics of Hadrons and Hadronic Matter: Lecture series
Shantiniketan, India: 06. – 09.11.2006

29. Hanhart, C.
The pi NN system: Recent progress
5th International Workshop on Chiral Dynamics: Theory & Experiment
Durham, Chapel Hill: 18. – 22.09.2006

30. Hanhart, C.
Towards an understanding of the light scalar mesons
QNP2006
Madrid, Spain: 05. – 10.06.2006

31. Hartmann, M.
The near-threshold production of ϕ mesons in pN collisions
MESON2006: 9th International Workshop on Meson Production, Properties and Interaction
Cracow, Poland: 09. – 13.06.2006

32. Hawranek, P.
Eta physics at GEM
MESON2006: 9th International Workshop on Meson Production, Properties and Interaction
Cracow, Poland: 09. – 13.06.2006

33. Kirilov, D.
Search for eta bound states at COSY
Eta workshop
Jülich: 09.05.2006

34. Kirilov, D.
The eta physics program at GEM
IVth International Conference on Quarks and Nuclear Physics (QNP06)
Madrid, Spain: 05. – 10.06.2006

35. Krebs, H.
Scalar two-loop diagrams on the lattice
Lattice QCD, Chiral Perturbation Theory and Hadron Phenomenology
ECT Trento, Italy: 10. – 14.10.2006

36. Krewald, S.
N^* physics
Institute of High Energy Physics, Seminar Talk
Beijing, China: 19.01.2006

37. Krewald, S.
Medium modifications of the nucleon-nucleon interaction
XI International Seminar on Electromagnetic Interactions of Nuclei
Moscow, Russia: 21. – 24.09.2006

38. Krewald, S.
Study of N^* excitations with the Juelich model
Thomas Jefferson National Laboratory : N^* Analysis Workshop
Newport News: 04. – 05.11.2006

39. Krewald, S.
Electric Dipole Strength in Heavy Nuclei
QCD and Few-Hadron Systems: 380th International Wilhelm and Else Heraeus Seminar
Bad Honnef, Germany: 13. – 17.11.2006

40. Lorentz, B.
Accelerator constraints for internal experiments
Joint Sino-German Symposium on Hadron Physics at COSY and CSR (HPC2)
Lanzhou, China: 13. – 18.01.2006

41. Machner, H.
Physics with WASA at COSY
Symposium QCD: Facts and Prospects
Oberwölz, Austria: 10. – 16.09.2006

42. Machner, H.
Recent Investigations at BIG KARL
XVIII Baldin ISHEPP
Dubna, Russia: 25. – 30.09.2006

43. Machner, H.
Recent Experiments at Big Karl
Seminar, Helsinki Inst. Physics
Helsinki, Finland: 10.10.2006

44. Meißner, U.-G.
Major Challenges in QCD
Joint Sino-German Symposium on Hadron Physics at COSY and CSR (HPC2)
Lanzhou, China: 13. – 18.01.2006

45. Meißner, U.-G.
Summary Talk of Hadron Physics at COSY and CSR
Joint Sino-German Symposium on Hadron Physics at COSY and CSR (HPC2)
Lanzhou, China: 13. – 18.01.2006

46. Meißner, U.-G.
B-Decays and the Scalar Sector of QCD
Workshop on Three-Body Charmless B Decays
Paris, France: 01. – 03.02.2006

47. Meißner, U.-G.
B-decays and the scalar sector of QCD
Workshop on Scalar Mesons
Bonn, Germany: 27. – 28.03.2006

48. Meißner, U.-G.
Form factors of the nucleon and its pion cloud
Workshop on Shape of Hadrons
Athens, Greece: 27. – 30.04.2006

49. Meißner, U.-G.
Modern Theory of Nuclear Forces
Universität zu Köln: Grosses Physikalisches Kolloquium
Köln: 23.05.2006

50. Meißner, U.-G.
Modern theory of nuclear forces
IVth International Conference on Quarks and Nuclear Physics (QNP06)
Madrid, Spain: 05. – 10.06.2006

51. Meißner, U.-G.
Modern theory of nuclear forces: Status and perspectives
18th International IUPAP Conference on Few-Body-Problems in Physics (FB 18)
Santos, Brazil: 21. – 26.08.2006

52. Meißner, U.-G.
Quark mass dependence of the nucleon mass and axial-vector coupling
Workshop on Soft-Pions in Hard Processes
Regensburg, Germany: 03. – 05.08.2006

53. Meißner, U.-G.
Hadronic atoms
Hadron TH'06 Workshop
Peniscola, Spain : 07. – 09.09.2006

54. Meißner, U.-G.
On the consistency of Weinberg's power counting
5th International Workshop on Chiral Dynamics: Theory and Experiment (CD 06)
Chapel Hill: 18. – 22.09.2006

55. Meißner, U.-G.
Recent developments in chiral perturbation theory
5th International Workshop on Chiral Dynamics: Theory and Experiment (CD 06)
Chapel Hill: 18. – 22.09.2006

56. Meißner, U.-G.
Thoughts on chiral extrapolations for excited states
ECT*-I3HP Workshop on Lattice QCD, Chiral Perturbation Theory, and Hadron Phenomenology
Trento, Italy: 02. – 06.10.2006

57. Meißner, U.-G.
Chiral dynamics with (non)strange quarks
Transregio 16: Tagung des Sonderforschungsbereichs
Bommerholz: 27. – 28.11.2006

58. Meißner, U.-G.
Modern theory of nuclear forces: Status and perspectives
Workshop of the SFB 634
Paradeismühle, Klingenberg: 06. – 08.12.2006

59. Moskal, P.
η and η' meson production at COSY-11
MESON2006: 9th International Workshop on Meson Production, Properties and Interaction
Cracow, Poland: 09. – 13.06.2006

60. Nikolaev, N.N.
Lectures on factorization theorems for hard processes in a nuclear environment St.Petersburg XL Winter-School on Nuclear and Particle Physics and XII School on Theoretical Physics : St.Petersburg Nuclear Physics Institute St. Petersburg, Russia: 20.02.2006 – 26.02.2006

61. Nikolaev, N.N.
Understanding the Spin Filtering in Storage Rings
Workshop on QCD with Antiprotons
ECT* Trento, Italy: 03. – 08.07.2006

62. Nikolaev, N.N.
QCD Physics with Antiprotons at FAIR GSI
Symposium QCD: Facts and Prospects
Oberwölz, Austria: 10. – 16.09.2006

63. Nikolaev, N.N.
Spin Filtering of Stored (Anti)Protons from FILTEX to COSY to AD to FAIR
17th International Spin Physics Symposium: SPIN2006
Kyoto University, Kyoto, Japan: 02. – 07.10.2006

64. Nogga, A.
Chiral 3N interactions and p-shell nuclei
Los Alamos National Lab, Seminar
Los Alamos: 12.01.2006

65. Nogga, A.
RG and EFT for nuclear forces
ECT* School on RG and Effective Field Theory Approaches to Nuclear Systems: 3 lectures
Trento, Italy: 27.02. – 10.03.2006

66. Nogga, A.
EFT approach
Workshop on Electron-Nucleus Scattering-IX
Isola d'Elba, Italy: 19. – 23.06.2006

67. Nogga, A.
Chirale und Niederimpulswechselwirkungen: ein systematischer Zugang zur Kernphysik
Universität Gießen, Seminar
Gießen: 14.07.2006

68. Nogga, A.
Application of chiral nuclear forces to light nuclei
5th International Workshop on Chiral Dynamics (CD06)
Duke University, Durham, Chapel Hill: 18. – 22.09.2006

69. Nogga, A.
Chiral nuclear interactions: a systematic approach to nuclear structure
University of Vancouver, TRIUMF, Seminar
Vancouver, Canada: 28.11.2006

70. Nogga, A.
Chirale und Niederimpulswechselwirkungen: ein systematischer Zugang zur Kernphysik
Technische Universität München, Seminar
München: 27.10.2006

71. Nogga, A.
Nuclear bound state predictions for chiral interactions
Workshop on QCD and Few-Hadron Systems
Bad Honnef: 13. – 17.11.2006

72. Oelert, W.
Experimente mit der Antimaterie — die geheimnsivolle Materie aus Antiteilchen
Universität Bonn, Kolloquium
Bonn: 28.04.2006

73. Oelert, W.
Experiments on making atoms totally of antimatter — why and how
Silesian University Katowice : Department of Physics, Kolloquium
Katowice, Poland: 17.01.2006

74. Oelert, W.
General thoughts to the Kaon pair production in the threshold region
MESON2006: 9th International Workshop on Meson Production, Properties and Interaction
Cracow, Poland: 09. – 13.06.2006

75. Oelert, W.
Physics with low Energy Antiprotons
Workshop on $\bar{p}$ Physics
Trento, Italy: 06.07.2006

76. Polinder, H.
Hyperon-nucleon interactions in effective field theory
IX International Conference on Hypernuclear and Strange Particle Physics
Mainz: 12.10.2006

77. Polinder, H.
Hyperon-nucleon interactions in effective field theory
Workshop on QCD and Few-Hadron Systems, 380th International Wilhelm und Else Heraeus Seminar
Bad Honnef: 16.11.2006

78. Ritman, J.
Physics with Antiprotons at FAIR
International Graduate School Basel-Tuebingen, Colloquium
Basel, Switzerland: 05.05.2006

79. Ritman, J.
Precision spectroscopy in the charmonium mass region using antiproton annihilation: PANDA at FAIR
Conference on Hadron Physics
Trento, Italy: 07.07.2006

80. Ritman, J.
Investigation of Fundamental Symmetries in Hadronic Systems: WASA at COSY
Technische Universität München, Colloquium
München: 27.07.2006

81. Ritman, J.
Charmonium Physics with PANDA at FAIR
Heavy Quarks and Leptons Conference
München: 17.10.2006

82. Ritman, J.
Symmetieverletzungen in der Hadronen-Physik
Ruhr Universität Bochum, Colloquium
Bochum: 04.12.2006

83. Schadmand, S.
Hadron Physics at COSY with the WASA Detector
Universität Mainz, Kernphysikalisches Institut, Seminar
Mainz: 02.01.2006

84. Schadmand, S.
Chasing Symmetries with WASA at COSY
Joint Symposium on Hadron Physics, GSI/Mainz, GSI/Darmstadt
Darmstadt: 26. – 27.01.2006

85. Schadmand, S.
Future Physics with WASA at COSY
QNP06: IVth International Conference on Quarks and Nuclear Physics
Madrid, Spain: 05. – 10.06.2006

86. Schadmand, S.
Two Pion Production from Nuclei
New Frontiers in QCD, Exotic Hadrons and Hadronic Matter: Yukawa International Seminar (YKIS) 2006
Kyoto, Japan: 04. – 08.12.2006

87. Speth, J.
Migdal's theory of finite Fermi systems, Nuclear Physics Seminar
Institute of Nuclear Physics, Colloquium
Cracow, Poland: 19.10.2006

88. Speth, J.
From Nuclear Physics to Financial Markets
Institute of Nuclear Physics, Colloquium
Cracow, Poland: 16.11.2006

89. Stassen, R.
Stochastisches Kühlsystem am Beispiel COSY und Weiterentwicklungen für HESR/FAIR
Universität Darmstadt, seminar talk
Darmstadt: 14.11.2006

90. Ströher, H.
Hadron Physics in Germany
Joint Sino-German Symposium on Hadron Physics at COSY and CSR (HPC2)
Lanzhou, China: 13. – 18.01.2006

91. Ströher, H.
Hadron Physics at COSY-Jülich
Universität Basel, Kolloquium
Basel, Switzerland: 04.05.2006

92. Ströher, H.
The Hadron Physics Program at COSY-Jülich
CGSWHP06, Spin in Hadron Physics
Tbilisi, Georgia: 04. – 08.09.2006

93. Ströher, H.
Spin in Hadronic Reactions at Medium Energy
SPIN2006: The 17th International Spin Physics Symposium
Kyoto, Japan : 02. - 07.10.2006

94. Ströher, H.
The Hadron Physics Program at COSY-Jülich
DAE-BRNS06: Physics and Astrophysics of Hadrons and Hadronic Matter
Santiniketan, India: 06. - 11.11.2006

95. Wirzba, A.
Casimir effect and trace formula
Nonlinearities '06 — from Turbulent to Magic
Nordita and Niels Bohr Institute Thematic Workshop
Copenhagen, Denmark: 17. – 20.05.2006

96. Wirzba, A.
Exact and semiclassical solutions to the Casimir effect
Lund University, Mathematical Physics, LTH, Seminar talk
Lund, Sweden: 03.07.2006

97. Wolke, M.
The Physics Case for WASA at COSY
HPC2, Hadron Physics at COSY and CSR
Lanzhou, China: 13. - 18.01.2006

98. Wolke, M.
Physik mit WASA an COSY
TU Dresden, Institut für Kern- und Teilchenphysik, Institutsseminar
Dresden: 13.07.2006

99. Zapatin, E.
Cornell cryostat structural analysis
Cornell LEPP Seminar
Ithaca, NY: 28.08.2006

100. Zapatin, E.
FZJ sc rf cavity developments
FermiLab Accelerator Seminar
Chicago, Ill.: 16.02.2006

101. Zapatin, E.
FZJ superconducting rf cavities
Cornell LEPP Seminar
Ithaca, NY: 14.08.2006

102. Zapatin, E.
High-gradient cavity mid-cell comparison
Cornell LEPP Seminar

E Awards & Offers for Professorships

J. Dietrich: *Dr. h.c.* by JINR Dubna (20.01.2006)

J. Dietrich: *Apl. Professor* by Univ. Dortmund (02.10.2006)

U.-G. Meißner: *Chair in Theoretical Nuclear Physics* by Univ. Mainz (June 2006)

F Funded Projects

Project	Responsible	Partner Institute	Funded by
CARE	R. Tölle		EU/FP6
TA-COSY	D. Grzonka		EU/FP6
Hadron Physics Theory Netzwerk	U.-G. Meißner	Network	EU/FP6
EtaMesonNet	W. Oelert	Network	EU/FP6
Pellet Target	M. Büscher	ITEP, MPEI Moscow (Russia)	EU/FP6
EURONS/EXL	D. Grzonka		EU/FP6
EUROTRANS/NUDATRA	F. Goldenbaum		EU/FP6
DIRAC Secondary Beams	R. Tölle		EU/FP6
DIRAC Secondary Beams PANDA-4	J. Ritman		EU/FP6
DIRAC Second. Beams PANDA-2	J. Ritman		EU/FP6
Strange and Charmed Scalar Mesonss	M. Büscher	ITEP, INR Moscow (Russia)	DFG
K^+ Production Mechanisms in Nuclei	H. Ströher	PNPI Gatchina (Russia)	DFG
Light Scalar Resonances $a_0/f_0(980)$	M. Büscher	ITEP, MPEI Moscow (Russia)	DFG
Isospin Violation	M. Büscher	IMP Lanzhou (China)	DFG
Jets in Hard Processes	N.N. Nikolaev	Landau Inst., ITEP Moscow (Russia)	DFG
Properties of Unstable Nuclei	S. Krewald	Petersburg State Univ., IPPE Obninsk (Russia)	DFG
Pion Reactions on Few Nucleon Systems	C. Hanhart	ITEP Moscow (Russia)	DFG
Quark-gluon degrees of freedom in the confinement region of QCD	J. Haidenbauer	UNESP Sao Paulo (Brasil)	DFG
ATRAP	W. Oelert	Univ. Mainz	DFG
Fundamental Research with Hadrons	W. Oelert	Jagellinian Univ. Cracow (Poland)	DFG
Broken Symmetries	H. Machner	Univ. Helsinki (Finland)	DAAD
PPP Poland	P.v. Rossen		DAAD
PPP Sweden	H. Ströher	Uppsala Univ. (Sweden)	DAAD
Short-range correlations in nuclear reactions	J. Haidenbauer	JINR Dubna (Russia)	Heisenberg-Landau Program
Eta-Meson Physics	H. Machner	BARC Mumbai (India)	Int. Büro BMBF
Target Development for nuclear physics experiments at COSY and AEA cyclotron	J. Ritman	AEA Cairo (Egypt)	Int. Büro BMBF
Medical Applications of Accelerators	J. Dietrich	iThemba LABS (South Africa)	Int. Büro BMBF
Advanced Residual Gas Profile Monitor	J. Dietrich		INTAS
Advanced Beam Dynamic for Storage Rings	A. Lehrach		INTAS
EM-processes in the peripheral collisions of relativistic and ultrarelativistic heavy ions	G. Baur	Belfast, Tashkent, Arkhangelsk	GSI-INTAS
Polarized Target	F. Rathmann	PNPI Gatchina (Russia)	ISTC
Few Nucleon Systems in χEFT	E. Epelbaum	Univ. Bonn	HGF
Planare Germanium Detektoren	D. Protic		GSI
Baryon Resonance Analysis	U.-G. Meißner	JLAB (U.S.A.)	JLAB

G COSY-FFE Projects

Project	Responsible	Institute
Θ^+ und Anti-decuplet	Prof. K. Goeke	Univ. Bochum
TOF-Entwicklung und Nutzung	Prof. H. Koch	Univ. Bochum
Frozen Spin Target	Prof. W. Meyer	Univ. Bochum
Zusammenarbeit von HISKP-Bonn an internen Experimenten an COSY	Prof. J. Bisplinghoff	Univ. Bonn
Polarisiertes Target für TOF	Dr. H. Dutz	Univ. Bonn
Theorectical studies of strangeness and charm production at COSY and PANDA/FAIR	Prof. H.-W. Hammer	Univ. Bonn
Entwicklung eines Partialwellenprogrammes für die Analyse von Daten von WASA	Prof. E. Klempt	Univ. Bonn
Zusammenarbeit an COSY H-Strahl Laserdiagnose	Prof. T. Weis	Univ. Dortmund
COSY-TOF detector	Prof. H. Freiesleben	TU Dresden
Bau von Detektoren für ANKE und K^--Nachweis	Prof. B. Kämpfer	FZ Dresden-Rossendorf
Theoretische Untersuchungen zur künftigen COSY-Physik	Prof. M. Dillig	Univ. Erlangen-Nürnberg
Bau eines Cherenkovdetektors für WASA at COSY	Prof. W. Eyrich	Univ. Erlangen-Nürnberg
Experimente mit COSY-TOF	Prof. W. Eyrich	Univ. Erlangen-Nürnberg
Polarization experiments with ANKE at COSY	Prof. E. Steffens	Univ. Erlangen-Nürnberg
Meson production and resonance properties in the coupled channel K-Matix approach	Prof. U. Mosel	Univ. Gießen
ANKE Experiment und Auswertung $pp \to dK^+\bar{K}^0$	Prof. H. Paetz gen. Schieck	Univ. Köln
Schwellenexperimente an COSY-11 und ANKE	Dr. A. Khoukaz	Univ. Münster
Installation und Inbetriebnahme des WASA-Detektors am COSY-Ring und Durchführung von Experimenten an WASA at COSY	Prof. H. Clement	Univ. Tübingen
Experimente an COSY-TOF	Prof. H. Clement	Univ. Tübingen
η-production on heavier nuclei	Dr. R. Tsenov	Univ. of Sofia (Bulgaria)
Polarized internal target for ANKE at COSY	Prof. M. Nioradze	Tbilisi State Univ. (Georgia)
Spin dependence in pd interactions	Prof. P. Dalpiaz	Univ. Ferrara (Italy)
Photonendetektor an ANKE	Prof. A. Magiera	Jagellinian Univ. Cracow (Poland)
WASA at COSY	Prof. M. Jezabek	INP Crakow (Poland)
Strange Baryon Produktion at ANKE	Prof. Z. Sujkowski	IPJ Otwock-Swierk (Poland)
Neutron tagging and strangeness production at ANKE	Dr. V. Koptev	PNPI Gatchina (Russia)
Set-up and research with the spectator/vertex detection system at ANKE-COSY	Prof. V. Komarov	JINR Dubna (Russia)
Investigation of scalar meson production in pp, pd and dd collisions	Prof. L. Kondratyuk	ITEP Moscow (Russia)
Development, commissioning and operation of components for the COSY experiments WASA and ANKE and spin-filtering studies at COSY as preparation of the PAX experiment in the framework of the FAIR project at GSI	Dr. A. Vasilyev	PNPI Gatchina (Russia)
Cooperation COSY-WASA for $pp \to pp\eta$ and $pp \to pp\eta\pi^0$	Prof. T. Johansson	Uppsala Univ. (Sweden)
Search for mixing between light mesons	Prof. A. Rudchik	INR Kiev (Ukraine)
Unified analysis of meson production in hadronic reactions	Prof. K. Nakayama	Univ. of Georgia (U.S.A.)
SPIN@COSY: Spin-Manipulating Polarized Deuterons and Protons	Prof. A. Krisch	Univ. of Michigan (U.S.A.)

H COSY Summer School CSS2006

From August 28 to September 1 the 3rd COSY Summer School (CSS2006) took place at the conference center Burg Hengebach in Heimbach — organized by the IKP in collaboration with the Universities Dresden and Cracow. It was attented by more than 30 Diploma and Ph.D. students from Germany, France, Ireland, Sweden, Finland, Poland, Ukraina, Russia und China.

Fig. 51: Participants and organizers of the COSY Summer School at Burg Hengebach.

During 12 theoretical and experimental lectures modern techniques and current hot topics in in hadron physics were presented with special emphasize on COSY relevant topics. In the second part of CSS2006 the participants were asked to work out — based on the contents of these lectures — experimental COSY proposals. These working groups were especially appreciated since they offered a possibility to apply the new knowledge to a "real case". The results were finally presented in talks by the students in which they had to "defend" their results against referees (*i.e.* the organizers of CSS2006). All proposals were so well worked out that all of the applied beam times could be "approved".
The agenda of the Summer School was complemented by an excursion to COSY and its detection systems as well as a hike through the lovely Eifel landscape. Due to the very positive feedback from the participants (one of the foreign guests wrote the organizers: "the best I had so far"), the next COSY Summer School is planned for the year 2008.
Financial support for the CSS2006 by the board of directors of the FZJ is gratefully acknowledged.

I Conferences (co-)organized by the IKP

I.1 HPC^2, Lanzhou (China)

On January 13–18 2006, the Joint Sino-German symposium on Hadron Physics at COSY and CSR (HPC^2) took place in Lanzhou, which is located in central China at the banks of the yellow river. The symposium was jointly organized by the Institute of Modern Physics (IMP) of the Chinese Academy of Sciences, and the IKP, and financed by the Sino-German Center for Research Promotion in Beijing. The workshop was attended by ∼80 participants, mostly from China and Germany.

Fig. 52: Some participants of HPC2 in front of the main building of the IMP, Lanzhou.

The IKP has been operating COSY for more than 10 years which provides proton and deuteron beams with momenta up to 3.7 GeV/c. A similar facility — with the CSRm and CSRe rings — has been built at IMP and is now in the commissioning phase.

At COSY several detection systems — like the ANKE dipole spectrometer and the non-magnetic COSY-TOF experiment — are used for hadron physics experiments. A disadvantage of these existing COSY detectors is that they are "photon blind". This will change with the start of operation of the Wide Angle Shower Apparatus WASA in 2007. WASA is a fixed-target 4π detector and designed for the detection of neutral and charged particles.

On the Chinese side a novel detector, HPLUS, is being prepared for hadron physics experiments. This device is conceptually designed for further studies of baryon resonances, scalar mesons and/or isospin violating effects. The R&D of the whole project has been started in the IMP with participation from other Chinese universities. Once operating, the WASA and HPLUS detectors allow one to investigate basic questions of non-perturbative quantum chromodynamics ("strong QCD"), for example through a precise study of symmetry breaking and very specific investigations of hadron structure. η and η' decays that vanish in the limit of equal-light quark masses explore the explicit isospin symmetry-breaking in QCD. Precision measurements of rare η and η' decays can be used to obtain new limits on the breaking of the charge, parity and time symmetries or their combinations. Last but not least, WASA and HPLUS can contribute to test various models offered to explain exotic and crypto-exotic hadrons — through precise measurements of decay chains and couplings to other hadrons.

These, together with other hot topics of strong QCD were discussed in about 40 talks during the 3-days workshop in order to coordinate the physics programs and share the technological expertise. Further common projects, focussing around measurements with WASA and the preparation of HPLUS, are now being launched.

I.2 International Workshop on η Physics

The International Workshop on Eta Physics was held from May 8–12 2006 at the IKP. The conference was a subgroup meeting of the EtaMesonNet network that coordinates activities and exchanges of information on the study of mesons, especially, η-mesons, at different European accelerator research infrastructures where they are produced with complementary processes.

The idea of this subgroup meeting was to bring together experts on various aspects of the field in order to understand better the complicated many-body problem posed by the η-nucleus dynamics. Most of the time of the meeting we will focus on the related theoretical aspects. However, for the first day we also invited representatives from the various experimental groups involved. There are currently or have been recently strong experimental efforts to investigate the η-nucleus system with various probes at BNL (USA), CELSIUS (Sweden), COSY (Jülich), and MAMI (Mainz). This first day was meant to define the problems to be studied in the following days, to get informed about experimental plans and possibilities, and to initiate the discussions.

Fig. 53: Participants of the η workshop in front of the COSY building.

There were in total 32 participants from 13 countries. The conference was characterized by very intense but constructive discussions. The talks can be found on the conference homepage under http://www.fz-juelich.de/ikp/etanucleus/ and the results of the meeting as well as the individual talks are summarized in http://arxiv.org/pdf/nucl-th/0610011.

The workshop was funded by the European Union and the FZ-Jülich.

I.3 MESON2006, Cracow (Poland)

The 9th MESON conference took place in 2006 as all previous conferences in Cracow, Poland, in the time from June 9–13. The topics covered were

- hadronic meson production in various reactions,
- hadronic meson production in various reactions,
- electromagnetic meson production meson interaction with mesons,
- nucleons and nuclei, structure of hadrons,
- mesons and fundamental symmetries,
- exotic systems.

The conference was organized by Jagellonian University, Cracow, Poland, Polish Academy od Sciences, Cracow, Poland, the Instituto Nazionale di Fisica Nucleare, Frascaty, Italy, and the FZJ. It was attended by more than 160 participants. The proceedings will appear as Vol. 22, Nos. 2 & 3 (30 January 2007) in the International Journal of Modern Physics A.

Fig. 54: Participants of the MESON2006 conference in front of the new Audimax of the Jagiellonian University.

I.4 CGSWHP2006, Tbilisi (Georgia)

The possibility of polarizing antiprotons at the upcoming Facility for Antiproton and Ion Research at GSI has stimulated widespread interest within the hadron community. Measuring the Drell-Yan process in high-energy proton-antiproton collisions offers the best way to study the transverse spin structure of protons (transversity). This was the focus at the second Caucasian-German School and Workshop on Hadron Physics (CGSWHP) in Tbilisi, Georgia, on 4-8 September. Around 70 participants attended, from nine countries.
Spin filtering, in which a beam of antiprotons acquires polarization by repeated passage through a polarized hydrogen target, is believed to be the most effective means of producing a useful beam for transversity experiments.

Fig. 55: Participants relax during an interlude at the highly charged CGSWHP'06 in Georgia.

CGSWHP'06 discussed preparatory spin-filtering tests using proton beams. These could be at COSY, where there is an extensive physics programme involving polarized beams and targets. Results from COSY were also presented at the meeting.
Georgian media covered several sessions, as well as the meeting of the organizers with the rector of Tbilisi State University, and some of the social programme. TV interviews publicized the workshop, with local graduate students discussing their research.
The EC Integrated Infrastructure Initiative project, Hadron Physics, supported the workshop, which was themed Spin in Hadron Physics and which was also sponsored by Forschungszentrum Jülich, the International Science & Technology Center, the Joint Institute for Nuclear Research and the Institute for High Energy Physics and Informatization, Tbilisi State University.

I.5 Carolina Isospin Violation Workshop

On December 1st and 2nd the Carolina Isospin Violation workshop was held at the Physics institute of the University of South Carolina located in Columbia, SC. This meeting was one of regular meetings where scientists interested in the subject of isospin violations come together, not only to discuss recent progress in the understanding of isospin violation in nucleon-nucleon and deuteron-deuteron induced pion production (one of the key experiments of WASA at COSY) but also new developments in the field as a whole. Out of the discussions emerged at least two concrete projects that will be carried out in the course of this year.
The workshop was funded by the Universtiy of South Carolina.

J Teaching Positions

Institute	Name	University
IKP-1	PD Dr. A. Gillitzer	Bonn
	PD Dr. F Goldenbaum	Wuppertal
	Prof. Dr. H. Machner	Duisburg-Essen
	Prof. Dr. W. Oelert	Bochum
	Prof. Dr. J. Ritman	Bochum
	PD Dr. S. Schadmand	Gießen
IKP-2	PD Dr. M. Büscher	Köln
	PD Dr. D. Gotta	Köln
	PD Dr. F. Rathmann	Erlangen-Nürnberg
	Prof. Dr. H. Ströher	Köln
	Dr. M. Wolke	Bochum
IKP-3	Prof. Dr. G. Baur	Basel
	Prof. Dr. E. Epelbaum	Bonn
	Univ. Doz. Dr. J. Haidenbauer	Graz
	PD Dr. C. Hanhart	Bonn
	Prof. Dr. S. Krewald	Bonn
	Prof. Dr. U.-G. Meißner	Bonn
	Prof. Dr. N.N. Nikolaev	Moscow
	Dr. A. Nogga	Bonn
	PD Dr. A. Wirzba	Bonn
IKP-4	Prof. Dr. Dr. h.c. J. Dietrich	Dortmund
	Dr. A. Lehrach	Bonn
	Prof. Dr. R. Maier	Bonn

K Beam Time at COSY 2006

Date	Experiment	Duration	Reaction
17.02.06–06.03.06	COSY-11	2 weeks	$pn \to d\eta'$
10.03.–20.03.	GEM	1 week	$pp \to d\pi^+ / pn\pi^+$
22.03.–29.03.	ANKE	1 week	cell tests
04.04.–02.05.	ANKE	4 weeks	$dd \to \alpha K^+ K^-$
05.05.–15.05.	GEM	1 week	$\vec{d}p \to ppn$
19.05.–29.05.	SPIN@COSY	1 week	
21.08.–04.09.	WASA	2 weeks	commissioning
08.09.–25.09.	GEM	2 weeks	$p\,^6\mathrm{Li} \to \eta + {}^7\mathrm{Be}$
29.09.–23.10.	COSY-11	3 weeks	$pp \to pp\eta'$
03.11.–20.11.	WASA	2 weeks	commissioning
22.11.–30.11.	ANKE	1 week	$\vec{d}\vec{p} \to ppn$
Total '06		20 weeks	

L Personnel

L.1 Scientific Staff

Msc. M.-M. Abdel-Bary (IKP-1) (until 31 March, 2006)

DP S. An (IKP-4) (until 28 January, 2006)

DP M. Angelstein (IKP-1) (1 April – 30 Sep., 2006)

F. Ballout (IKP-3) (since 1 July, 2006)

Prof. Dr. G. Baur (IKP-3)

Dr. U. Bechstedt (IKP-4)

Dr. K. Bongardt (IKP-4)

DI N. Bongers (IKP-4)

DI W. Borgs (IKP-2)

DI R. Brings (IKP-4)

PD Dr. M. Büscher (IKP-2)

Dr. R. Castelijns (IKP-1) (until 30 November, 2006)

DP A. Chechenin (IKP-4)

DP D. Chiladze (IKP-2)

Prof. Dr.Dr.h.c. J. Dietrich (IKP-4)

Dr. A. Djalois (IKP-1)

DP A. Dzyuba (IKP-2)

Dr. R. Engels (IKP-2)

Prof. Dr. E. Epelbaum (IKP-3) (since 1 April, 2006)

DI F.-J. Etzkorn (IKP-4)

M. Evers (IKP-3) (until 28 February, 2006)

Dr. P. Fedorets (IKP-2)

Dr. O. Felden (Rs)

M. Freunek (IKP-3) (since 1 July, 2006)

Dr. W. Gast (IKP-1)

Dr. R. Gebel (IKP-4)

PD Dr. A. Gillitzer (IKP-1)

PD Dr. F. Goldenbaum (IKP-1)

PD Dr. D. Gotta (IKP-2)

Dr. F. Grümmer (IKP-3)

Dr. D. Grzonka (IKP-1)

DI W. Günther (IKP-4)

Univ. Doz. Dr. J. Haidenbauer (IKP-3)

PD Dr. C. Hanhart (IKP-3)

Dr. M. Hartmann (IKP-2)

Dr. V. Hejny (IKP-2)

DI K. Henn (IKP-4)

Dr. F. Hügging (IKP-1)

D. Jamanidze (IKP-2) (1 April – 30 September, 2006)

Dr. V. Kamerdjiev (IKP-4)

Dr. I. Keshelashvili (IKP-2)

DP D. Kirillov (IKP-4)

DP P. Klaja (IKP-1) (since 1 February, 2006)

A. Klingler (IKP-2) (since 1 April, 2006)

DP A. Kowalczyk (IKP-1) (since 6 November, 2006)

Dr. H. Krebs (IKP-3) (since 1 April, 2006)

Prof. Dr. S. Krewald (IKP-3)

DI K. Kruck (IKP-4)

Dr. A. Lehrach (IKP-4)

DP V. Lensky (IKP-3)

DP V. Leontyev (IKP-2)

DP M. Lesiak (IKP-1) (until 31 August, 2006)

Dr. B. Lorentz (IKP-4)

Prof. Dr. H. Machner (IKP-1)

Dr. Y. Maeda (IKP-2) (until 31 March, 2006)

Prof. Dr. R. Maier (IKP-4)

J. Majewski (IKP-2)

Dr. S. Martin (IKP-4) (until 30 April, 2006)

Prof. Dr. U.-G. Meißner (IKP-3)

DP M. Mertens (IKP-1) (since 16 October, 2006)

M. Mittag (IKP-2) (1 April – 30 September, 2006)

DI I. Mohos (IKP-4)

Dr. H.-P. Morsch (IKP-1) (until 31 December, 2006)

Dr. M. Nekipelov (IKP-2)

Prof. Dr. N.N. Nikolaev (IKP-3)

Dr. A. Nogga (IKP-3)

DP M. Odoyo (IKP-1) (1 March – 31 August, 2006)

Prof. Dr. W. Oelert (IKP-1)

DP D. Oellers (IKP-2)

Dr. H. Ohm (IKP-2)

DI N. Paul (IKP-1)

Dr. C. Pauly (IKP-1) (since 1 September, 2006)

DP F. Pavlov (IKP-3) (until 20 August, 2006)

DP B. Piskor-Ignatowicz (IKP-1) (until 28 Feb., 2006)

DP P. Podkopal (IKP-2)
Dr. H. Polinder (IKP-3)
Dr. D. Prasuhn (IKP-4)
DP D. Protic (Dt)
DP J. Przerwa (IKP-1) (since 1 February, 2006)
PD Dr. F. Rathmann (IKP-2)
DP Ch.F. Redmer (IKP-1)
DI A. Richert (IKP-4)
Prof. Dr. J. Ritman (IKP-1)
Dr. E. Roderburg (IKP-1)
Dr. P. v. Rossen (IKP-4) (until 31 December, 2006)
DI J. Sarkadi (El)
DP P. Saviankou (IKP-3)
Dr. H. Schaal (IKP-1)
PD Dr. S. Schadmand (IKP-1)
E. Schlauch (IKP-3) (since 15 August, 2006)
Dr. R. Schleichert (IKP-2)
Dr.-Ing. A. Schnase (IKP-4) (until 30 September, 2006)
DI H. Schneider (IKP-4)
DI G. Schug (IKP-4)
Dr. Th. Sefzick (El)
DI E. Senicheva (IKP-4)
Dr. Y. Senichev (IKP-4)
DI M. Simon (IKP-4)
Dr. A. Sokolov (IKP-1)
Dr. R. Stassen (IKP-4)
Dr. H. Stockhorst (IKP-4)
Dr. T. Stockmanns (IKP-1)
DP Th. Strauch (IKP-2) (since 1 June, 2006)
Prof. Dr. H. Ströher (IKP-2)
T. Tolba (IKP-1) (since 1 August, 2006)
Dr. R. Tölle (IKP-4)
DP Y. Valdau (IKP-2)
DI T. Vashegyi (IKP-4)
Dr. N. Vasiukhin (IKP-4)
DP P. Vlasov (IKP-1)
Chr. Weidemann (IKP-2) (since 1 November, 2006)
DP D. Welsch (IKP-4)
Dr. P. Wintz (IKP-1)
PD Dr. A. Wirzba (IKP-3)
DI J.-D. Witt (IKP-4)
Dr. M. Wolke (IKP-2)
L. Yurev (IKP-2)
Dr. E. Zaplatin (IKP-4)
DP D. Z. Zhang (IKP-1)

L.2 Technical and Administrative Staff

C. Berchem (El)

P. Birx (IKP-4)

M. Böhnke (IKP-4)

H. Bongen (IKP-1) (since 22 February, 2006)

J. Borsch (Rs)

P. Brittner (IKP-4)

J. But (Ws)

M. Comuth-Werner (Ad)

B. Dahmen (IKP-4)

C. Deliege (IKP-4)

W. Derissen (Co)

N. Dolfus (El)

G. D'Orsaneo (IKP-2)

R. Dosdall (IKP-1)

R. Enge (IKP-4)

B. Erkes (IKP-4)

W. Ernst (El)

K. Esser (Ad)

H.-P. Faber (IKP-4)

G. Fiori (Dt)

H.-W. Firmenich (Ws)

J. Göbbels (Rs)

H. Hadamek (Ws)

R. Hecker (IKP-4)

E. Heßler (Co)

M. Holona (Ws)

H.-M. Jäger (IKP-1)

H. J. Jansen (Ws)

M. Karnadi (IKP-2)

A. Kieven (IKP-4)

Ch. Krahe (Ws)

M. Kremer (Ws)

Th. Krings (Dt)

G. Krol (IKP-4)

M. Küven (Ws)

K.-G. Langenberg (IKP-4)

H. Metz (Dt)

S. Müller (Ad)

R. Nellen (El)

St. Nießen (Dt)

H. Pütz (IKP-4)

G. Roes (Ad)

N. Rotert (IKP-4)

D. Ruhrig (IKP-4)

T. Sagefka (IKP-4)

F. Scheiba (IKP-4)

H. Schiffer (El)

J. Schmitz (IKP-4)

F. Schultheiß (Ws)

K. Schwill (Dt) (until 30 June, 2006)

H. Singer (IKP-4)

D. Spölgen (IKP-2)

G. Sterzenbach (IKP-1)

J. Strehl (Ws)

R. Stumm (IKP-1) (until 31 January, 2006)

J. Uehlemann (IKP-1)

P. Wieder (IKP-2)

Th. Willems (IKP-2) (until 31 January, 2006)

J. Wimmer (IKP-1)

H. Zens (IKP-4)

Ad = Administraion
Co = Construction
Dt = Detectors
El = Electronics
Rs = Radiation Safety
Ws = Workshop

M Contents of the Attached CD

1. This report as pdf file

2. Detailed reports for the Annual Report 2006